UNIVERSITÀ DEGLI STUDI DI TRENTO

Doctorate School in Civil, Environmental and
Mechanical Engineering

---

# STREAMFLOW GENERATION IN ALPINE CATCHMENTS

## The role of hydrological and geochemical information

Karina Cano Paoli

March 2016

Doctoral thesis in Environmental Engineering
$27^{th}$ Cycle
Department of Civil, Environmental and Mechanical Engineering
University of Trento
**Supervisor**: Prof. Ing. Alberto Bellin

*This research was partially supported by the European Communities 7th Framework Programme under Grant Agreement No. 603629-ENV-2013-6.2.1-Globaqua.*

Academic year 2014/2015

Front Cover: Vermigliana catchment (North-Eastern Italy) during summer and winter seasons.

*To Simone*

# Acknowledgements

The completion of this PhD represents the end of a long and challenging journey, which has been possible only thanks to the support and encouragement of numerous people over the past four years. Therefore I wish to express my sincere appreciation to those who have contributed in many different ways to made of this journey an unforgettable experience.

Foremost, I would like to express my gratitude to my supervisor, Alberto Bellin, not only for his scientific contribution, but most of all, for his support, guidance and encouragement, in particular during the last stage of this thesis. My sincere gratitude is reserved also to Gabriele Chiogna, whom even if not an official supervisor, guide me through this path with much enthusiasm and patience, always encouraging me with positive thoughts. Under the guidance of both, I have successfully overcome many difficulties and learned so much along the way.

I would also like to thank Prof. Mario Schirmer for his great sense of hospitality during my short visit to the EAWAG institute and to Behnam Doulatyari, for his contribution to Chapter 5, his endless patience and for the good moments outside academia.

I gratefully acknowledge Prof. Mario Putti, Damiano Pasetto, Prof. Claudio Paniconi, Prof. Stefano Orlandini, Giovanni Moretti and Marcello Fiorentini for their support and availability during the first years of my PhD, even though my path change afterwards, the period shared with them for sure contributed positively to this experience.

A very special acknowledgement goes to my dear office mates: Giorgia, Diego, Ines, Elisa, Elena and Stefano. For all the coffee breaks and other good moments shared together, in particular for their words of encouragement during the last period. This experience would have not been the same without you.

My gratitude and appreciation goes also to the rest of the people in my research group, Bruno, Alessandra, Oscar, Sebastiano, for sharing their work and life experiences and for all the good advices. Likewise, to the rest of my colleagues and friends spread around the world. I hope we may meet again some time in the future, in particular I will like to thank Elisa, Lydia, Marialaura, Giulia, Enrico and Carlotta.

A heartfelt thank goes to my dear family, my mum, my dad and my sister, who even from the distance have always shown their love and support. Thanks for all of the sacrifices that you have made on my behalf. The same way, a warm thank is reserved for my husband's entire family, who accepted me from the first

moment and gave me their unconditional love and support.

I am beyond grateful to the trentinian-paraguayan group in Trento, "la fiebre trentina", whom I discover not only as true friends but also as a big family that help me so much throughout this journey. In particular many thanks to Luca Cernuzzi, for encouraging me years ago back in Paraguay to depart for this trip.

A special thanks goes to Enrico, Daniele, Barbara, Anna and Enrico, for their support and for the great times spent together over these last years.

Finally, I would like to express my deepest gratitude to the most important person in my life, my beloved husband Simone, foremost the greatest addition along this journey, who has been a constant source of strength and inspiration, always by my side with a big smile. For sure I could not have succeed without his love and support. I cannot thank you enough for your constant encouragement and distractions. This journey has definitively been much easier together.

# Abstract

Headwaters in Alpine regions represent the large majority of streams in natural or nearly natural conditions, which provide essential ecosystem services. These catchments are particularly sensitive to temperature changes and may suffer significant changes because of climate variations. Thus, identifying the main mechanisms controlling streamflow generation and understanding the nature and variability of streamflow in Alpine streams, represent a very important contribution towards a better understanding of these complex systems.

Among the multiplicity of streamflow sources (e.g., rain, snow-melt, ice-melt and groundwater), in particular snow and ice-melt play a fundamental role on the hydrological cycle of Alpine catchments and strongly affect streamflow regime. Despite several research efforts over the past decades focused on understanding the complex dynamics of the hydrological processes that characterize these environments, there is still much to disclose. Hence, the interpretation of streamflow sources can become very difficult with water discharge as the sole observed variable. The previous calls for the use of alternative data sources and methods for data analysis and visualization.

This doctoral thesis aimed to contribute with new insights into the multifaceted aspects of streamflow generation in Alpine river catchments, exploring the different roles played by hydrological and geochemical information and the use of several techniques, such us tracer-based analysis, continuous wavelet transform, wavelet coherence, cross-correlation and Hovmöller diagrams; in order to investigate the mechanisms controlling streamflow generation on real case studies at different temporal scales. Hence, the present thesis is based on four main elements.

In the first part of this work we show how tracer data (i.e., electrical conductivity and stable isotopes of stream water) can be used to separate the contribution of pre-event and event waters applying a two-component mixing analysis on four single rainfall events identified in the Vermigliana catchment ($78.94 km^2$), North-Eastern Italian Alps. The separation of streamflow into two different components allowed us to improve the conceptual model of the catchment introducing constraints that are impossible to envision counting only on streamflow measurements. Moreover, we show that the relative contribution of event water with respect to pre-event water does not change only according to the magnitude of the precipitation event and on the variations in air temperature, but it also depends on the presence and thickness of the snowpack present during the event.

Second, we explored the correlation between stream water electrical conduc-

tivity (EC) and water discharge (Q) using continuous records collected during two melting periods of the Vermigliana catchment. The analysis of the hysteresis relating EC and Q at the annual scale evidenced the limitations of the use of EC measurements as a proxy of Q in these type of catchments. In addition, the combined analysis of the correlation between both signals using wavelet coherence and cross-correlation, evidenced the nature of their relationship (i.e., out of phase) and the existence of relatively constant time lag between both signals. Wavelet coherence proved to be likewise useful to identify specific periods of significant changes in the dynamics controlling streamflow generation. Furthermore, the analysis of EC and Q diurnal cycles allowed us to obtain new insights related to snow-dynamics and were also used to estimate the daily contribution to streamflow from snow-melting processes. The previous contributions may support future research on the different transfer functions that characterize water and solute transport in snow and ice-melting dominated catchments.

Third, the need to understand how short and long-term climate variations may influence streamflow variability in Alpine environments lead us to the use of alternative techniques to analyse traditional long-term hydrological time series, i.e., precipitation (P), temperature (T) and streamflow (Q). We compared streamflow variability and explored the relationship between atmospheric forcing and streamflow of two case studies: Vermigliana and Sarca di Genova catchments ($77.52 km^2$), both located in the same region and presenting similar features, like the presence of glaciers in their upper part. Hovmöller diagrams and continuous wavelet transform were used to investigate daily and seasonal climate influences on streamflow variability, while wavelet coherence analysis was used to explore the periods on which two time series experienced oscillations at a similar frequency. Moreover, the use of these alternative techniques for data analysis and visualization, provided further insights into the hydrological response and sensitivity of the systems under study to climate changes, leading to the improvement of current conceptual models and allowing us to define a suitable framework for modelling applications, as foreseen within the following research element.

The fourth element of this thesis, includes the application of an existing stochastic analytical modelling framework to the two case studies mentioned above, with the aim of characterizing and predicting streamflow distribution in these glacierized catchments. Results evidence that the size of glacier coverage on these type of catchments represents a very important feature of the system that needs to be taken account for, in fact, glaciers store a large amount of water as snow and ice, which can be rapidly released affecting significantly the magnitude and distribution of streamflow.

Overall, the results obtained during this thesis provide new insights into the multi-faceted aspects of streamflow generation in snow and glacier dominated catchments, where geochemical data as an addition to hydrological information on real case studies played an essential role. Likewise, the application of different techniques for data analysis and visualization considering a variability of temporal scales provided valuable information about the sensitivity of Alpine systems to climate changes, which may serve as a support for water resources management in these important environments. Moreover, testing the applicability of an stochastic analytical approach to this complex context allowed us to understand

the influence of the presence and size of glaciers on streamflow variability. Thus, the outcomes of this study may contribute to the improvement and development of new modelling structures.

**Keywords:** Alpine catchment, diurnal streamflow cycles, electrical conductivity, glacier, hydrological modelling, hysteresis, Sarca di Genova, stable isotopes, two-component mixing analysis, Vermigliana, wavelet analysis.

# Contents

# List of Figures

# List of Tables

*Chapter* 1

# Introduction

Headwaters represent the large majority of streams in natural or nearly natural conditions providing important ecosystem services, including clean drinking water, habitat for aquatic life, rapid processing and uptake of nutrients (Elmore and Kaushal, 2008). In Alpine regions, headwaters are very sensitive to temperature changes due to the dominance of snow and glacier melting in streamflow generation (Penna et al., 2014; Engel et al., 2015). These catchments are therefore expected to be significantly affected by the rise of temperature due to climate change (Barnett et al., 2005). Moreover, the sharp elevation gradients as well as the heterogeneous geology and land use, makes them a challenging benchmark for hydrological modelling (Weekes et al., 2014).

From a functioning point of view, Alpine headwaters are dominated by water storage as snow and ice, which induces both dial variations of streamflow during the melting season, as well as significant seasonal variations with glaciers playing a relevant role in regulating inter-annual variability (Kuhn and Batlogg, 1998; Stewart, 2009). At the origin of these complex dynamics are a multiplicity of streamflow sources, such as rain, snow-melt, glacier-melt and groundwater, operating on scales ranging from a few minutes (in case of intense rainstorm events) to seasons or longer time scales for groundwater contribution. Therefore, quantifying these sources, including their seasonal variability, becomes essential to characterize catchment's hydrological functioning and introduce effective constraints into the conceptual model, which are essential to reduce epistemic uncertainty (see e.g., Theakstone, 1988; Unnikrishna et al., 2002; Lee et al., 2010; Cable et al., 2011; Chiogna et al., 2014).

The high complexity characterizing Alpine catchments calls for alternative data sources, as seen from earlier studies which have suggested supplementing traditional hydrological observations with environmental tracers data (e.g., Behrens et al. (1971),Collins (1979), Gurnell and Fenn (1985), Christophersen et al. (1990), Laudon and Slaymaker (1997), Brown et al. (2006)). Among natural tracers, water stable isotopes (i.e., $\delta D$ and $\delta^{18}O$) and electrical conductivity (EC) have shown a great potential to separate the sources of streamflow in Alpine and snow-melt dominated catchments (Leibundgut et al., 2011).

High resolution sampling of tracer data may thus represent a fundamental step

to gain a comprehensive view of the relevant hydrological processes occurring in these catchments (see e.g., Evans and Davies, 1998; Dzikowski and Jobard, 2012; Ohlanders et al., 2013). Although data collection can be a challenging task in Alpine catchments due to the strong gradients and scarce accessibility of some areas (Simoni et al., 2011), in the last decade, as more hydrological and geochemical data became available a wealth of studies using natural tracers have investigated hydrological functioning of mountain catchments (Tetzlaff et al., 2007), to disentangle the contribution of multiple sources of streamflow and identify their time variability (Yuan and Miyamoto, 2008), estimate catchment mean transit times (Speed et al., 2011), predict streamflow (Weijs et al., 2013), to characterize spatial and seasonal patterns (Chiogna et al., 2014), and to estimate streamflow sources through hydrograph separation techniques (Liu et al., 2004; Williams et al., 2009; Suecker et al., 2000; Huth et al., 2004; Penna et al., 2014).

A renowned method to identify source components of streamflow is the tracer-based hydrograph separation, which dates back to the end of 1960s (see Pinder and Jones, 1969; Crouzet et al., 1970; Dincer et al., 1970; Martinec et al., 1974; Martinec, 1975) and brought along significant progress into catchment hydrology at the time. This method assumes that the stormflow hydrograph is made of two components, i.e., event (e.g., rain or snow) and pre-event water (e.g., groundwater), which can be separated based by applying mass balance (Sklash and Farvolden, 1979). Further developments that go beyond two components, accounting for other sources (e.g., hillslope, riparian zone) can also be found (see e.g., Suecker et al., 2000; McGlynn and McDonnell, 2003; Uhlenbrook and Hoeg, 2003) and are likewise based on a mass balance approach as the classic version. Studies comparing the use of two or more components on hydrograph separation have shown similar results (see Wenninger et al., 2004; Carey and Quinton, 2005; Muñoz-Villers and McDonnell, 2012). For an extensive review on the method the reader may refer to Buttle (1994) and Klaus and McDonnell (2013).

A widely used technique for performing hydrograph separation is the end-member mixing analysis (EMMA) proposed by Hooper et al. (1990) and Christophersen and Hooper (1992), based on the linearity of mixing, the conservative behaviour of tracers and the time invariance of end-member (i.e., pre-event and event water) compositions (Hooper, 2001, 2003). The applications of EMMA include very few studies performing high-resolution sampling during specific storm events in Alpine catchments (see e.g., Engel et al., 2015; Penna et al., 2015). The former suggests that our current knowledge about the complex hydrological dynamics of Alpine catchments can still be enriched by additional field scale experiments, therefore studies set to investigate streamflow generation in these catchments during single storm events based on two-component mixing analysis may represent a valuable contribution to improve the conceptual models of these complex systems.

Moreover, with the current advancements in technology, field measurements of stream water EC can now be obtained with very high resolution using data loggers, which allow us to further investigate the relationship or link between EC and streamflow (Q) measurements, already evidenced in previous studies (see e.g., Collins, 1979; Gurnell and Fenn, 1985; Evans and Davies, 1998; Dzikowski and Jobard, 2012), which have also shown how this relationship can be quite com-

plex and sometimes characterized by the presence of lags and hysteresis. While there has been a recent increase of hydrological studies suggesting the use of EC measurements for different purposes, e.g., to quantify streamflow; to understand geochemical processes; or to differentiate among different water sources (Weijs et al., 2013; Hayashi et al., 2012; Penna et al., 2014; Engel et al., 2015; Penna et al., 2015). To our knowledge, new studies focused mainly on studying the nature and variability of the relation between EC and Q using continuous data from Alpine study cases have not yet been discussed.

Exploring the nature and variability of the relationship between EC and Q using continuous data, may play a fundamental role in the study of the complex hydrological processes controlling streamflow generation in Alpine catchments, which can additionally lead to a more rigorous application of the EC-Q relationship for various hydrological and geochemical purposes. An interesting tool to disentangle periods of variations between two time series (i.e., EC and Q), that can also allow us to identify their change of strength in time is wavelet analysis (Torrence and Compo, 1998), a technique widely applied in geophysics and hydrology (see e.g., Kumar and Foufoula-Georgiou, 1993; Foufoula-Georgiou and Kumar, 1994; Venugopal and Foufoula-Georgiou, 1996; Saco and Kumar, 2000; Gaucherel, 2002; Coulibaly and Burn, 2004; Grinsted et al., 2004; Zolezzi et al., 2009; Carey et al., 2013), which has proved to be very effective in the analysis of oscillating transient signals. More precisely, wavelet coherence (Torrence and Compo, 1998; Grinsted et al., 2004) may be particularly useful to study the correlation between the two signals at the level of the single modes of variability. In addition, quantitative analysis of the relationship between EC and Q to estimate the time lag or delay between both series can be performed with a cross-correlation analysis (see e.g., Gurnell and Fenn, 1985).

Another interesting feature linking EC and Q are the diurnal and inverse fluctuations on both signals, as it has been observed on some pro-glacial systems (see Collins, 1979; Gurnell and Fenn, 1985). Natural diurnal fluctuations on streamflow and likewise on electrical conductivity, in catchments fed by snow and glacier-melt, are an important characteristic of these complex systems and can therefore be used to study the processes controlling streamflow generation. There have been a few studies focusing on the analysis of diurnal fluctuations on streamflow (see e.g., Caine, 1992; Lundquist and Cayan, 2002; Lundquist et al., 2005; Lundquist and Dettinger, 2005; Mutzner et al., 2015) and electrical conductivity (Hayashi et al., 2012) in Alpine catchments. However, there are currently no studies, that we are aware of, suggesting a combined analysis of both EC and Q diurnal cycles. We believe that learning about similarities or differences between EC and Q diurnal fluctuations may not only reveal interesting features on catchment functioning, but may also represent a step forward towards potential uses or applications of continuous EC measurements.

Furthermore, traditional long-term time series (i.e., precipitation, temperature and streamflow) can also provide valuable information which can be used to study streamflow variability. The relationship between precipitation (P) and streamflow has been explored for decades using long-term time series, leading to significant applications in hydrology which are currently used for streamflow prediction. Current studies at the catchment scale concentrated on the relationship P-Q and the

link between storage and discharge to define a joint concept for catchment response (Kirchner, 2009; Ali et al., 2011; Peters and Aulenbach, 2011; Shook and Pomeroy, 2011). However, Alpine catchments are very sensitive to temperature (T) changes, which drive the main mechanisms controlling streamflow generation, i.e., melting and snow accumulation (see e.g., Kuhn and Batlogg, 1998; Barnett et al., 2005; Stewart, 2009; DeBeer et al., 2010; Tobin et al., 2013; Penna et al., 2014; Engel et al., 2015); which highlights the importance to explore likewise the nature of variability of the relationship T-Q. The identification of patterns and scales of variability over long-term hydrological time series and a more in-depth analysis of the relationship between atmospheric forcing and streamflow variability, can have significant implications in catchment hydrology, that may allow us to improve existing conceptual models or to define a suitable framework for future model applications.

In addition, the need to explore alternative methods of data analysis and visualization that improve our understanding on catchment functioning (Carey et al., 2013), which can be particularly useful in complex environments like Alpine regions, has lead to the use of alternative techniques for the analysis of hydrological time series, among which we can mention: (i) Hovmöller diagrams (Hovmöller, 1949), commonly used for plotting meteorological data, although they have also been used to plot the time evolution of vertical profiles of scalar quantities (Marengo et al., 2011); and (ii) wavelet analysis (see e.g., Torrence and Compo, 1998; Kumar and Foufoula-Georgiou, 1993; Foufoula-Georgiou and Kumar, 1994; Venugopal and Foufoula-Georgiou, 1996; Saco and Kumar, 2000; Gaucherel, 2002; Coulibaly and Burn, 2004; Grinsted et al., 2004; Zolezzi et al., 2009; Carey et al., 2013), on which wavelet coherence becomes central to study the correlation between P-Q and T-Q at different temporal scales. Moreover, catchment inter-comparison implementing novel methods for data analysis and visualization can meaningfully contribute to study the nature of streamflow variability and its consequent association to climate patterns, thus providing further insights into the hydrological response or the sensitivity of Alpine systems to climate changes, constituting an important tool for climate change assessment.

Besides a comprehensive knowledge on streamflow variability in Alpine rivers, as the result of many intertwined ecohydrological and climate processes occurring at the catchment scale (Ceola et al., 2010), another central problem addressed in hydrology comprises the adequate characterization and prediction of this variability (see e.g., Chow et al., 1964; Brutsaert, 2005), which may have significant scientific and social implications. Fluctuations on streamflow can be described by the probability distribution function (pdf) of daily water discharge or the related flow duration curve (see e.g., Searcy, 1959; Moore, 1985; Sharma et al., 1997; Doyle et al., 2005; Castellarin et al., 2007; Botter et al., 2007a,b,c, 2008, 2009).

A stochastic analytical framework recently proposed by Botter et al. (2009), as an extension from pioneer works (Rodriguez-Iturbe et al., 1999; Rodríguez-Iturbe and Porporato, 2005), incorporates the effect of non-linear recessions on streamflow regimes. Applications of this model have shown its capability to reproduce the main features of observed streamflow statistics on different environments (e.g., Ceola et al., 2010; Doulatyari et al., 2014, 2015). Moreover, streamflow dynamics in Alpine catchments can be strongly dominated by snow and ice-melting dur-

ing the summer while by snow accumulation during winter, which may cause a temporal disconnection of one part of the catchment from the active streamflow network (DeBeer et al., 2010; Tobin et al., 2013). The are currently very few analytic descriptions of snow-dominated streamflow dynamics (Allamano et al., 2009; Molini et al., 2011), the latest was proposed by Schaefli et al. (2013) as an extension of the work by Botter et al. (2007a,b,c, 2008, 2009), describing winter streamflow pdf based on a non-responsive part of the catchment during winter.

Catchment inter-comparison throughout the application of streamflow probability distribution models may provide further insights on the characterization and prediction of streamflow variability in hydrological complex contexts like in Alpine regions; while assessing the applicability of these models to this context may improve conceptual and analytical frameworks, thus contributing to water resources management on such important environments.

In this doctoral thesis, we aim at contributing with new analyses to broaden our understanding of the multi-faceted aspects of streamflow generation in Alpine region catchments, thus we explore throughout each chapter, the different roles played by hydrological and geochemical information to investigate the mechanisms controlling streamflow generation on real case studies and applying several methods. The specific objectives of this thesis are:

i) to show how geochemical and hydrological data can be combined to investigate streamflow generation at the scale of single precipitation events;

ii) to explore the nature and variability of the relationship between electrical conductivity and streamflow at the seasonal scale applying different data analysis techniques (i.e., wavelet analysis, cross-correlation and analysis of diurnal cycles);

iii) to explore the variability of the relationship between atmospheric forcing and streamflow at long-term scale applying alternative methods for data analysis and visualization and comparing different case studies within the Alpine region;

iv) to apply an existing stochastic framework to characterize and predict streamflow variability on two Alpine catchments characterized by the presence of glaciers.

Thus, the present thesis is organized in four research elements, which can be summarized as follows:

**Chapter 2 (Tracer-based analysis):** tracer data is used to separate the contribution of event and pre-event water in the Vermigliana catchment ($78.9 km^2$), North-Eastern Italian Alps. Two-component mixing analysis is applied to separate old (i.e., pre-event) from new (i.e., event) water contributions during four single events and also at the annual scale. The specific objectives of this chapter are: i) to quantify the relative contribution of pre-event and event water to streamflow generation during single precipitation events using EC and stable isotope data and to analyse differences emerging in streamflow separation when using different tracers; ii) to explore streamflow-EC relationships at the temporal scale

of single rainfall events; iii) to further comprehend the influence of the presence and thickness of snowpack on the catchment's response during these events.

**Chapter 3 (The role of electrical conductivity):** electrical conductivity and streamflow were measured continuously during two melting periods (June-November of 2012-2013) in the Vermigliana catchment ($78.9km^2$) and the analyses performed aimed to: (i) to identify limitations on the use of EC data as a proxy of Q in Alpine catchments; ii) to develop a methodology to fully explore the correlation between EC and Q and its use in the identification of timing of the main streamflow sources; iii) investigate the use of diurnal cycles of EC and Q to determine the daily contribution from snow-melting to streamflow.

**Chapter 4 (Temporal variability of long-term hydrological time series):** long-term hydrological time series (i.e., precipitation, temperature and streamflow) are used to study the nature of variability in two Alpine catchments located in the North-Eastern Italian Alps: Vermigliana ($78.9km^2$) and Sarca di Genova ($77.52km^2$); with the following specific objectives: (i) to explore patterns and scales of variability of the hydrological time series of two case studies within the Alpine region using two different tools (i.e., Hovmöller diagrams and continuous wavelet transform); (ii) to further investigate the link between the variability of P-Q and T-Q using the wavelet coherence.

**Chapter 5 (Characterization of streamflow):** daily records of observed precipitation, temperature and streamflow from the period 1996-2014 are used to predict streamflow pdf, applying an existent stochastic analytical framework (Botter et al., 2009) to the two case studies analysed on the previous Chapter, Vermigliana and Sarca di Genova, both characterized by the presence of glaciers. The specific objectives are:(i) to test the model's ability to predict streamflow distribution on glacierized catchments on a seasonal basis and; (ii) to apply the model extension proposed by Schaefli et al. (2013) in order to predict winter streamflow pdf and further investigate the size of the non contributing part of the catchment during winter.

*Chapter* 2

# Tracer-based analysis of single events

## 2.1 Introduction

Streamflow variability can be influenced by a multiplicity of factors such as climatic conditions, rainfall intensity, morphology, vegetation, soil characteristics and in the case of Alpine catchments, additional effects due to the snow cover. Quantifying the different sources contributing to streamflow generation, e.g., rain, snow-melt, glacier-melt and groundwater, including their temporal variability, constitutes a fundamental step towards a better characterization of the catchment's hydrological functioning, which may allow us to introduce new constraints into the conceptual model, which are crucial to reduce epistemic uncertainty (see e.g., Theakstone 1988, Unnikrishna et al. 2002, Lee et al. 2010, Cable et al. 2011).

The complexity of Alpine environments has lead former studies to explore alternative data sources, suggesting to complement traditional hydrological observations with environmental tracers data (e.g., Behrens et al., 1971; Collins, 1979; Gurnell and Fenn, 1985; Brown et al., 2006). A widely applied method particularly useful to separate streamflow source components is the tracer-based hydrograph separation (Pinder and Jones, 1969)(Crouzet et al., 1970; Dincer et al., 1970; Martinec et al., 1974; Martinec, 1975; Sklash and Farvolden, 1979; Laudon and Slaymaker, 1997; Ladouche et al., 2001; Laudon et al., 2002; Uhlenbrook and Hoeg, 2003; Soulsby et al., 2003; Muir et al., 2011; Maurya et al., 2011) and the latest applications of this method rely on the End Member Mixing Analysis (EMMA) technique (Hooper et al., 1990; Christophersen and Hooper, 1992).

To apply such methods or techniques, high resolution sampling (in time) of tracer-based data in Alpine catchments becomes of fundamental importance in order to gain a comprehensive view of the relevant hydrological processes (e.g. Gurnell and Fenn, 1985; Evans and Davies, 1998; Dzikowski and Jobard, 2012; Ohlanders et al., 2013), for example, to characterize the catchment's response (Tetzlaff et al., 2007; Yuan and Miyamoto, 2008) or to identify the travel time distribution (Speed et al., 2011; Birkel et al., 2012; Botter et al., 2011; Chiogna et al., 2014).

Current studies based on tracer data that focused within the Alpine region

include the following applications: use of stable isotopes and electrical conductivity as tracers to identify runoff sources and their seasonal variability (Penna et al., 2014); characterization of spatial and seasonal patterns of the isotopic signature of surface waters, groundwater and rainfall (Chiogna et al., 2014); analysis of individual melt-induced runoff events applying EMMA analysis; study of the seasonal variability of streamflow sources by using hydrometric, isotopic, and electrical conductivity data together with two and three-component hydrograph separation and end-member mixing analysis (Penna et al., 2015).

Overall, our knowledge about the complex hydrological dynamics of Alpine catchments is still incomplete. The need of further knowledge on the origin of the different sources contributing to streamflow generation as well as on the variations of solute concentration of stream water during single rainfall events (Kirchner, 2003; Lischeid, 2008), evidence the importance of additional field scale experiments to improve our understanding of system functioning and to provide experimental evidence to support or falsify standard models based on the excess infiltration concept (Burt and McDonnell, 2015). Therefore, studies set to investigate streamflow generation in Alpine catchments during single rainfall events, represent a valuable contribution to improve the conceptual models of these complex systems.

In this chapter, we show how tracer data can be used to separate the contribution of new and old water in the Vermigliana catchment ($78.9 km^2$), North-Eastern Italian Alps. Thus, we apply a two-component mixing analysis to separate old (i.e., pre-event) from new (i.e., event) water contributions on four precipitation events, which have been carefully selected in order to understand the response of the catchment under different snow depth and snow cover conditions.

The specific objectives are: i) to quantify the relative contribution of old and new water to streamflow generation during single precipitation events using EC and stable isotope data and to analyse differences emerging in streamflow separation when using different tracers; ii) to explore streamflow-EC relationships at the temporal scale of single rainfall events; iii) to further comprehend the influence of the presence and thickness of snowpack on the catchment's response during these events.

## 2.2 The Vermigliana catchment

The Vermigliana creek is one of the main headwaters of the Noce, a tributary of the Adige river, the second longest river in Italy (Chiogna et al., 2015). It drains a catchment area of $78.94 km^2$ until the streamflow gauging station located at Vermiglio (see point P2 on figure 2.1). The catchment presents a very complex morphology, with elevations that range from 1165 m.a.s.l. to 3558 m.a.s.l. (figure 2.2). Vermigliana has two main tributaries, the Presanella and Presena creeks, which are fed by two glaciers bearing the same names, with peaks at 3558 m.a.s.l. and 3069 m.a.s.l. respectively. For further information on the catchment and glaciers the reader may refer to Chiogna et al. (2014) and Meteotrentino (2011).

The current climate shows the typical characteristics of Alpine regions, with cold winters (mean temperature of $-4.5\,°C$) and relatively warm summers (mean

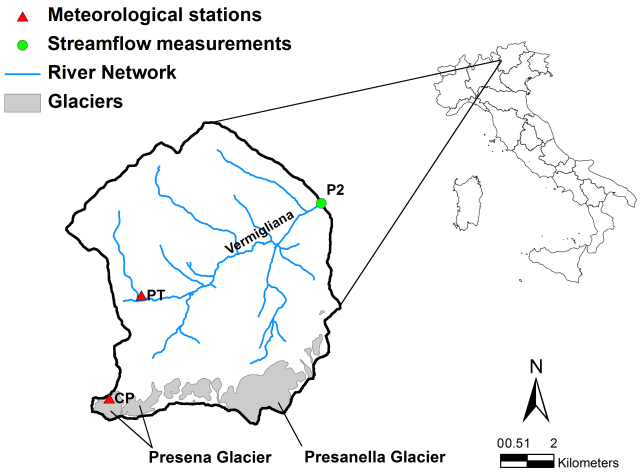


Figure 2.1: Map of the Vermigliana catchment and location of the monitoring stations. Grey polygons indicate glaciers (Presena and Presanella). Red triangles show the location of the two meteorological stations within the catchment: CP and PT. The green dot indicates the gauging station for the continuous monitoring of streamflow and electrical conductivity. The upper right inset shows the location of the catchment within the Italian territory.

temperature of $11.6\,°C$) and a mean annual air temperature of $3.7\,°C$. Annual precipitation averages to $1300\,mm$ and falls as snow from early November to April. Mean temperature and precipitation were estimated considering available records from the last twenty years at PT (Passo del Tonale) station (figure 2.1). Additional details on the main morphological and climatic characteristics of the catchment are listed in table 2.1. Land use information and morphological characteristics were obtained from the official $10\,m$ resolution Digital Terrain Model (DTM) of the Autonomous Province of Trento and can be observd on figure 2.2, while soil types were classified in the range from 1 to 4 from the most to the less permeable soils, according to the classification used in the SCS-CN model (McCuen et al., 1982).

## 2.3 Methods

### 2.3.1 Data collection

Precipitation and air temperature at hourly resolution and daily snow depth data were provided by Meteotrentino (http://www.meteotrentino.it) for the two meteorological stations located within the catchment, CP (Capanna Presena) and PT (Passo del Tonale). Water discharge records at hourly intervals from the gauging station of Vermiglio (point P2 in Figure 2.1) were provided by the Ufficio Dighe

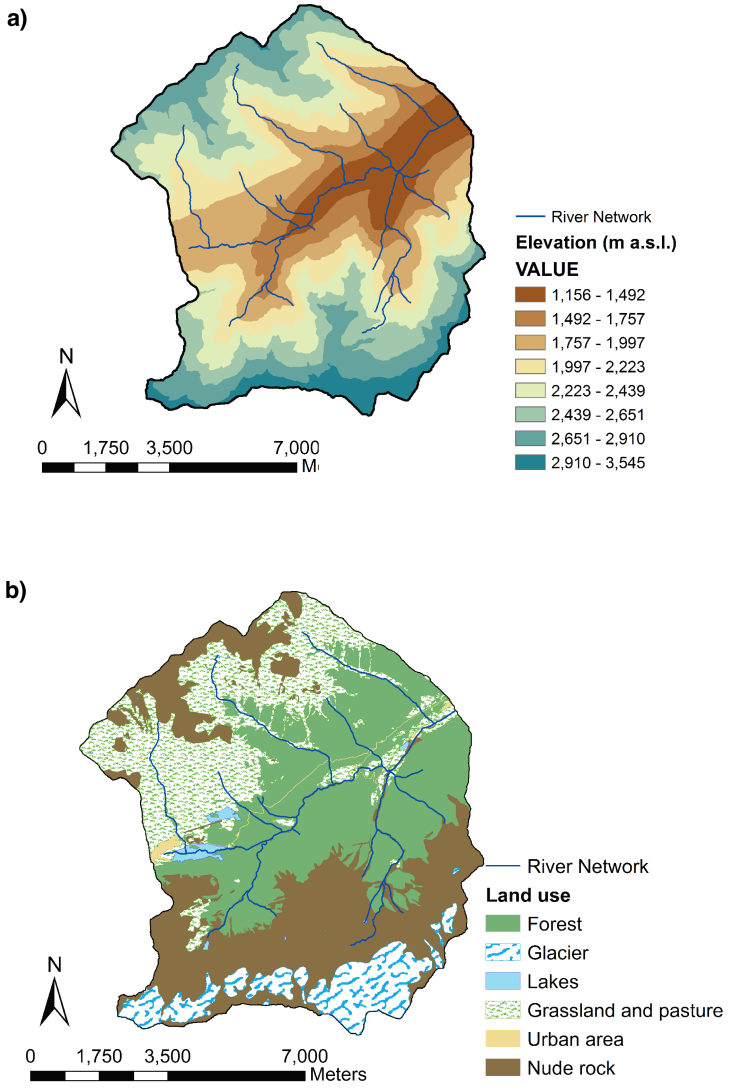


Figure 2.2: Vermigliana catchment maps: a) 10 $m$ DTM and; b) land use.

Table 2.1: Main geomorphological and climatic characteristics of the Vermigliana catchment.

| **Main characteristics** | | **Soil type** | **(%)** | **Land cover** | **(%)** |
|---|---|---|---|---|---|
| Drainage area ($km^2$) | 78.94 | 1 | 31.08 | Forest | 34.18 |
| River length until P2 ($km$) | 9.5 | 2 | 19.21 | Nude rock | 31.65 |
| Mean annual precipitation ($mm$) | 1300 | 3 | 2.49 | Grassland, pasture | 24.18 |
| Mean annual temperature ($^\circ C$) | 3.7 | 4 | 47.23 | Glacier | 8.55 |
| Mean summer streamflow ($m^3/s$) | 4.4 | | | Lakes | 0.79 |
| Mean winter streamflow ($m^3/s$)] | 0.94 | | | Urban area | 0.64 |
| Mean slope (%) | 1 | | | | |
| Min. elevation (m a.s.l.) | 1165 | | | | |
| Max. elevation (m a.s.l.) | 3558 | | | | |

of the Province of Trento (http://www.floods.it).

Tracer-based information instead were collected through experimental field work. For this purpose, an automatic Aqua TROLL 200 multi-parametric sensor (figure 2.3) was installed at point P2 in order to record continuous electrical conductivity measurements of stream water with instrumental precision of 0.1 $\mu S/cm$. Hence, electrical conductivity measurements were recorded at hourly intervals on the following periods: September 2011, April-November 2012 and May-November 2013. Table 2.2 reports further details on the type of data collected at each monitoring point.

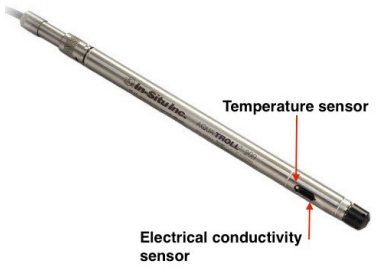


Figure 2.3: Aqua TROLL 200 data logger by In-Situ Inc, used for recording stream water temperature and electrical conductivity point P2.

The Aqua TROLL 200's primary conductivity measurement is the so-called actual conductivity, which is the ability of an aqueous solution to carry an electric current and is dependent on temperature. In order to observe changes on stream water EC independent of any changes in temperature, actual conductivity values measured by the instrument are then referred to a standard reference temperature of $20^\circ C$, and then expressed as specific conductivity (SC) using the following

Table 2.2: Observational data collected at the monitoring points within the Vermigliana catchment.

| Monitoring point | Name | Lat | Long | Altitude m a.s.l. | Type of data |
|---|---|---|---|---|---|
| PT | Passo del Tonale | 46.26251044 | 10.59682317 | 1875 | Precipitation, air temperature, snow depth |
| CP | Capanna Presena | 46.22799303 | 10.58013033 | 2730 | Precipitation, air temperature, snow depth |
| P2 | Vermiglio | 46.2904248 | 10.684067 | 1165 | Surface water monitoring: streamflow, temperature, electrical conductivity, stable isotopes in stream water. |

general equation (see Standard Methods 2510B **?**):

$$SC = \frac{AC}{1 + 0.0191(T - T_{ref})} \tag{2.1}$$

where $AC$ and $T$ are stream water actual conductivity and temperature, respectively, measured by the instrument at each interval. $T_{ref}$ corresponds to the reference temperature.

Moreover, an ISCO 6712 automatic sampler was also installed at monitoring point P2, to collect stream water samples during significant hydrological events (see figure2.4) for isotope analyses of $\delta D$ and $\delta^{18}O$. Thus, a 5-day long sampling campaign was conducted during 17-21 September of 2011, on which the ISCO 6712 was programmed to collect samples at time intervals of 4 hours. Water samples were stored automatically by the sampler in glass vials of 300 $ml$ and covered for transport with Butyl-Polytetrafluorethylene (PTFE) caps. Altogether, 23 samples were collected. After the event, the bottles were removed from the automatic sampler, sealed and stored in the dark to avoid potential contamination from external agents and isotopic fractionation induced by evaporation and gas-diffusion (Bolto et al., 2012). Finally, the samples were dispatched to the isotope laboratory of the Edmund Mach Foundation, San Michele, Trento (Italy) for stable isotopes analysis (for further details please refer to Chiogna et al., 2014).

### 2.3.2 Identification of single events

High resolution data collected during precipitation events provide valuable insights on system functioning characteristics, in particular for fast responses which cannot be assessed with daily data. Thus, we identified four significant hydrological events that occurred in the Vermigliana catchment during the observation period. The data collected for this purpose were useful to distinguish two different type of responses to precipitation input: (i) an event with rapid runoff generation in late summer (Event 1) and, (ii) events with a slow yet enhanced runoff generation observed in mid spring (Event 2) and late autumn (Events 3 and 4).

Figure 2.4: ISCO 6712 installed at point P2 for stream water sampling during a significant hydrological event.

Table 2.3: Identification of significant hydrological events

| Event | Date | Description | Tracer |
|---|---|---|---|
| 1 | 17-21 September 2011 | Regular flood | $\delta D$, $\delta^{18}O$ and EC |
| 2 | 29 April to 3 May 2012 | RoS | EC |
| 3 | 3-8 November 2012 | RoS | EC |
| 4 | 21-26 October 2013 | RoS | EC |

The second type (i.e., Events 2, 3 and 4) were identified as rain on snow (RoS) events and are known to occur often in Alpine catchments with strong elevation gradients (Merz and Blöschl, 2003; Singh et al., 1997; Garvelmann et al., 2015). An event is typically classified as RoS when it occurs in combination to a maximum daily temperature greater than $0°C$ and a reduction of the snowpack (McCabe et al., 2007; Surfleet and Tullos, 2013). At the early stages of these events rain water is stored within the snowpack, but later runoff in excess to rainfall is produced by the release of melted snow and water initially stored within the snowpack, often resulting in severe floods. Additional details on the events are listed on table 2.3.

### 2.3.3 Two-component mixing analysis

The contributions from new and old water are separated on each event by applying an End Member-Mixing Analysis (EMMA) using streamflow and tracer concentration data. This technique imposes mass conservation after assuming that the observed tracer concentration depends on mixing of new and old waters, called end-members, which tracer concentration is known (Burns et al., 2001; Christophersen et al., 1990; Christophersen and Hooper, 1992).

Under stationary conditions mass balance of water and solute read as follows (Sklash and Farvolden, 1979):

$$Q_t = Q_p + Q_e \tag{2.2}$$

and

$$C_t Q_t = C_p Q_p + C_e Q_e \tag{2.3}$$

respectively. In equations (2.2) and (2.3) $Q$ is streamflow $[L^3/T]$, $C$ $[M/L^3]$ is tracer concentration and subscripts $t$, $p$ and $e$ refer to the total streamflow, pre-event and event components, respectively.

In order to determine $Q_p$ and $Q_e$ with a two-component mixing analysis, the following additional assumptions are needed: (i) streamflow can be approximated as the mix of two components, (ii) tracer concentration of the event and pre-event components should differ significantly, (iii) the tracer concentration of each component is assumed to be known and, (iv) surface storage contributes minimally to streamflow (Sklash and Farvolden, 1979).

Therefore, the relative contribution of event water, $\alpha_{C,i}$, to streamflow can be obtained at each time step $i$ by combining equations (2.2) and (2.3) as follows:

$$\alpha_{C,i} = \frac{Q_e}{Q_t} = \frac{C_{t,i} - C_p}{C_e - C_p} \qquad i = 1, ..., N \tag{2.4}$$

where event and pre-event components are assumed at constant concentration, $C_e$ and $C_p$, respectively, and $C_{t,i}$, $i = 1, ..., N$, is the recorded time series of the stream water concentration with $N$ being the length of the time series. Likewise, the pre-event water contribution $\beta_{C,i}$ can also be determined from equation (2.2) and reads as:

$$\beta_{Ci} = \frac{Q_p}{Q_t} = 1 - \alpha_{C,i} \qquad i = 1, ..., N \tag{2.5}$$

**Comparison between different tracers**

For the case of Event 1, we compare the use of three different tracers (i.e., $\delta D$, $\delta^{18}O$ and EC). In order to reduce the adverse effect of possible variations of the isotopic signature of rainfall, within the same event and in consecutive rainfall events (Uhlenbrook and Hoeg, 2003), we consider the following objective function, which assigns the same weight to the information carried by each one of the three tracers:

$$s = \sqrt{\sum_{i=1}^{N} \left(\alpha_{EC,i} - \alpha_{\delta D,i}\right)^2} + \sqrt{\sum_{i=1}^{N} \left(\alpha_{EC,i} - \alpha_{\delta^{18}O,i}\right)^2} + \sqrt{\sum_{i=1}^{N} \left(\alpha_{\delta^{18}O,i} - \alpha_{\delta D,i}\right)^2} \tag{2.6}$$

where $\alpha_{EC}$, $\alpha_{\delta^{18}O}$ and $\alpha_{\delta D}$ are the fractions of event water contribution, with respect to the total water discharge, computed by using EC, $\delta^{18}O$ and $\delta D$ as tracer concentration, respectively. Equation (2.6) quantifies the differences of the relative contribution of event water inferred by the three tracers using equation (2.4). Similar approaches have been used in Genereux (1998); Burns et al. (2001); Laudon et al. (2002); Uhlenbrook and Hoeg (2003).

## 2.4 Results and discussions

### 2.4.1 Event characterization

A detailed description of the events defined on section 2.3.2 is here presented, facing both hydrological and geochemical information, followed by a brief discussion of the main features characterizing streamflow generation on each case.

#### Event 1: Regular flood event - September 2011

Figure 2.5a depicts a regular flood event occurred in September of 2011. A total runoff of 15 $mm$ was generated between September 17 at 17:00 and September 19 at 9:00. Total precipitation during the entire event amounts to 86 $mm$ at CP and 101 $mm$ at PT, while mean air temperature values are of 2.2°$C$ at CP and 6.9°$C$ at PT (figures 2.5b and 2.5c). Effective precipitation (i.e., rainfall responsible for runoff generation) can be divided into three main blocks which are created in sequence: the first starting from 17:00 of September 17 to 4:00 of September 18, the second lasts until 18:00 of September 18 and the third, until 8:00 of September 19.

The first block of precipitation causes a mild rise on streamflow, which mimics, with some smoothing and delay reflecting the catchment travel time distribution, the temporal distribution of precipitation, observed at both meteorological stations (Figures 2.5b, and 2.5c). After a short pause due to the decrease of precipitation intensity, streamflow increases again, faster this time (from 6:00 of September 18), when the second block of precipitation, more intense than the first, hits the catchment. Water discharge reaches a peak (near $10m^3/s$) and then declines slightly as precipitation intensity starts decreases between 17:00 and 18:00 of September 18. The third block of precipitation causes water discharge to climb again reaching out the maximum observed value during the entire event equal to $14.6m^3/s$, at 23:00 of September 18, with a delay of two hours from the maximum precipitation intensity of this block. While precipitation ceases, air temperature decreases sharply and streamflow declines to pre-event values. The classical recession curve is interrupted by a very small rise due to a smaller precipitation event that occurred on September 19 from 11:00 to 17:00. This fourth block was left outside the analysis given that the initial and most significant contribution comes from the first three blocks previously described. Notice that due to technical problems with the sensor, air temperature records are not available at PT from September 19 at 11:00 to September 20 at 17:00.

A significant reduction is observed on EC values, i.e., from $77\mu S/cm$ to $27\mu S/cm$, along the entire event (Figure 2.5a), although later EC rises again up to about $60\mu S/cm$. In addition, both $\delta D$ and $\delta^{18}O$ concentrations in stream water mirror the increase on streamflow, reaching the maximum, $-72.6$‰ and $-10.2$‰ respectively, and declining to pre-event values about two days after the end of the third block of precipitation. The previous suggests that the pre-event water component (i.e., composition of stream water prior to the event), marked by larger EC values and less depleted isotopic signatures with respect to the new water component, mixes with event water during the rising limb of the event.

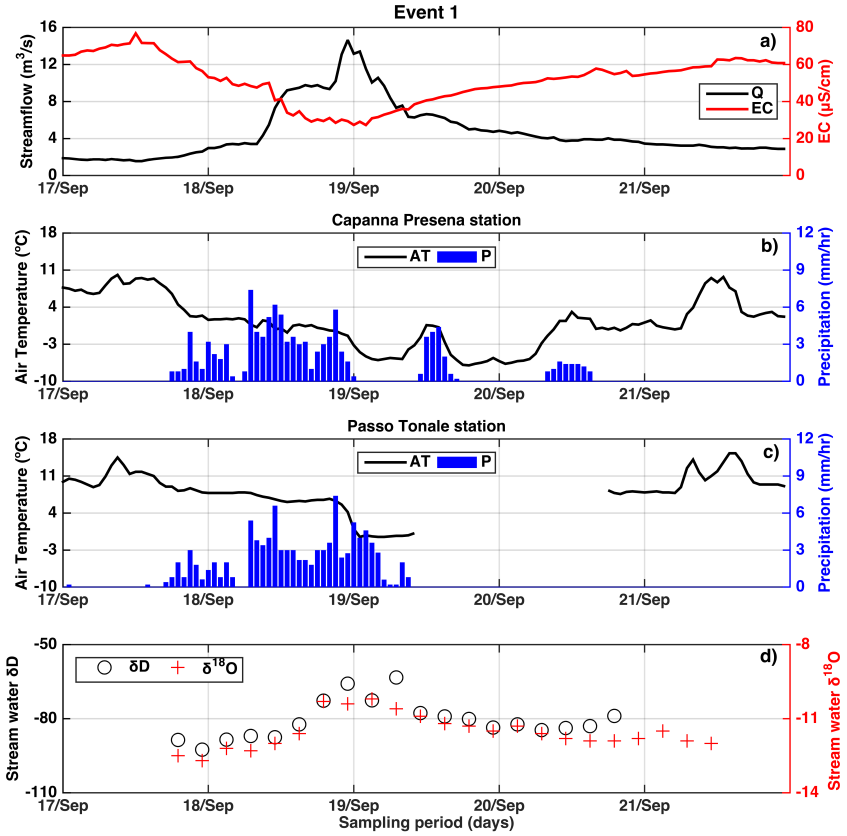


Figure 2.5: Event 1. Regular flood event during 17-21 September, 2011; a) streamflow (black line) and electrical conductivity (red line) data recorded at monitoring point P2; b) and c) air temperature (black line) and precipitation (blue bars) registered at meteorological stations of Capanna Presena and Passo del Tonale, respectively (there are no available records of snow depth during this period); d) stable isotope values for $\delta D$ (black circles) and $\delta^{18}O$ (red plus sign) at monitoring point P2, where stream water samples were taken automatically at 4-hour intervals.

### Event 2: Rain on snow event - April-May 2012

Event 2 corresponds to a RoS event identified on mid spring, during April-May of 2012 (figure 2.6), generating a total runoff of $4.2\,mm$ between April 30 at 14:00 and May 2 at 22:00. Total precipitation during the entire event amounted to $62\,mm$ at CP and $31\,mm$ at PT, while mean air temperature values were of $-4.3°C$ at CP and $6°C$ at PT (figures 2.6b and 2.6c). Effective precipitation was

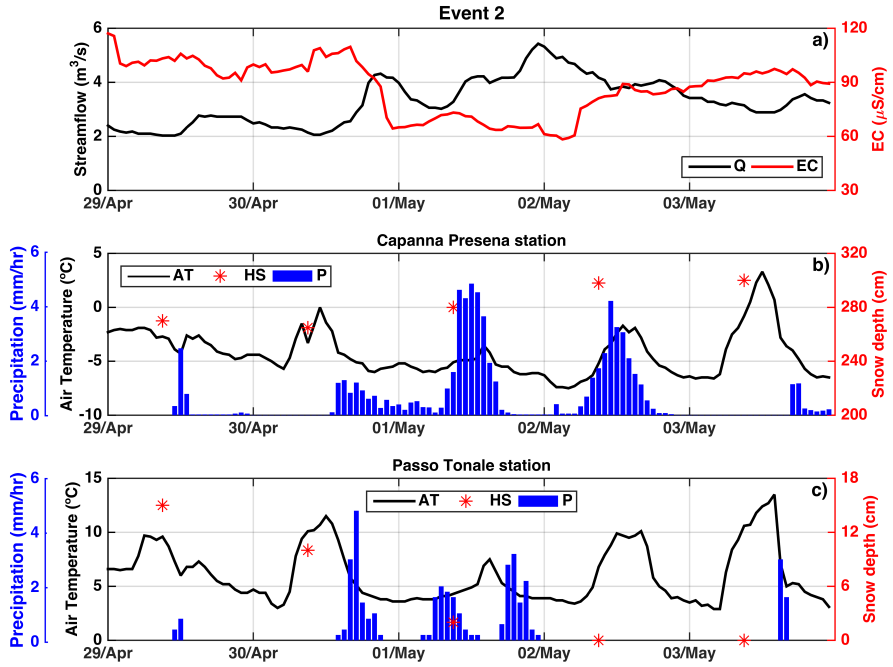


Figure 2.6: Event 2. Rain on snow from 29 April to 3 May, 2012; a) streamflow (black line) and electrical conductivity (red line) data recorded at monitoring point P2; b) and c) air temperature (black line), precipitation (blue bars) and snow depth (red stars) registered at meteorological stations of Capanna Presena and Passo del Tonale, respectively.

divided into three main blocks: the first goes from April 30 at 14:00 to May 1 at 5:00, resulting on $10mm$ at CP and $12mm$ at PT; the second, from May 1 at 6:00 until 17:00, contributing with $29mm$ and $9mm$ at CP and PT respectively; the last block goes until May 1 at 23:00 and contributes with $10mm$ at PT. A last block appears on May 2 and is observed only at CP with a total precipitation of $23mm$. Notice this last block does not cause a peak on streamflow, instead interrupts the recession curve caused by the previous event.

The first block of precipitation causes an initial increase on water discharge that goes from $2.29m^3/s$ to $4.32m^3/s$ on April 30, which after decreases again towards initial values due to the reduction of precipitation intensity. Water discharge slightly increases again when the second block of precipitation hits the catchment. The recession is interrupted by the third block of precipitation, which leads to the maximum peak on water discharge equal to $5.43m^3/s$ at 23:00 of May 1 (see figure 2.6a), with a delay of 4 hours from the maximum precipitation intensity of this block. While precipitation ceases, air temperature decreases sharply and streamflow gradually declines. The classical recession curve is once

more interrupted by a fourth block of precipitation, consequently baseflow values show a slight increase with respect to initial values. Right before the event, air temperature shows a significant increase on April 30, from $-5.7°C$ to $0.7°C$ at CP and from $3.6°C$ to $11.5°C$ at PT (figures 2.6b and 2.6c). This sudden increase on air temperature leads to a reduction on the snow cover, $5cm$ at CP and $13cm$ at PT, which combined with the first block of precipitation results on a RoS event.

Under these conditions, EC shows a significant decrease starting exactly at the same time as the first precipitation block, from $108.9\mu S/cm$ to $64.4\mu S/cm$ in 7 hours (figure 2.6a), although later EC rises again up to about $95\mu S/cm$. Again in this case, the pre-event water component, marked by larger EC values with respect to the new water component, mixes with event water during the rising limb of the event.

Moreover, assigning a snow density of $70\,Kg/m^3$ and $200\,Kg/m^3$ at PT and CP, respectively, a rough estimate of $9.1\,mm$ and $10\,mm$ of snow water equivalent (SWE) can be obtained from the drop of snow depth at the same stations. These values of snow density were measured by Meteotrentino on April 24 and May 1, 2012, and are assumed to apply also during this event. These values are larger than the runoff of $4.2\,mm$ measured at Vermiglio, evidencing the emergence of slow contribution (notice that water discharge tends to stabilize to $3.2\,m^3/s$ against to $2.3\,m^3/s$ before the event) and storage within the catchment.

**Event 3: Rain on snow event - November 2012**

Figure 2.7a shows a typical late autumn event of Rain on Snow (RoS), between 4 and 5 November of 2012, followed by a period of slightly declining streamflow. The event is characterized by a maximum water discharge of $11.1\,m^3/s$, corresponding to a total runoff of $7.8\,mm$, while total precipitation amounted to $84mm$ and $62mm$ at CP and PT, respectively. The peak of water discharge occurred $4\,h$ later than the maximum precipitation intensity. Along with precipitation and air temperature increase, a reduction of the snow depth of about $15\,cm$ is observed at both CP and PT at the end of the event (see figures 2.7b and 2.7c). However, an accurate inspection of figure 2.7 reveals differentiated dynamics at CP and PT between November 3 and 4. During this period, snow depth slightly declines at PT while slightly increases at CP, suggesting that precipitations were liquid at the former and solid at the latter. This is also confirmed by air temperature, which is above freezing and rising at PT and below freezing, though also rising, at CP.

The relatively constant EC and Q values prior to the event (figure 2.7a), suggest that rainfall and snow-melt originating from the lower portion of the catchment was stored. However, starting on the afternoon of November 4, air temperature increases over the threshold value of $0\,°C$ and this change is accompanied by intense precipitation and a steadily declining of the snow depth at both stations. Driven by these changes, the combined contribution of snow-melt and rainfall becomes evident in the following days, starting from November 4 at 15:00, when EC dropped from $112\,\mu S/cm$ to $48\,\mu S/cm$ in 16 hours.

Furthermore, assigning a snow density of $160\,Kg/m^3$ and $90\,Kg/m^3$ at PT and CP, respectively, a rough estimate of $24\,mm$ and $13.5\,mm$ of snow water equivalent

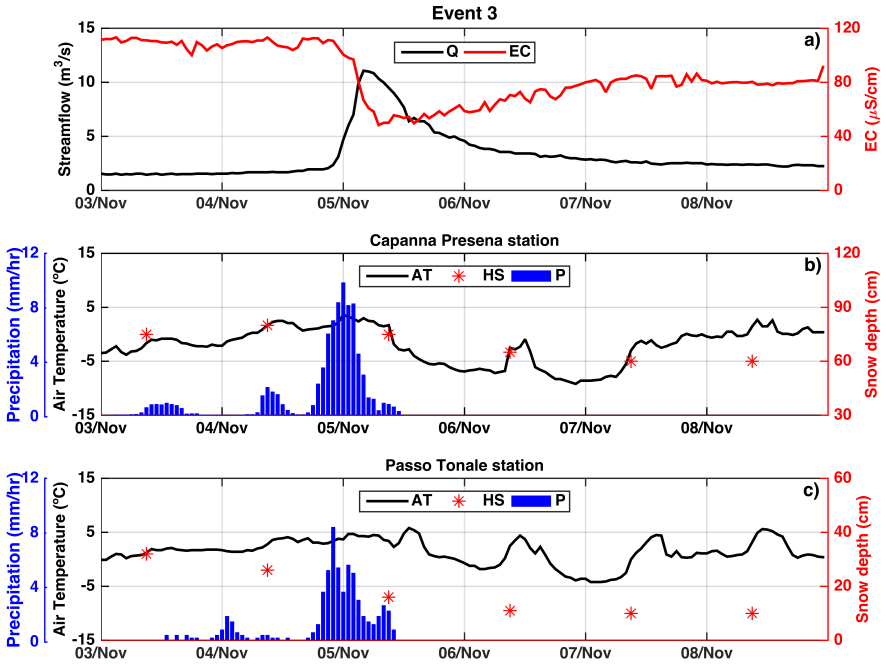


Figure 2.7: Event 3. Rain on snow during 3-8 November, 2012. On top: a) streamflow (black line) and electrical conductivity (red line) data recorded at monitoring point P2; b) and c) air temperature (black line), precipitation (blue bars) and snow depth (red stars) registered at meteorological stations of Capanna Presena and Passo del Tonale, respectively.

(SWE) can be obtained from the drop of snow depth at the same stations. Snow density value were measured by Meteotrentino on November 1 and 2 of 2012 and are assumed to apply also during this event. SWE values are larger than the runoff of 7.8 $mm$ measured at Vermiglio, evidencing the emergence of slow contribution (notice that water discharge tends to stabilize to 2 $m^3/s$ against to 1.5 $m^3/s$ before the event) and storage within the catchment, similar to what observed on Event 2.

### Event 4: Rain on snow event - October 2013

Another typical autumn RoS event was identified between 21-27 October of 2013, with an important peak on water discharge equal to 18.6$m^3/s$, observed at 22:00 of October 23 (figure 2.8a), corresponding to a total runoff of 17.4 $mm$, while total precipitation amounted to 150$mm$ at PT (figure 2.8c). The peak of water discharge occurred 9 $h$ later than the maximum precipitation intensity.

Along with precipitation and the increase in air temperature, we observe a

reduction on the snow depth, 10 $cm$ and 2 $cm$ at CP and PT (see figures 2.8b and 2.8c). Although in this case, since there are no available records of precipitation at CP during this period, it becomes more complicated to determine whether there is a difference on the dynamics at CP and PT. Nevertheless, snow depth decreases on both stations, which suggests that precipitations could have been liquid on both cases, while air temperature is above freezing and slightly rising at both stations.

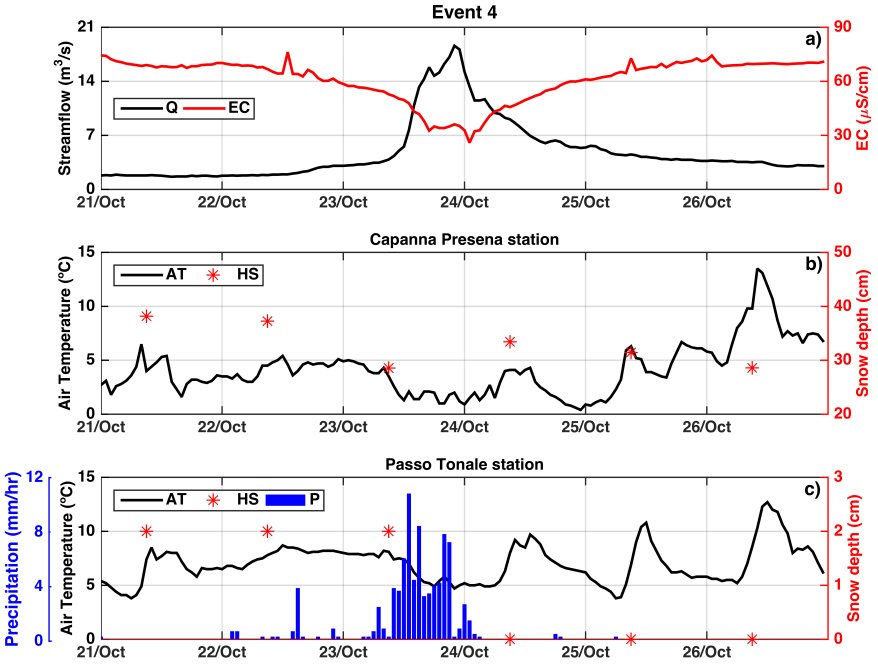


Figure 2.8: Event 4. Rain on snow during 21-26 October, 2013. On top: a) streamflow (black line) and electrical conductivity (red line) data recorded at monitoring point P2; b) and c) air temperature (black line), precipitation (blue bars) and snow depth (red stars) registered at meteorological stations of Capanna Presena and Passo del Tonale, respectively.

EC and Q are relatively constant prior to the event, suggesting that rainfall and snow-melt were stored during this time. However, as soon as rainfall started on October 23, EC values gradually decreased (figure 2.8a), in combination to a slight increase on air temperature and the reduction on snow depth at both stations. The combined contribution of snow-melt and rainfall becomes evident in the following days, when EC drops from $60 \mu S/cm$ to $25.9 \mu S/cm$ in 24 hours reaching the minimum on October 24 at 1:00.

Assigning a snow density of 60 $Kg/m^3$ and 150 $Kg/m^3$ at PT and CP, respectively, a rough estimate of 1.2 $mm$ and 15 $mm$ of snow water equivalent (SWE)

can be obtained from the drop of snow depth at the same stations. These values of snow density were measured by Meteotrentino on November 6 and December 20 of 2013 and are assumed to apply also during this event. SWE value at CP is very close to the runoff value of $17.4\,mm$ measured at Vermiglio, evidencing the emergence of a very fast contribution. Moreover, baseflow tends to stabilize at $2.8\,m^3/s$ against the value of $1.7\,m^3/s$ observed before the event.

### 2.4.2 Two-component mixing analysis of specific events

The results of the two-component mixing analysis were divided into two different parts: on the first we present the results only for Event 1 and discuss the differences emerging when using different tracers (i.e., $\delta D$, $\delta^{18}O$ and EC), while on the second part, we present and compare results of all four events using only EC as tracer, then discuss the existence of a time lag between maximum water discharge and maximum new water contribution.

#### Comparison between three different tracers: Event 1

Quantitative estimates of the relative contributions of event (i.e., rainfall) and pre-event (i.e., baseflow attributed chiefly to groundwater) water during this flood event were obtained by using equations (2.4) and (2.5). For the single case of Event 1, data were collected considering three different tracers and the following constraints have been considered: (i) EC of event and pre-event water are assumed both constant in time and equal to $EC_{e1} = 8.0\,\mu\,S/cm$ and $EC_{p1} = 68.4\,\mu S/cm$, respectively. The latter is the mean EC value of stream water observed before the event, after a long period without significant precipitations, while the former assumption is in line with previous studies showing that in this area of the Alps rainfall EC is stable with small deviations from the mean value of $8.0\,\mu S/cm$ (Penna et al., 2014); (ii) similarly to EC, the isotopic signature of pre-event water is assumed constant in time and equal to $\delta D_{p1} = -94.8‰$ and $\delta^{18}O_{p1} = -12.85‰$, which are the values observed in samples collected on September 9 of 2011 on a former study (see Chiogna et al., 2014) and can be considered constant since only seasonal variability has been observed.

We minimized equation (2.6) by considering both isotopic signatures of event water piecewise constant, with maximum three different values corresponding to the three blocks of precipitation described for this event (see description of Event 1 on section 2.4.1). This approximation was introduced because the only rainfall water sample available in September was taken 8 days before the beginning of the event. The best fit was obtained with isotopic signatures of event water equal to $\delta D_{e1} = -72.28‰$ and $\delta^{18}O_{e1} = -10.59‰$ between September 17 at 17:00 and September 18 at 18:00 (i.e., for the first two blocks of precipitations), and with $\delta D_{e2} = -54.05‰$ and $\delta^{18}O_2 = -8.56‰$ in the remaining of the event.

Despite the assumptions and the limitations affecting the proposed approach (see Laudon and Slaymaker, 1997; Uhlenbrook and Hoeg, 2003), the mean relative differences between event water contribution computed using the three tracers do not differ by more than 6.1%. Furthermore, the inferred isotopic signatures of event water contribution are consistent with both the signatures of the only

rainfall sample taken on September 2011 as well as the local meteoric water line provided by Chiogna et al. (2014).

Figure 2.9a shows the relative contribution of new water to streamflow associated to the three tracers (i.e., $\alpha_{EC}$, $\alpha_{\delta D}$ and $\alpha_{\delta^{18}O}$). Event water contribution during the first block of precipitation reaches a maximum of 34%, 29% and 32%, according to the time series of $\delta D$, $\delta^{18}O$ and EC, respectively. As rainfall continues (i.e., second block of precipitation), $\alpha_{\delta D}$ and $\alpha_{\delta^{18}O}$ increase up to 55% while $\alpha_{EC}$ increases up to 59%. With the third block of precipitation, contribution due to event water reaches the maximum values: 71% for $\alpha_{\delta D}$, 62% for $\alpha_{\delta^{18}O}$ and 68% for $\alpha_{EC}$. In addition, a 3 hour time lag is observed between streamflow maximum peak and maximum new water contribution obtained with EC data ($\alpha_{EC}$). For the case of stable isotopes, it was not possible to obtain precise information because unlike EC, isotopic data were available at a minimum time step of 4 hours.

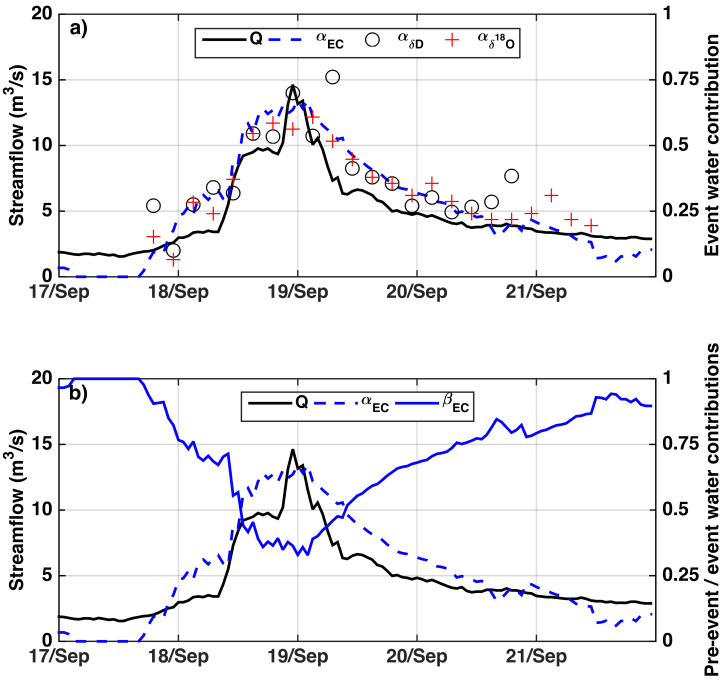


Figure 2.9: Event 1. a) Relative contributions of event water during the entire flood event estimated from tracer data: $\alpha_{EC}$ (blue dashed line), $\alpha_{\delta D}$ (black circles) and $\alpha_{\delta^{18}O}$ (red plus sign). b) Pre-event and event water separation using only EC data: blue dashed line corresponds to contribution from event water ($\alpha_{EC}$) while the blue continuous line to the pre-event water component ($\beta_{EC}$). Black continuous line depicts the observed streamflow on both panels.

Furthermore, the contribution of pre-event and event water is then compared using only EC data (figure 2.9b): pre-event water is the main component of

discharge (i.e., $\beta > 0.5$) up to 18 September at 12:00. After this, the pre-event water contribution decreases up to its minimum (32%) on 19 September at 0:00. During the recession limb of the hydrograph, the contribution of event water reduces to the 10% and correspondingly, pre-event water contribution increases to a value of 90%, which characterizes pre-event conditions. A slight increase on baseflow is however observed at the end of this event (from $1.8m^3/s$ to $3m^3/s$).

The results of the two-component mixing analysis suggest that mixing between pre-event water and event water occurs almost instantaneously during a regular flood event, hence indicating a very quick response of the catchment in the absence of snowpack. Moreover, the mean relative differences between event water contribution computed using the three different tracers is less than 6.1%. Considering the many advantages of recording continuous EC measurements with respect to collecting water samples for stable isotope analysis (i.e., lower costs, immediate available measurements, high resolution data), on the following analyses we used only EC data as tracer.

**Comparison between all events using only EC as tracer**

Two-component mixing analysis was likewise applied to Events 2, 3 and 4, under the main assumption that during a RoS event, both rainfall and snow-melt may contribute to streamflow generation. Experimental work on a similar environment showed that in this area of the Alps both snow-melt and rainfall present very low mean EC values, $EC_e = 20.0\,\mu\,S/cm$ and $EC_e = 8.0\,\mu\,S/cm$ respectively (Penna et al., 2014). Moreover, the results of the two-component mixing analysis are not significantly influenced by considering a mixed composition of the event water, indeed, considering $EC_e = 8.0\,\mu\,S/cm$ (i.e., only rainfall water contribution) or $EC_e = 20.0\,\mu\,S/cm$, (i.e., only snow-melt water contribution), leads to a difference in the maximum contribution of event water smaller than 8%.

The difference between these two estimates is therefore small, such that they can hardly be separated using EC data, hence, the following constraints have been considered: (i) EC of event water is assumed to be constant and equal to $EC_e = 8.0\,\mu\,S/cm$ for all events and; (ii) EC values of pre-event water correspond to the mean values of stream water EC observed days prior to every single event, therefore vary on each case and are equal to: $EC_{p2} = 118.8\mu S/cm$, $EC_{p3} = 111.7\mu S/cm$ and $EC_{p4} = 77.1\mu S/cm$ respectively. Notice that $EC_p$ values of Event 1 (September 2011) and Event 4 (October 2013) are significantly smaller than those of Event 2 (May 2012) and Event 3 (November 2012), this can be attributed to the fact that during September and October a significant amount of melting water is still present in the catchment system, while in May and November streamflow is mainly characterized by baseflow conditions.

The two-component mixing analysis allowed us to further investigate the dynamics of event water contribution comparing different events and to identify a relatively constant time lag between maximum streamflow and maximum event water contributions (see figure 2.10), hence providing new insights into the system functioning of the Vermigliana catchment. Results are shown as panels, where the black continuous line represents streamflow, the red dashed line depicts the event water contribution estimated using stream water EC and the light blue shade

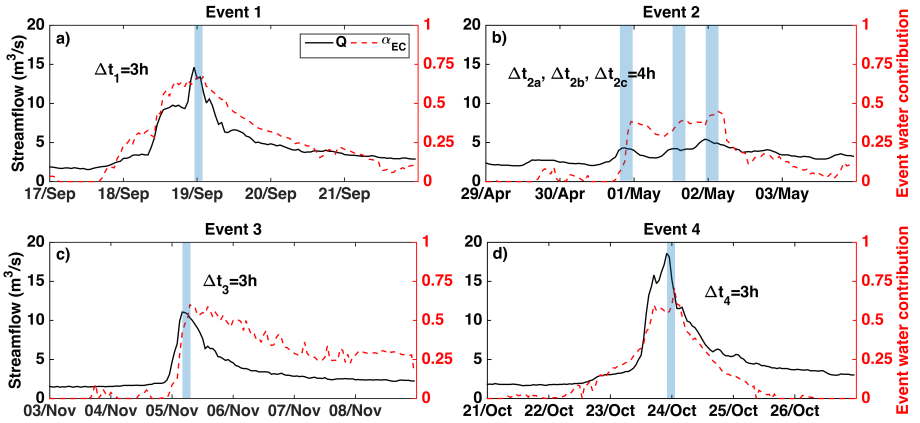


Figure 2.10: Relative contribution of event water (red dashed line) and streamflow Q (black continuous line): a) Event 1; b) Event 2; c) Event 3 and; d) Event 4. The shaded polygon (light blue) indicates the time lag $\Delta t$ between the maximum values of Q and maximum $\alpha_{EC}$.

indicates the time lag $\Delta t$ between the peak values of Q and $\alpha_{EC}$.

Maximum contribution of event water ranges between 45% (Event 2) and 71% (Event 4) with a significant difference in the rate of increase of the rising part of the hydrograph. The time lag $\Delta t$ for Events 1, 3 and 4 is equal to 3 hours. Event 2 is the most complex between the cases under study, since there are three separated rainfall events falling on a snowpack of different thicknesses (see figure 2.6), thus we evidenced the time lag between the maximum value of Q generated after each block of precipitation (defined as 2a, 2b and 2c), which in all cases is equal to 4 hours. Interestingly, despite the significant differences in the amount of precipitation and snow depth, all events present relatively the same time lag, hence suggesting that the difference in the arrival time of the maximum streamflow is anticipated with respect to the maximum contribution of new water by about 3 hours. The previous can be explained by the difference celerity between streamflow signal and the celerity of a dissolved solute, such as electrical conductivity (see e.g., Toffolon et al., 2010).

Moreover, while Events 1 and 4 show a smooth increase in the contribution of event water, Events 2 (i.e., during the first block of precipitation) and 3 present a very steep increase on the event water contribution. Thus, we also observed the dynamics of maximum $\alpha_{EC}$ with respect to precipitation time series. Figure 2.11 shows all events as panels, on which blue bars correspond to precipitation data obtained from records at Passo del Tonale station, the red dashed line corresponds to the event water contribution and the shaded polygons (light orange) indicate the time lag, $\Delta t_p$, between the peak of precipitation and the consequent peak value of $\alpha_{EC}$: Events 1 and 4 respond almost instantaneously to the precipitation input (figures 2.11a and 2.11d) with maximum time lags equal to 5 and 4 hours respectively, showing a gradual increase on $\alpha_{EC}$ as soon as rainfall begins. Events

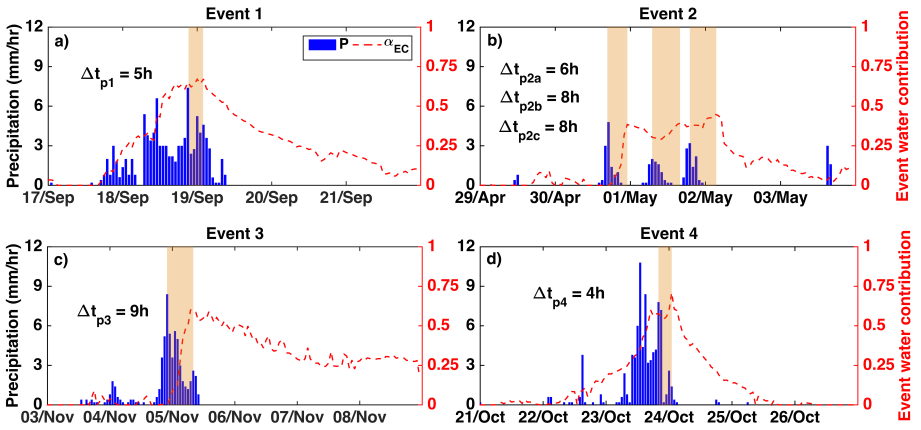


Figure 2.11: Relative contribution of new water (red dashed line) and precipitation (blue bars) at Passo del Tonale station: a) Event 1; b) Event 2; c) Event 3 and; d) Event 4. The shaded polygons (light orange) indicate the time lag $\Delta t_p$ between precipitation peak and subsequent maximum $\alpha_{EC}$.

2 and 3 instead (figures 2.11b and 2.11b) display a longer delay between the start of precipitation and the appearance of event water contribution, indeed, the maximum time lag between precipitation peak and maximum event water contribution is of 8 and 9 hours respectively.

The above analyses indicate that the thickness of the snowpack present during the event directly affects the dynamics of event water contribution. In the cases with no snow cover at all (Event 1) or with very thin snowpack (Event 4), the delay between peak precipitation and maximum event water contribution is much smaller than the cases with thicker snowpack (Events 2 and 3). The previous suggests that when the snowpack is thick enough, it can potentially store water, hence increasing the catchment's storage capacity and causing a delay between the beginning of precipitation and runoff generation. Once the storage capacity is saturated, the water previously stored within the snowpack in addition to melted water can be released very rapidly, resulting on a sharp increase in the new water contribution, as observed on Events 2a and 3.

### 2.4.3 Hysteresis between streamflow and tracer concentration

Hysteresis loops can be observed when plotting streamflow against the concentration of dissolved species (Evans and Davies, 1998), caused by the occurrence of a delay between the two signals. We analysed the relationship between EC concentration and Q during each event (figure 2.12) to verify the existence or not of this hysteresis and its main characteristics.

Event 1, additionally allowed us to compare the use of three different tracers on this analysis. During the rising limb of the hydrograph, $\delta D$ and $\delta^{18}O$ con-

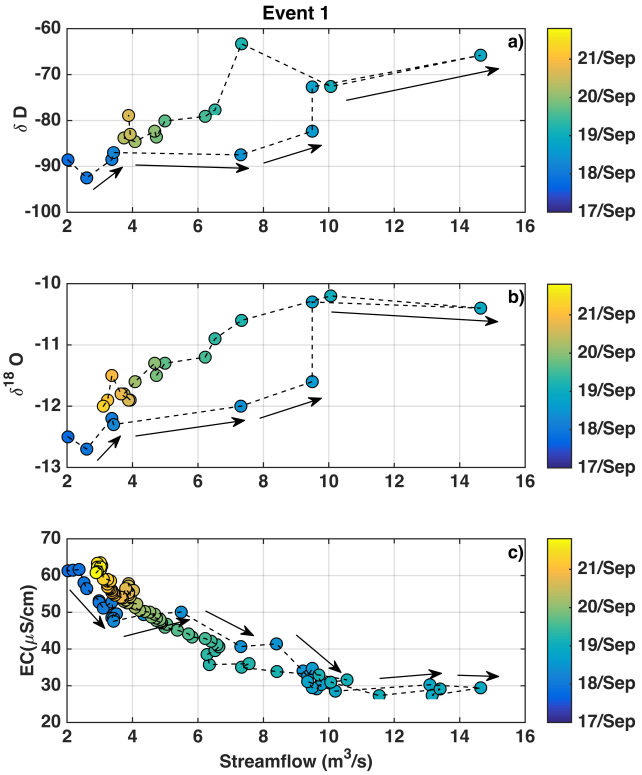


Figure 2.12: Event 1. Relationship between Q and: a) $\delta D$; b) $\delta^{18}O$ and; c) EC. The colour bar indicates the days with beginning and ending of the sampling represented in dark blue and yellow, respectively.

centrations (figures 2.12a and 2.12b) increase very rapidly at the same time as water discharge, EC concentration (figure 2.12c) instead decreases towards the minimum value while water discharge increases. This is followed by the recession limb, on which all three tracers return gradually near to pre-event values (i.e., $\delta D$ and $\delta^{18}O$ decrease and EC increases). Isotopic data thus display a relatively wide counter-clockwise hysteresis loop while EC presents a very tight and small clockwise hysteresis loop between $11m^3/s$ and $14m^3/s$.

Moreover, when looking at the relationship between streamflow and EC concentration of all four events we find different type of hysteresis loops according to the case (see figure 2.13). During Event 1 (figure 2.13a) no hysteresis is observed and the EC-Q relation is the same both during the rising as well as during the recession phase of the hydrograph. Event 3 instead is characterized by an unique and very wide clockwise hysteresis loop (figure 2.13b): during the rising limb of the hydrograph, EC values are significantly high for a given value of Q, this initial stage is followed by a gradual decrease of EC and increase of Q until this last reaches its peak value. The recession limb shows at the beginning a slight

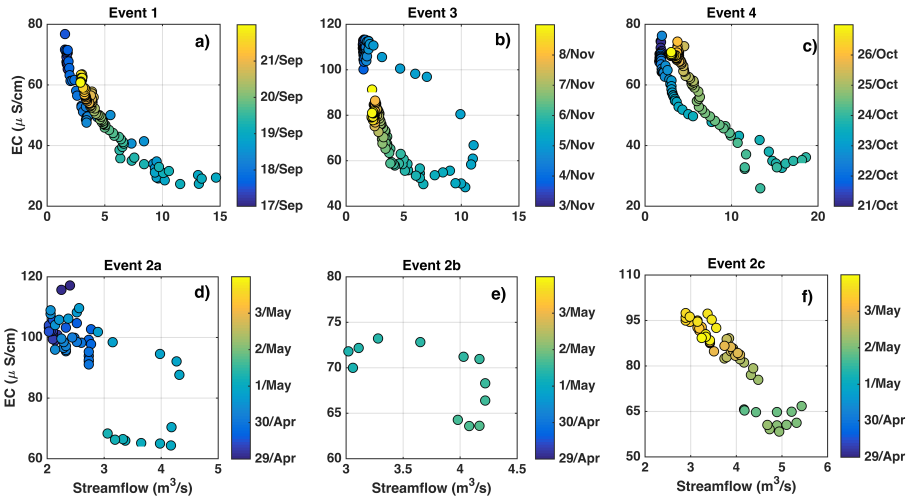


Figure 2.13: Relationship between Q and EC at the event scale: a) Event 1; b) Event 3 and; c) Event 4; d) Event 2a; e) Event 2b and f) Event 2c. The colour bar indicates the days with beginning and ending of each event represented in dark blue and yellow, respectively.

decrease on both EC and Q, then a gradual decrease of Q while EC remains relatively constant. On the final part of the loop, Q remains relatively constant while EC decreases towards values similar to pre-event conditions.

During Event 4 (figure 2.13c) we observe an initial decrease on EC for a given value of Q, then as Q increases due to event water contribution, EC gradually decreases. After Q achieves its peak value, EC remains relatively constant while Q decreases, after this point a very small clockwise hysteresis loop appears between $10m^3/s$ and $15m^3/s$, as both EC and Q increase and decrease respectively, returning to pre-event conditions.

On the other hand, Event 2 was separated in three panels considering the three main blocks of precipitation as observed on figure 2.6: the first part (Event 2a) presents a wide clockwise loop (figure 2.13d), suddenly interrupted by the occurrence of the second block of precipitation (Event 2b), which causes a second smaller clockwise hysteresis loop (figure 2.13e). Again, the cycle is interrupted by a third block of precipitation (Event 2c) without the presence of hysteresis, followed by a gradual decrease on streamflow and increase of EC as both return to values similar to the pre-event conditions (figure 2.13f). Notice the observed hysteresis pattern between EC and Q is always in the clockwise sense.

Furthermore, the occurrence as well as the size of the loop can be related to the presence and thickness of the snowpack during the event. In Events 1 and 2c no snowpack is present and as consequence no hysteresis patterns are observed. However, in Events 4 and 2b, a $2cm$ thick snowpack is present and thus a small hysteresis appears. During Events 2a and 3 instead, a thicker snowpack is present, $10cm$ and $25cm$ respectively, leading to much wider loops than the

previous cases. Notice the snow depth values reported here are referred to records at Passo del Tonale station. A more detailed analysis of the influence of the presence and thickness of the snowpack during each event is presented in the following subsection.

### 2.4.4 Influence of the presence and thickness of the snowpack

The hypothesis that the occurrence and width of the hysteresis loops observed on each event are related to the presence and thickness of the snowpack on each case was tested by considering the existence of a delay time $\Delta t_{EC}$ between EC and Q, which in the end causes the appearance of the loop.

Thus, we translated EC signal with respect to $Q(t)$, were $t = 0$ and represents the beginning of the event. By plotting $Q(t)$ against the translated signal of EC, i.e., $EC(t+\Delta t_{EC})$, we expect the hysteresis loop to disappears in all the cases, as shown on figure 2.14. The delay time used to suppress the hysteresis is different on each event and more important, is correlated with snow depth values as shown in Figure 2.15. Specific values of $\Delta t_{EC}$ are reported on table 2.4.

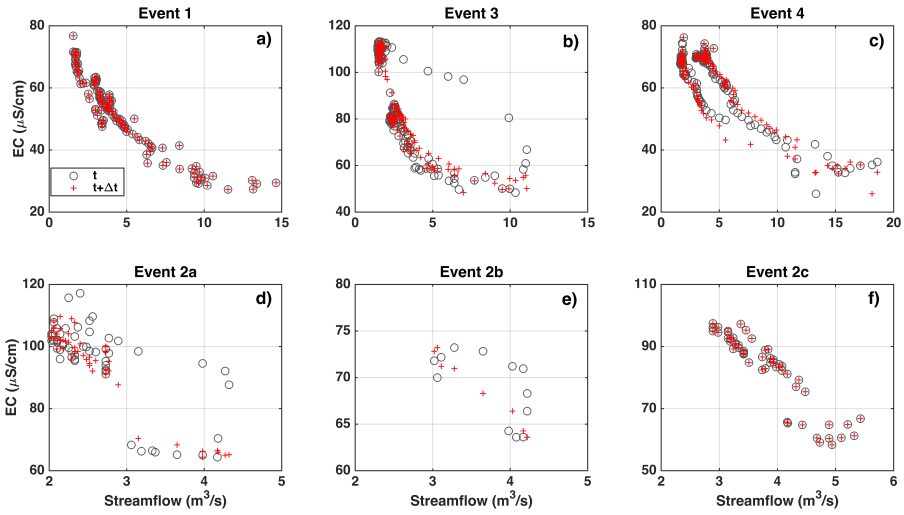


Figure 2.14: Hysteresis between EC and Q at time $t$ (dark grey circles) and suppressed hysteresis considering the time $t + \Delta t_{EC}$ (red plus sign): a) Event 1; b) Event 3 and; c) Event 4; d) Event 2a; e) Event 2b and f) Event 2c.

At Passo del Tonale station (figure 2.15a) we observe that the thicker the snowpack (HS) the longer is the delay time $\Delta t_{EC}$. This behaviour reflects the following dynamics: at the beginning of the precipitation event, water with low values of EC is accumulated in the system and after it is rapidly released mixing with pre-event water. At Capanna Presena station (figure 2.15b), Events 1, 3 and 4 show similar correlation between the delay $\Delta t_{EC}$ and the thickness of the snowpack, however, a different dynamic is observed during Event 2, where the delay

Table 2.4: Main features related to the hysteresis observed on each event

| Event | Loop feature | Snow depth at CP (cm) | Snow depth at PT (cm) | $\Delta t_{EC}$ hr |
|---|---|---|---|---|
| 1 | no hysteresis | 0 | 0 | 0 |
| 2a | wide | 265 | 10 | 4 |
| 2b | small | 280 | 2 | 3 |
| 2c | no hysteresis | 298 | 0 | 0 |
| 3 | very wide | 80 | 26 | 5 |
| 4 | small | 37 | 2 | 3 |

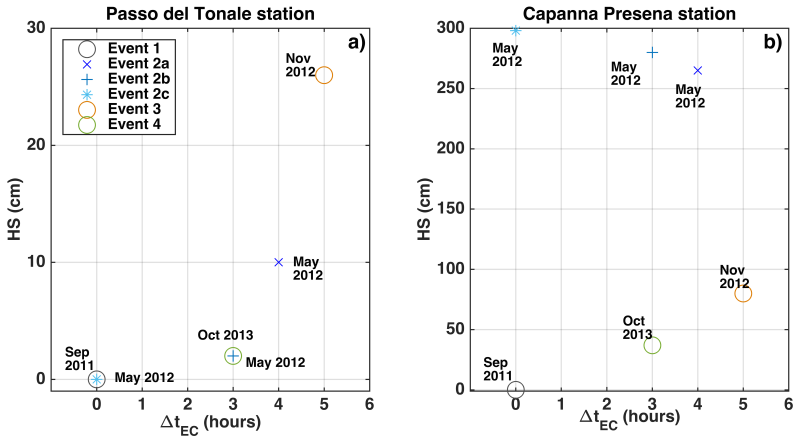


Figure 2.15: Correlation between $\Delta t_{EC}$ considered for supressing the hysteresis on each event and the snow depth level (HS) measured at: a) Passo Tonale and b) Capanna Presena stations.

time $\Delta t_{EC}$ instead decreases while the snowpack becomes thicker. Considering the altitude difference between both stations, it can be expected to observe different dynamics at higher elevations, while at PT precipitation is only liquid and additionally snow-melted water is released due to the increase in air temperature (figure 2.6c), at CP precipitation is liquid but also falls solid as snow (figure 2.6b), thus there is no additional contribution from snow-melted water.

Notice that Events 1, 3 and 4 correspond occur within the autumn season, while Event 2 occurs during late spring, therefore suggesting that the increase of $\Delta t_{EC}$ due to the increase of the thickness of the snowpack during precipitation events is valid during the winter season, on which snow accumulation is the main processes controlling streamflow generation. However, during late spring and summer, when snow-melting is triggered, the dynamics controlling streamflow generation are different, in particular at lower elevations due to the higher air temperatures.

## 2.5 Conclusions

Streamflow in Alpine headwaters is shaped by several generation mechanisms, from snow and glacier melting during the summer, and rainfall, often mixed with snowfall at high elevations in spring and autumn, while in winter streamflow is chiefly sustained by groundwater contribution. This peculiar characteristic of Alpine headwaters results in large variability of streamflow over many temporal scales. We explored this complexity by analysing the contributions to streamflow generation during four precipitation events identified in the Vermigliana catchment, a headwater catchment in the Alpine region, North-Eastern Italy.

Two-component mixing analysis was applied using electrical conductivity measurements of stream water as tracer in order to quantify the relative contribution of pre-event and event water to streamflow generation on each event. The maximum contribution of event water estimated ranged between 45% and 71%. In addition, one specific case (Event 1) was used to study the differences emerging in streamflow separation using two additional tracers, i.e., $\delta^{18}O$ and $\delta D$. Results indicate that different tracers can provide similar estimates of event water contribution, within an average error of 6.1% for our study case.

Correlation between tracer data and discharge or precipitation time series during single events is in general complex, nevertheless an adequate interpretation may allow us to build an in depth knowledge on the system functioning. The detailed observation of the dynamics of the relative contribution of event water during each event evidenced that this contribution does not change only according to the magnitude of the precipitation input but it also depends on the amount of snow accumulated prior to the event. Hence, we further explored the relationship between EC and Q during each event (figure 2.13), observing hysteresis loops with clockwise patterns. It was found that the occurrence as well as the size of the loops can be related to the presence and thickness of the snowpack: in the cases with very thin snowpack or no snow cover at all, small loops were observed, while in the cases with thick snowpack, very wide loops appeared.

Furthermore, we showed that the hysteresis can be suppressed considering the existence of a delay between EC and Q (figure 2.14), which is correlated to the thickness of the snowpack present during each event, suggesting that the thicker the snowpack the longer the delay time. However, the comparison between two meteorological stations located at different altitudes (figures 2.15a and 2.15b) showed that this correlation is found only for events occurring in autumn, when snow accumulation is the main process controlling streamflow generation and similar dynamics are observed at both low and high elevations. During late spring instead, snow-melting processes are triggered at lower elevations, causing a different behaviour with respect to points at higher elevations due to the increase on air temperature.

Overall, our results indicate that hydrological data complemented with other sources of information, such as electrical conductivity, provide important additional insights on system functioning. Hence, we believe that this study can motivate future research on streamflow generation dynamics on snow-dominated catchments based on hydrometric and high resolution tracer data.

*Chapter* 3

# The role of electrical conductivity measurements

## 3.1 Introduction

Electrical conductivity (EC) and streamflow (Q) signals are expected to be correlated, owing to the dependence of streamflow on the distribution of water residence times, though the inherent unsteadiness of flow makes this dependence complex Rinaldo et al. (2015). The general idea is that snow and ice waters, as well as rainfall, are characterized by a very low electrical conductivity when they enter the catchment, and therefore the EC at the control section should depend on the time water remains in contact with rocks dissolving geogenic components. Besides flow unsteadiness, the analysis is complicated by heterogeneity in the distribution of geogenic components. These difficulties notwithstanding, which make the relationship between EC and Q highly non-linear and transient (in time), earlier studies have evidenced the existence of some types of relationship between stream water electrical conductivity and discharge signals (e.g. Collins, 1979; Gurnell and Fenn, 1985; Evans and Davies, 1998; Dzikowski and Jobard, 2012). Thus, EC measurements have been used in several applications in hydrology, such as to quantify streamflow (Weijs et al., 2013), to differentiate among different water sources (e.g., Penna et al., 2014), to understand geochemical processes (e.g., Hayashi et al., 2012) and to perform hydrograph separation (e.g., Engel et al., 2015; Penna et al., 2015).

The above difficulties complicate the analysis and ultimately call for a better understanding of the relationship between electrical conductivity and water discharge. Exploring the nature and variability of the relationship between EC and Q may play a fundamental role in the study of the complex hydrological processes controlling streamflow generation in Alpine catchments, consequently leading to a more rigorous application of the EC-Q relationship for hydrological and geochemical purposes. To our knowledge, new studies focused mainly on studying the nature and variability of the relation between EC and Q and its potential applications have not yet been discussed. Therefore, the aim of this chapter is

to show that an in depth analysis of electrical conductivity and water discharge signals can reveal information about the hydrological characteristics of the catchment, which otherwise could not be obtained if each signal were to be analysed separately.

We investigated continuous records of electrical conductivity and water discharge time series of two melting periods (June-November) of the Vermigliana, an Alpine headwater stream located in the North-Eastern Italian Alps. A full description of the catchment, including, location, morphology, climate regime, monitoring points, can be found in Chapter 2. To this end, we analysed the hysteresis relating EC and Q at the annual scale (see e.g., Hooper et al., 1990; Walling and Webb, 1986; Evans and Davies, 1998); explored similarities between the fluctuations of both signals applying the wavelet coherence (see e.g., Torrence and Compo, 1998; Grinsted et al., 2004), which was complemented with a cross-correlation analysis used to study the similarity of the two signals as a function of the lag of one relative to the other (see e.g., Gurnell and Fenn, 1985), which allowed us to verify and estimate the existence of a time lag between both signals during the melting period and; analysed EC and Q diurnal cycles to estimate the daily contribution to streamflow from snow-melting (see e.g. Caine, 1992; Lundquist and Cayan, 2002; Lundquist et al., 2005; Lundquist and Dettinger, 2005; Mutzner et al., 2015).

More specifically, the main objectives of this study are: i) to identify limitations of the use of EC data as a proxy of Q in Alpine catchments; ii) to develop a methodology to fully explore the correlation between EC and Q and its use in the identification of timing of the main streamflow sources; iii) investigate the use of diurnal cycles of EC and Q to determine the daily contribution from snow-melting to streamflow.

## 3.2 Methods

In this section we present the available data and the tools used to analyse the signals and evidence their correlation across the scales of variability.

### 3.2.1 Data collection

At the gauging station located at Vermiglio (see monitoring point P2 in figure 2.1, Chapter 2) we supplemented the streamflow data, provided by the Ufficio Dighe of the Province of Trento (http://www.floods.it), with electrical conductivity data recorded at 1-hour time intervals with an Aqua TROLL 200 multiparametric probe. The instrumental precision of the two sensors mounted in the probe is of 0.1 $\mu S/cm$ and 0.01°$C$ for EC and water temperature respectively. EC values were after referred to a standard temperature of 20°$C$ following the methods described in Section 2.3.1. of Chapter 2. Moreover, data collection with this instrument was limited to the period between June 1 to November 20 of 2012 and 2013, thus including data mainly from the melting period.

The graphs reported on figure 3.1 show the entire dataset of precipitation, air temperature and snow depth at the meteorological stations of Capanna Presena

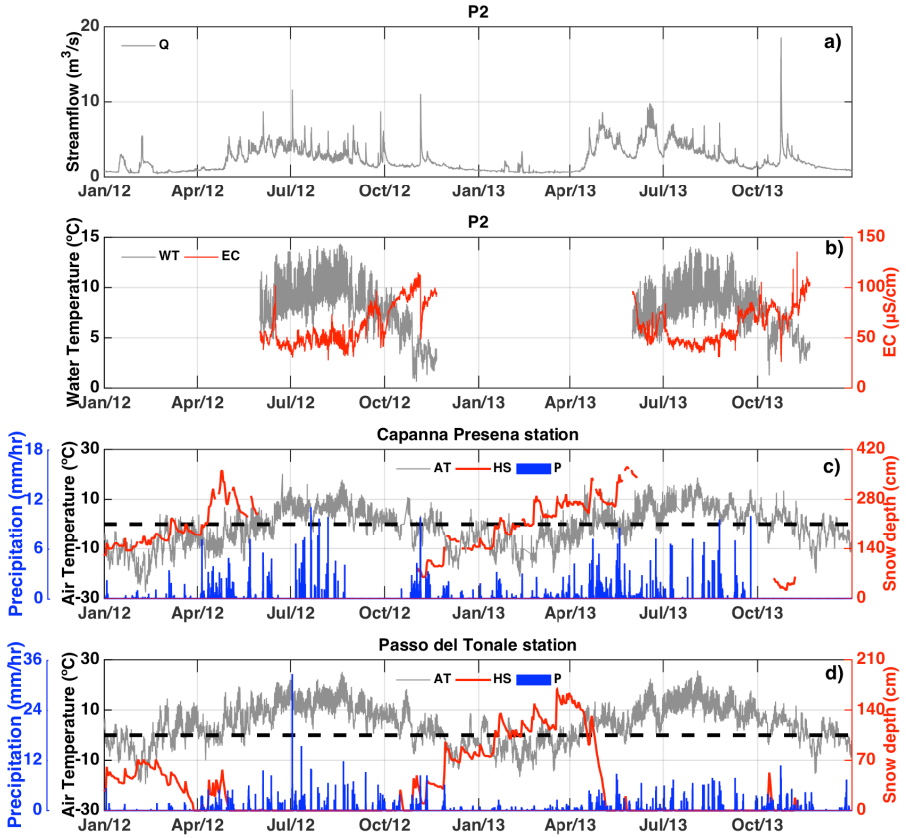


Figure 3.1: Data collected on the period 2012-2013: a) hourly time series of streamflow (grey line) at P2; b) hourly time series of air temperature (grey line), precipitation (blue bars) and daily time series of snow depth (red line) at Capanna Presena station (CP); c) hourly time series of air temperature (grey line), precipitation (blue bars) and daily time series of snow depth (red line) at Passo del Tonale station (PT); d) hourly time series of water temperature (grey line) and electrical conductivity (red line) recorded at Vermiglio gauging station (P2).

(figure 3.1b) and Passo del Tonale (figure 3.1c), provided by the local meteorological survey (http://www.meteotrentino.it), along with water discharge and electrical conductivity (figure 3.1a) at the Vermiglio gauging station. Streamflow time series (figure 3.1a) shows the typical seasonal variability of Alpine catchments (i.e. warm wet summers and autumns followed by dry winters), with minimum in winter due to precipitation falling as snow (Chiogna et al., 2014), while the maximum seasonal streamflow is observed in summer due to the contribution of snow-melting and glacier-melting, which are driven by air temperature. This cyclical behaviour is intertwined by random flood events occurring chiefly in autumn, as for example the case of Events 3 and 4 analysed on Chapter 2, which occurred on 3-8 November 2012 and 21-26 October 2013 with peaks on water discharge of $11.1 m^3/s$ and $18.6 m^3/s$, respectively. Air temperature (figures 3.1b and 3.1c) presents also a very marked seasonal variability, which is the main driver of the melting processes that control streamflow fluctuations. A black dashed line has been drawn at $0°C$, to easily identify the periods below freezing conditions. On the other hand, snow depth presents higher values and longer snow cover duration in 2013 with respect to 2012. Furthermore, electrical conductivity and temperature of stream water (figure 3.1d) show as well a marked seasonal variability, where EC presents relatively low values during summer while higher values during winter, that range from 26 to 136 $\mu S/cm$; oppositely water temperature shows low values during winter ($0.6°C$) and higher values during summer ($14.5°C$).

### 3.2.2 Continuous wavelet transform and signal coherence

The continuous wavelet transformation of a discrete signal $x_n$, $n = 1, ...., N$, sampled at constant time intervals $\delta t$, is defined as follows (Grinsted et al., 2004):

$$W_n(s) = \sum_{n'=0}^{N-1} x_{n'} \psi^* \left[ \frac{(n' - n)\delta t}{s} \right] \tag{3.1}$$

where $\psi(\eta)$ is a band-pass filter and the superscript $*$ indicates the complex conjugate. Mathematically, the transform of equation (3.1) is the convolution of the signal $x_n$ with the scaled version of the wavelet function $\psi$, which is obtained from a "mother wavelet" $\psi_o(\eta)$ normalized at each scale $s$ such that to respect the following condition: $\sum_{k=0}^{N-1} |\psi(s\,\omega_k)|^2 = N$, where $\omega_k$ is the angular frequency and $s$ is the wavelet scale (Torrence and Compo, 1998), which assumes the following expressions: $\omega_k = 2\pi k/(N\delta t)$ for $k \leq N/2$ and $\omega_k = -2\pi k/(N\delta t)$ for $k > N/2$.

Similarly to other studies analysing variability in climate and hydrological signals (see e.g., Kumar and Foufoula-Georgiou, 1993; Foufoula-Georgiou and Kumar, 1994; Lau and Weng, 1995; Venugopal and Foufoula-Georgiou, 1996; Saco and Kumar, 2000; Coulibaly and Burn, 2004; Zolezzi et al., 2009; Guan et al., 2011; Carey et al., 2013), the Morlet function was used as "mother wavelet" for its ability to evidence fluctuations oscillating transient signals:

$$\psi_o(\eta) = \pi^{-1/4} e^{i\,\omega_o \eta} e^{-\eta^2/2} \tag{3.2}$$

where $\omega_o$ is dimensionless frequency and $\eta$ is dimensionless time. Following Torrence and Compo (1998), $\omega_o$ is set to 6, such that the wavelet scale is almost identical to the corresponding Fourier period.

The wavelet transform (i.e., equation (3.1)) is then computed for a selection of scales $s_j = s_0^{2j\,\delta_j}, (j = 1, 2, ..., J)$, where $s_0$ is the smallest scale considered in the analysis and $J = \delta_j^{-1} log_2(N\delta_t/s_0)$ is the largest scale. In addition, $s_0$ should be chosen such that the equivalent Fourier period is approximately $2\,\delta t$.

The wavelet power spectrum, defined as $W_n\,(s)\;W_n^*\,(s)$, represents the energy of the scale $s$ and is useful in the identification of fluctuation scales with the largest influence on the signal.

Since the wavelet transform is not completely localized in time, the discontinuity at the beginning ($t = 0$) and at the end of the time series introduces spurious effects at the edges of the spectrum. Therefore, at each scale the spectrum is limited to a time interval: $[\tau_s, n\,\delta t - \tau_s]$, where $\tau_s$ is the folding time influenced by edge effects. For the Morlet wavelet, $\tau_s = \sqrt{2}\,s$.

The variability across temporal scales and reciprocal dependence between EC and Q may reveal interesting features. The wavelet coherence between two time series can be interpreted as the squared correlation coefficient of the time series components (see Torrence and Webster, 1999). Similarly to the correlation coefficient, coherence varies between 0 (uncorrelated) to 1 (fully correlated). Therefore the coherence analysis becomes interesting because evidences the modes of variation (periods) which are correlated in the two signals.

Wavelet coherence (WTC) is defined as follows (Torrence and Webster, 1999; Grinsted et al., 2004):

$$R_n^2\,(s) = \frac{\left|S\left[s^{-1}W_n^{XY}(s)\right]\right|^2}{S\left[s^{-1}\left|W_n^X(s)\right|^2\right]\,S\left[s^{-1}\left|W_n^Y(s)\right|^2\right]} \tag{3.3}$$

where $S$ is a smoothing operator, given by $S\,(W) = S_{scale}\,\{S_{time}\,[W_n(s)]\}$, while $S_{scale}$ denotes smoothing with respect to scales $s$ and $S_{time}$ smoothing in time. For details on the smoothing functions the reader may refer to Torrence and Webster (1999) and Grinsted et al. (2004).

### 3.2.3 Cross-correlation analysis

Cross-correlation is a standard method useful to determine the time lag between two time series $x_i, y_i$ with $i = 0, 1, 2, ..., N$, where $N$ is the length of the time series. It is defined as follows:

$$r_{x,y}(k) = \frac{\frac{1}{N-1}\sum_{i=1}^{N}\left[(x_i - \mu_x)(y_{i-k} - \mu_y)\right]}{\sigma_x\sigma_y}; k = 0, \pm1, \pm2, ... \tag{3.4}$$

where $k$ indicates the time lag between the two time series, $\mu_x$ and $\mu_y$ are the sample means and $\sigma_x$ and $\sigma_y$ the sample standard deviations of the time series (Box et al., 2011).

We considered the time series of $EC$ and $log_{10}Q$, similarly to the method described in Gurnell and Fenn (1984), with the time series of $Q$ logarithmically

transformed to reduce possible effects from outliers, like very high values that may significantly affect the statistics. The cross-correlation (equation 3.4) is then computed by keeping one of the two time series fixed and shifting the other by a given time lag. Several time lags are applied and then the one providing the maximum correlation is identified. Sample size is equal to $N = 24h$, which allows us to obtain the maximum correlation and time lag between the two time series on each single day.

### 3.2.4 Estimation of the daily contribution to streamflow due to snow-melting

Following the approach proposed on Mutzner et al. (2015), we analysed streamflow and electrical conductivity diurnal cycles, excluding from the original series days with precipitation events and likewise, the first subsequent day after each precipitation event. In this way the initial portion of the recession curve is directly excluded from the analysis. The amplitude of the resulting (modified) daily time series $t_i$, with $i = 1, 2, 3...N$ and $N$ being the length of the entire time series, can be defined as the difference between the maximum and the minimum values of each day $i$. A previous study (see Lundquist and Cayan, 2002) showed that in the case of streamflow, the ratio between the amplitude and mean daily streamflow value can indicate the dynamic dominating streamflow generation. Thus, we tested the applicability of this relationship using also electrical conductivity time series. The daily contribution to snow-melting is then defined as:

$$C_{SM}(t_i) = \frac{A(t_i)}{\overline{t_i}} \tag{3.5}$$

where $A(t_i)$ is the daily amplitude of either EC or Q signals and $\overline{t_i}$ is the mean daily value. Values of $C_{SM}$ greater close to 1 indicate streamflow dynamics dominated by snow or ice melting, while values close to 1 are representative of periods without significant melting. Results were compared and we evaluated the mean relative difference on the use of electrical conductivity with respect to water discharge measurements.

## 3.3 Results and discussions

### 3.3.1 Annual hysteresis between electrical conductivity and water discharge

Figures 3.2a and 3.2b show EC against Q for the two melting seasons of the hydrologic years 2012 and 2013, respectively. The colour of the symbols allows to identify the month in which the data have been collected. In general, EC is high at the beginning of the melting season (i.e., about $80\mu S/cm$ in 2012 and $100\mu S/cm$ in 2013), decreasing considerably (to about $38\mu S/cm$) during the summer, when the contribution from snow and ice-melting dominate streamflow generation. As soon as the melting ends (from September), EC rises again. Data within dashed circles indicate the occurrence of rain-on-snow (RoS) events, which were the main

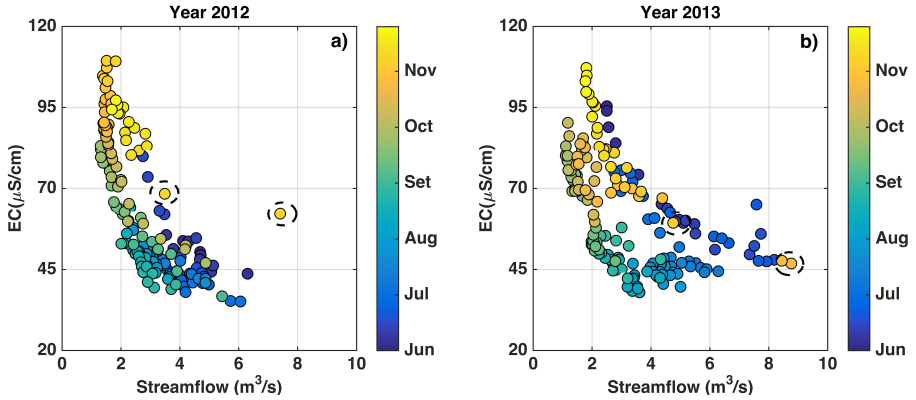


Figure 3.2: Relationship between daily averaged values of EC and streamflow measurements at the Vermiglio gauging station (P2): data recorded from June to November of a)2012 and b)2013. Symbols are coloured according to the month they refer (see the colour bar at the left of each panel) and dashed circles indicate the occurrence of RoS events

flood events registered in both 2012 and 2013. Overall, figures 3.2a and 3.2b show a wide hysteresis cycle relating EC and Q at the annual time scale and interestingly, RoS events fall apart from this cycle.

Hysteresis cycles relating water discharge and tracer concentration (i.e., electrical conductivity) have been observed to occur when streamflow mixes contributions from sources with different dominant scales of variability (e.g., Hooper et al., 1990; Walling and Webb, 1986; Evans and Davies, 1998). Evans and Davies (1998) proposed a classification of hysteresis based on the combination of the following three characteristics: rotational pattern (clockwise or counter-clockwise), curvature (convex or concave) and trend (positive or negative) applicable only if the loop is concave. A positive trend indicates low solute concentration on the baseflow or pre-event component, while a negative trend implies the opposite, that the pre-event component has the highest solute concentration.

Following the previous criteria, our data shows a clockwise rotational pattern with concave curvature and a negative trend on both years, which means that water discharge generated from events (i.e., snow-melting) has lower solute concentration than water discharge generated from pre-event or existing water within the stream, which main component is assumed to be groundwater.

We have seen in Chapter 2 that the width of the hysteresis cycle between electrical conductivity and water discharge can be affected by the thickness of the snowpack present during single events, caused by the delay on the catchment's response to precipitation input due to the storage of rain water within the snowpack. A simultaneous inspection of the snow depth data in figures 3.1b and 3.1c and the hysteresis cycles observed in the years 2012 (figure 3.2a) and 2013 (figure 3.2b) provides evidence that a similar behaviour can be found at the annual scale. In 2013, average snow depth values were 223 $cm$ and 47 $cm$ at CP and PT, while in 2012 equal to 180 $cm$ and 23 $cm$, thus, 2013 showed an increase of around 20%

and 50% at CP and PT with respect to 2012. In addition, snow cover duration was around 20% longer at CP and 40% at PT in 2013 with respect to 2012.

The former features suggest that at the annual scale, the width of the hysteresis loop between EC and Q is influenced by the snow dynamics: high average snow depth values and long periods with snow cover produce very wide loops (figure 3.2b), while the opposite case results on much narrower loops (figure 3.2a).

The seasonal variation of EC can be used to identify periods in which rainfall or snow-melting contribution dominate streamflow generation (see e.g. Richards and Moore, 2003). The hysteresis cycles shown in figures 3.2a and 3.2b resemble the shape of an irregular trapezium, which has been observed and described for the first time by (Collins, 1979). The first side of the trapezium goes from the upper left part of the graph, where Q is low and EC is high due to the dominance of groundwater (in early spring), to the lower right part where Q is high and EC is low due to dilution with melting water. A second stage follows in which Q decreases with EC remaining nearly constant, or slightly varying (from mid July to mid August). The third stage shows a further reduction of Q accompanied by a slight increase of EC (from mid August to mid September). Finally, in the fourth stage Q remains nearly constant or slightly reduces while EC experiences a strong increase towards the starting point of the first stage (from mid September).

Recently, Weijs et al. (2013) showed that under certain conditions, EC can be used to infer water discharge at locations not equipped with stream gauges and where their installation is not possible or reliable rating curves cannot be obtained. Conversion of EC measurements into water discharge is performed by using a power law relationship similar to rating curves.

Figures 3.2a and 3.2b show that in our case a single power law cannot be defined to transform EC data into water discharge, because of the rather wide and transient (i.e., changing from year to year) hysterical cycle. More specifically: the rather wide hysteresis cycles suggest that no unique relationships can be identified between Q and EC. In addition, between June and July EC is low and almost constant, while the water discharge varies wildly, thereby preventing the use of EC to infer water discharge.

When attempting to represent separately the two limbs of the hysteresis cycle, regression of the experimental data with the following expression $Q = a\,EC^m$, two different values of the exponents are obtained from June to November ($m = -1$), when groundwater dominates streamflow, and from July and October ($m = -1.3$), when groundwater mixes with significant rainfall, snow and glacier-melting. Notice that the width of the hysterical cycle is not constant through the winter seasons, depending on the amount of snowpack at the beginning of the melting season and snow cover duration. In addition, rain-on-snow events fall apart from the annual hysteresis cycle. Therefore estimating Q from a non-linear time invariant EC-Q relationship is error prone and leads to estimations affected by a significant uncertainty in glacial and snow fed rivers.

### 3.3.2 Correlation analysis between electrical conductivity and water discharge signals

The wavelet power spectra of precipitation (P), water discharge (Q) and electrical conductivity (EC) time series are shown as panels in figure 3.3. The colour bar ranges from dark blue, indicating low energy, i.e., small amplitude of the fluctuation with that period, to yellow, indicating high energy. The thick black contours indicate the 5% significance level against red noise and the light shading shows the region influenced by edge effects excluded from the analysis.

The signal of P (figures 3.3a and 3.3b) shows localized high energy regions at different temporal scales (i.e., from 16 to 256 hours), caused by the occurrence of very intense precipitation events. The most evident are the large yellow regions observed in November 2012 and October 2013, that correspond to Events 3 and 4 studied in Chapter 2. On the other hand, the signal of Q (figures 3.3c and 3.3d) shows a localized diurnal periodicity (i.e., 24 hours) due to the contribution of snow and ice-melting, with the latter dominating streamflow from spring and the former from July to August, when an important contribution to streamflow originates from ablation of the glaciers. From September to November diurnal periodicity attenuates because the ablation of the glaciers reduces as the temperature decreases (see figures 3.3c and 3.3d).

In the absence of rainfall, the signal of Q shows low energy content with the most energetic modes of variability centered around the periods of 24 hours and 7 days, i.e., 168 hours (figures 3.3c and 3.3d). Localized in time high energy modes of variation, spanning a wider range of periods are observed during flood events in both years, in November 2012 and October 2013, as an effect of the meteorological forcing, which introduces additional modes of variation with respect of the periods without rainfall, and possibly by the activation of flow pathways not contributing when streamflow is dominated by snow and ice melting. The presence of significant contributions from snow and glaciers makes streamflow signal statistically non-stationary and more complex with respect to catchments dominated by rainfall.

EC signal shows a distribution of the energy similar to the one of Q (figures 3.3e and 3.3f), but the diurnal variation (i.e., the 24 hours period) is attenuated with respect to that of Q, with the highest energy is localized in August, when melting water comes entirely from glacier ablation. The broaden of the periods with high energy in correspondence of the high flow events (November 2012 and October 2013), so evident in the streamflow signal, is observed also in the 2012 EC signal, though more localized in time, but it is barely visible in 2013, thereby evidencing, once again, that non-stationarity effects and non-linearities prevent the identification of a simple relationship between Q and EC also during flooding events. Overall, the energy localized around the 24 hours period on the electrical conductivity signal is higher in 2012 than 2013.

Moreover, as exposed on the previous section, snow cover was higher and more persistent in 2013 than in 2012, according to both CP and PT meteorological stations, thereby leading to a larger contribution of ice-melting water in 2012 with respect to 2013. The large energy of the diurnal variation of EC in 2012 with respect to 2013 (see figures 3.3e and 3.3f) is therefore justified by the larger contribution of ice-melting water with EC lower than that of snow-melting water.

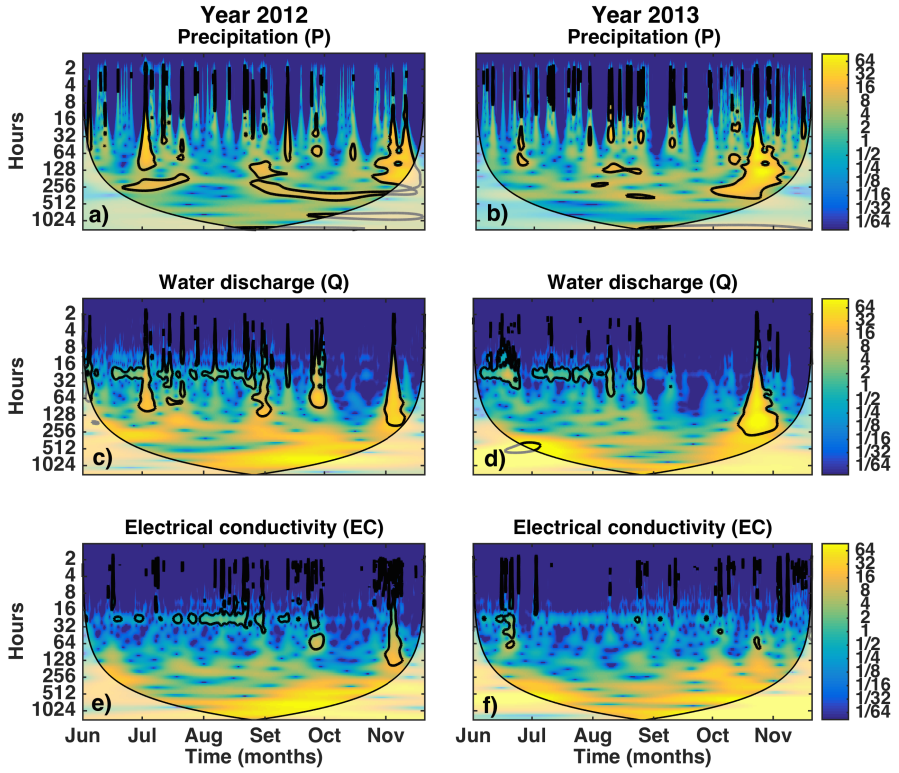


Figure 3.3: Continuous wavelet spectrum, on top: a-b) precipitation for the years 2012 and 2013, respectively; middle: c-d) water discharge for the years 2012 and 2013; bottom: e-f) electrical conductivity for the years 2012 and 2013.

The lower EC values of ice-melting with respect to snow-melting water has been observed in previous studies conducted in the same region (Penna et al., 2014; Engel et al., 2015).

The analysis of the wavelets spectra confirms what already discussed on the previous section: the relationship between EC and Q is complex, statistically non stationary, and dominated by non-linearities, which complicate the identification of a simple relationship between the two signals.

### Wavelet coherence analysis

Figure 3.4 present the results of the wavelet coherence analysis between P-Q and EC-Q. Results are shown as panels where the colour bar indicates the correlation coefficient between the two signals analysed, varying from 0 (uncorrelated) to 1 (fully correlated). Arrows show the phase relationship between the two signals: pointing right when the signals are in phase and pointing left when they are out of phase. Thick contour lines and light shading have the same meaning as in figure 3.3.

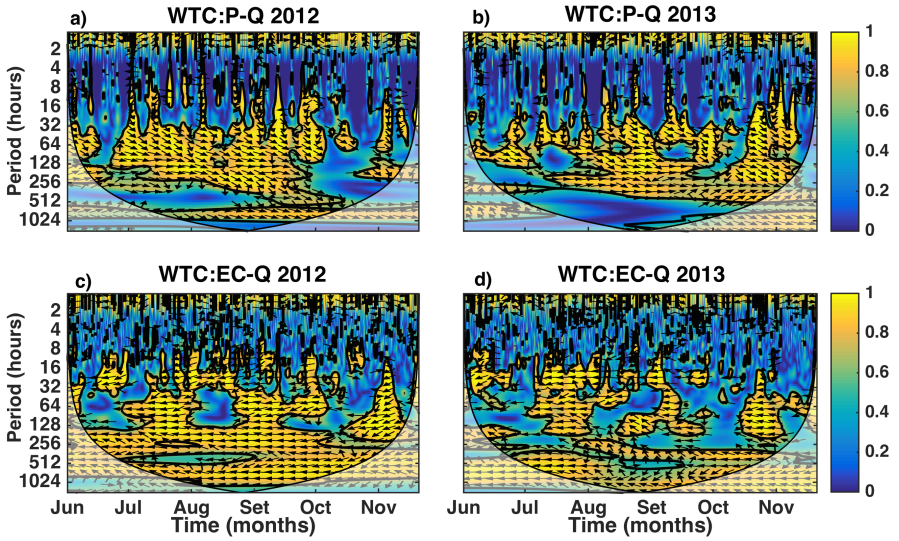


Figure 3.4: Wavelet coherence analysis, on top: a-b) between P and Q signals for the years 2012 and 2013 respectively; bottom: c-d) between EC and Q signals for the years 2012 and 2013.

The coherence between P and Q (figures 3.4a and 3.4b) is similar on both years, extending over a broad range of scales, i.e., 16 to 256 hours. Correlation is particularly high and relatively constant from July to September on both years, although a high correlation region emerges again in November 2012 and at the from the end of October 2013, which coincides with big flood events (Events 3 and 4 described in Chapter 2). Arrows point towards right although showing some variability on the phase angle, which means that P and Q are mostly in-phase, i.e., an increase in precipitation intensity causes also an increase in water discharge, which is expected, with some delay in the catchment's response.

On the other hand, the coherence between EC-Q is mainly out of phase when correlation is significant (i.e., coherence larger than 0.5), as evidenced by predominance of the arrows pointing left (figures 3.4c and 3.4d). This reflects the simple fact that an increase of water discharge causes a reduction of EC, and vice versa a reduction of water discharge leads to and increase of EC. The reduction of EC occurring when Q increases is the consequence of dilution of the groundwater component with large EC caused by the contribution of low EC water from either rainfall or snow-or ice-melting. Nevertheless, in 2013, arrows within the 128-256 hours period show more variability in the phase angle with respect to 2012, where arrows point straight into the left direction.

Moreover, some differences were found in the coherence between EC-Q in 2012 and 2013, with the latter showing high coherence extending over a different range of periods in July (from about 16 to 142 hours in 2013 against 64-256 hours in 2012). In August high coherence is limited around the 24 hours period in both years, while in September a significant coherence of this period is observed only in

the first 10 days. In general, coherence between EC and Q remains high for longer time and extends over a broader range of periods, when the low EC contribution is mainly due to ice-melting water rather than snow-melting. Autumn high flows cause a broadening of the periods with high coherence, but this effect is more localized in time, with respect to the similar broadening of high energy modes in the two signals

The results of the wavelet coherence demonstrate that only when evidencing the modes of variation (periods) on which EC and Q are correlated (present similar fluctuations), it is possible to disclose relevant information in regards to the nature and variability of their relationship. The most interesting features found with this analysis are: (i) it is possible to separate or identify the periods dominated by snow and ice-melting during the year and to observe a significant change on the scales of variability when the catchment shifts from snow-dominated to rainfall dominated regime; (ii) we verify the existence of a correlation between EC and Q signals, i.e., out of phase. In the next section, we further explore the correlation and estimate the time lag between EC and Q.

**Cross-correlation analysis**

We performed a cross-correlation analysis considering the time series of EC and $log_{10}Q$ (see further details on section 3.2.3). Figures 3.5a and 3.5b show the daily maximum correlation coefficient (XC) for the years 2012 and 2013 respectively, computed according to equation 3.4. In addition, we show the variation of the time lag on which this maximum correlation occurs (figures 3.5c and 3.5d). In addition, the black dashed line indicates a positive lag of 3 hours to be used as reference value.

According to figures 3.5a and 3.5b, cross-correlation between EC and $log_{10}Q$ is always negative, which is consistent with the out of phase relationship observed on the wavelet coherence analysis performed in the previous section, with a maximum absolute value of 0.98 on both 2012 and 2013. Absolute values of correlation equal or larger than 0.5 are almost exclusively located between July to mid September, when streamflow is dominated by snow and glacier-melting.

Cross-correlation also allowed us to identify and quantify a relative constant time lag of 1 to 3 hours between EC and Q time series (see figures 3.5c and 3.5d), which starts earlier in the year 2012 (mid June) with respect to 2013 (July). The previous served as an indicator of the earlier snow-melting in 2012, which, due to the thinner snowpack produced during this year, determines an earlier glacier-melting, further verifying what observed with the continuous wavelet transform. Outside the melting season, cross-correlation values decrease (figures 3.5a and 3.5b) and the time lag oscillates between positive and negative lags. The positive and relatively constant time lag during the melting season suggests that variations on EC followed the variations of Q and the propagation of EC is slower than the one of Q. On the other hand, the large variations on the time lag (positive and negatives) observed mainly from October occur because with the end of snow and ice-melting contribution, the larger contribution of rainfall events strongly affect the relationship between EC and Q.

Moreover, cross-correlation analysis further support the wavelet coherence re-

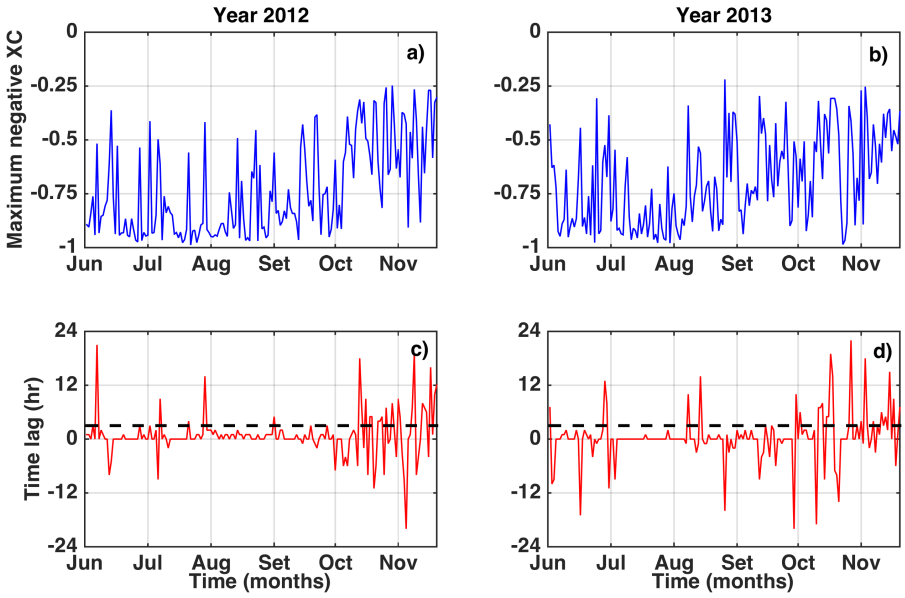


Figure 3.5: Cross-correlation analysis between *EC* and the logarithmic transformation of *Q* time series of the years 2012 and 2013: a-b) Maximum negative cross correlation (XC); c-d) time lag on which the maximum negative XC occurs.

sults, there is a significant change in the temporal scales of variability and correlation between EC and Q as the catchment shifts from a snow and ice-melting regime to a rainfall controlled regime.

### 3.3.3 Analysis of the diurnal cycles of streamflow and electrical conductivity

While the amplitude and timing of occurrence of maximum and minimum values are important characteristics of the diurnal streamflow cycles and have been used on previous studies to identify the hydrological processes contributing to streamflow generation (see e.g. Lundquist and Cayan, 2002; Lundquist et al., 2005; Lundquist and Dettinger, 2005; Mutzner et al., 2015), the use of similar characteristics of EC diurnal cycles for this purpose is rare. We analyse both EC and Q diurnal cycles and compare the daily contribution to streamflow from snow-melting in the Vermigliana catchment obtained with both time series.

Figures 3.6 and 3.7 show the minimum and maximum values of electrical conductivity and streamflow diurnal cycles of the years 2012 and 2013 respectively. The symbols are coloured according to the Julian days and go from dark blue (June) to yellow (November). The radial plots indicate the hours of occurrence within the day in the clockwise direction and dark grey rings denote the range of values of either Q (figures 3.6a, 3.6b, 3.7a and 3.7b) or EC (figures 3.6c, 3.6d, 3.7c and 3.7d).

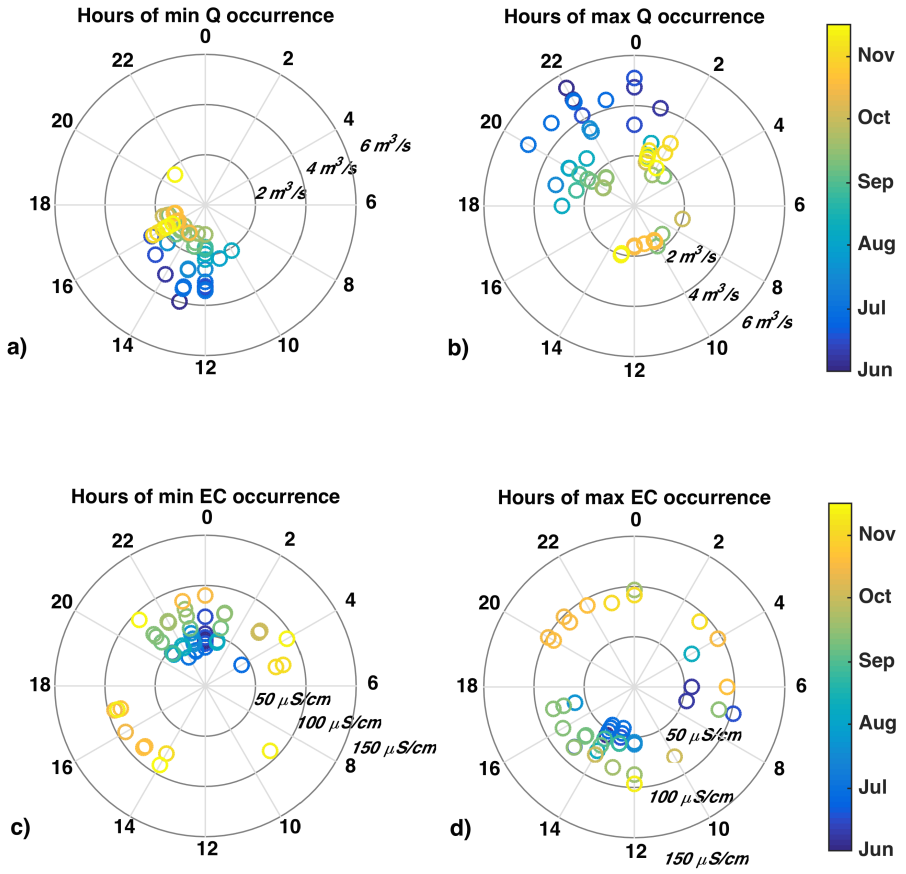


Figure 3.6: Radial plots indicating the hours of occurrence of: a-b) minimum and maximum Q, c-d) minimum and maximum EC of the year 2012 as a function of the 24 hours within a day. The symbols are coloured according to the month and go from dark blue (June) to yellow (November). Grey rings indicate the range of value of Q or EC according to the case.

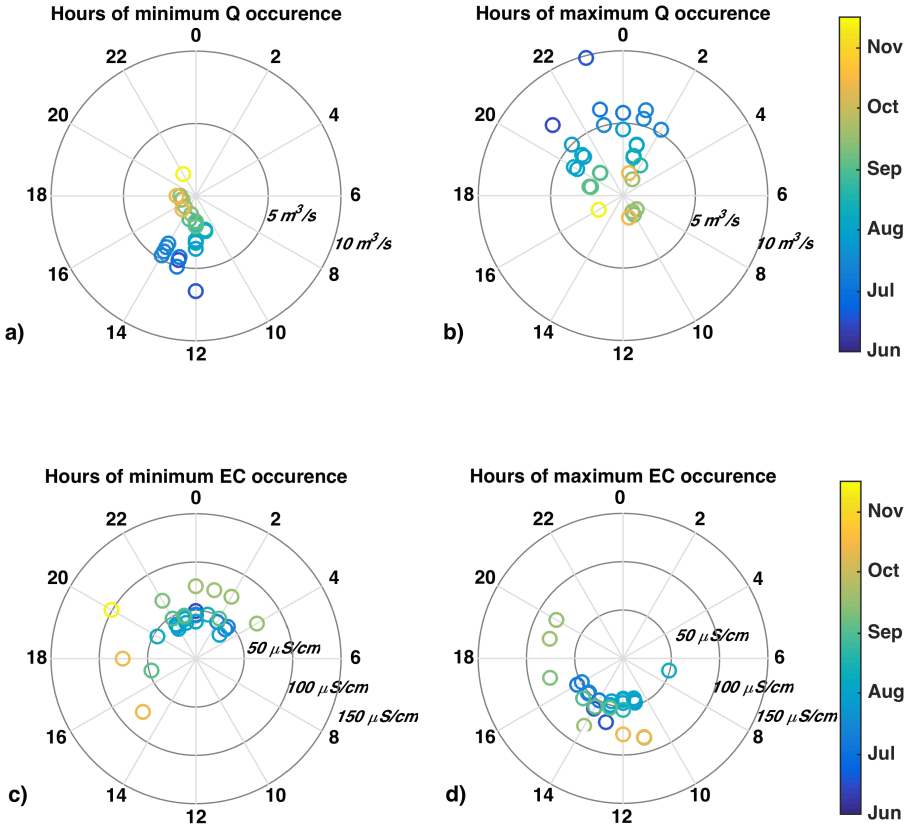


Figure 3.7: Radial plots indicating the hours of occurrence of: a-b) minimum and maximum Q, c-d) minimum and maximum EC of the year 2013 as a function of the 24 hours within a day. The symbols are coloured according to the month and go from dark blue (June) to yellow (November). Grey rings indicate the range of value of Q or EC according to the case.

From mid June to mid September, minimum Q (figures 3.6a and 3.7a) and maximum EC (figures 3.6d and 3.7d) occur mainly from late morning to afternoon, between 10:00 and 16:00 on 2012 and from 11:00 to 14:00 on 2013, with minimum Q preceding maximum EC. Maximum Q (figures 3.6b and 3.7b) and minimum EC (figures 3.6c and 3.7c) occur instead from evening to early morning, between 18:00 and 1:00 on 2012 and from 19:00 to 2:00 on 2013 (with maximum Q that precedes minimum EC).

Similar variations in the timing of occurrence of maximum Q along the season were observed in another study as a result from the increasing heterogeneity of snow depth and melt rates (see Lundquist and Dettinger, 2005). The heterogeneity on snow depth may depend on two factors: the elevation gradient and the variability in the precipitation events, which can change from year to year according to the characteristics of the events.

Typically melting starts at low elevations and snow covered areas retreat to higher elevations as the season advances, hence postponing the time of occurrence of maximum Q due to longer travel times. Moreover, the delay in the travel time at the beginning of the melting season decreases with the progress of the season due to the reduction on the thickness of the snowpack, consequently, the timing of occurrence of maximum Q shifts to earlier in the day. Therefore a long delay reflects deeper snowpacks and long travel times (Lundquist and Dettinger, 2005).

Table 3.1: Main features of the diurnal cycle of Q

| **Year** | **Snow depth value** | **Snow cover duration** | **Prevailing mechanism** | **Catchment travel time** | **Timing of max Q** |
|---|---|---|---|---|---|
| 2012 | low | short | water storage within the snowpack | short | anticipated |
| 2013 | higher | longer | water storage within the snowpack and snow retreating to higher elevations | longer | mainly postponed |

We observe different mechanisms on each year (see details on table 3.1): 2012 presents low average snow depth values during the season and short snow cover duration, with maximum Q (figure 3.6b) occurring later during the day in June (between 22:00 and 1:00) than in July and August (between 18:00 and 1:00). Thus, daily maximum Q values are anticipated with the progress of the season. Instead 2013 presents 45% higher average snow depth value and 30% longer snow cover duration with respect to the previous year, while maximum Q (figure 3.7b) occur late during the day from June until the end of July (between 21:00 and 2:00) and that shifts to earlier in the day (between 19:00 and 1:00) starting from August. Notice that minimum EC daily values show similar dynamics to maximum Q values, yet the shifting in the timing of occurrence is not so clear, we observe instead overlapping due to the delay with respect to the signal of Q.

In addition, we looked in detail at the difference in the timing of occurrence (i.e., time lag) between maximum Q and minimum EC. Hence, figures 3.8 and 3.8 show the evolution in time of this delay: in both years, we observe a relative constant value between 1 and 3hours from June to the beginning of September.

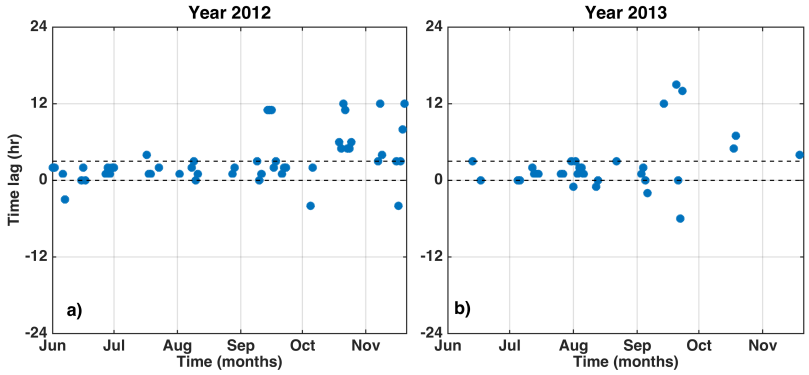


Figure 3.8: Evolution in time of the difference between the timing occurrence of maximum Q and minimum EC: a) 2012; b) 2013. The dashed black lines indicate values between 0 and 3 hours time lag.

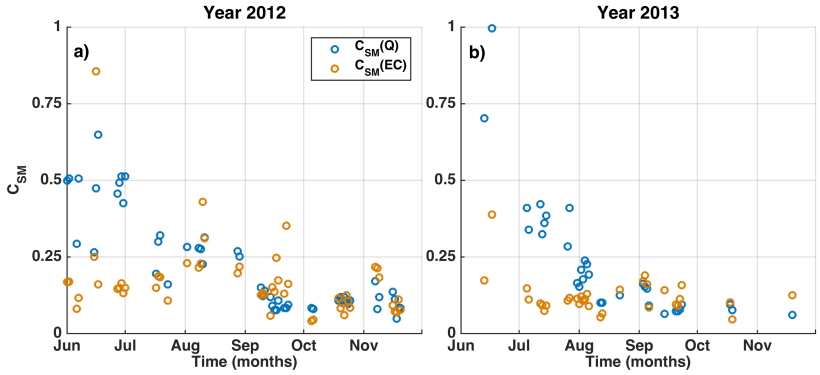


Figure 3.9: Daily contribution from snow-melting to streamflow using Q (blue) or EC (orange) data during the melting seasons of: a) 2012 and b) 2013.

From mid September, the lag between daily extremes of Q and EC shows larger variations, in agreement with the wavelet coherence and cross-correlation analyses (see section 3.3.2). Thus, the timing of occurrence of maximum Q ca also provides further insights into catchment functioning.

Given the similarities found between Q and EC diurnal cycles, we estimated the amplitude of both signals in order to estimate the daily contribution due to snow-melting $C_{SM}$, by computing equation 3.5. Figures 3.9a and 3.9b show the results for $C_{SM}$ estimated with Q (blue) and EC (orange) for the years 2012 and 2013, respectively. Similar shapes are observed on both years and 2013 presents higher values than 2012 as a result of larger daily streamflow fluctuations due to the larger contribution from snow-melting in this year. The ratio defined by equation 3.5 ranges from 5% to 99% if estimated with Q and from 5% to 85% if estimated with EC.

In both years, snow-melting contribution presents a decrease similar to an

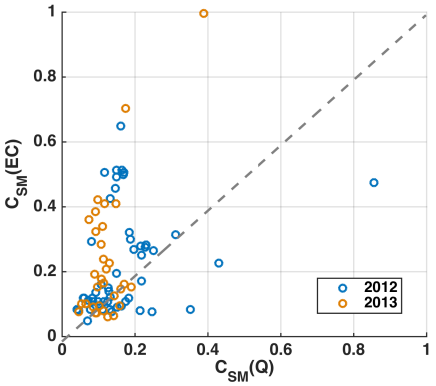


Figure 3.10: Probability plot between the contribution due to snow-melting estimated with Q ($C_{SM}(Q)$) and with EC ($C_{SM}(EC)$).

exponential decay when estimated with water discharge data (blue circles) and a steeper decrease is observed in the snow-melting contribution in 2013 (figure 3.9a) with respect to 2012 (figure 3.9b). The contribution estimated with EC (orange circles) underestimates the first part of the snow-melting (June and July) in both years, while during August, when most of the contribution comes from ice-melting, values obtained with EC are closer to the ones obtained with Q. The mean relative difference found when using EC instead of Q to estimate this ratio is of 12%. Moreover, figure 3.10 shows the agreement between the contribution estimated with Q (blue circles) and the one estimated with EC (orange circles). In 2012 the agreement between the contribution estimated with Q and with EC is relatively good up to quantiles of 0.4, while higher quantiles are mostly underestimated by EC. In 2013 instead the agreement is good only up to quantiles of 0.2 and the rest are underestimated by EC.

Overall, the analysis of EC and Q diurnal cycles of the Vermigliana catchment showed how the timing of occurrence of minimum and maximum values can be used to obtain valuable information into catchment functioning. EC and Q diurnal cycles can give important information relating the dynamics of the snowpack during the melting season, which is different every year in accordance to the meteorological forcing. Yet, the use of the EC signal alone for this purposes does not provide reliable results.

## 3.4 Conclusions

This chapter shows how stream water electrical conductivity together with streamflow measurements can give valuable insights into the complex hydrological characteristics of Alpine catchments. Thus, the analyses performed on the experimental dataset of the Vermigliana catchment can serve as a reference tool for similar environments.

We first analysed the limitations on the use of EC data as a proxy of Q and

observed the wide hysteresis cycle relating EC and Q at the annual scale. The annual hysteresis is influenced by the amount of snow fallen in the previous winter season and by the snow cover duration within the catchment, with some points that significantly depart from this cycle due to the occurrence of rain-on-snow events. All the previous reasons complicate the use of a single EC-Q relationship for the prediction of water discharge based on EC measurements.

Second, we developed a methodology to fully explore the correlation between EC and Q and its use in the identification of timing of the main streamflow sources. The temporal variability of EC and Q can be investigated by applying the continuous wavelet transform to each signal separately. However, the information of most interest can only be obtained when evidencing the modes of variation (periods) on which EC and Q are correlated (present similar fluctuations). Thus wavelet coherence analysis evidenced the out of phase (i.e., an increase on streamflow leads to an decrease of electrical conductivity values) correlation between EC and Q, which extends over a range of scales and whose amplitude changes in time. In addition, wavelet coherence allowed us to identify the periods dominated by snow and ice-melting during the year and to observe a significant change on the scales of variability when the catchment shifts from snow-dominated to rainfall dominated regime. Moreover, we further explored the correlation between EC and Q with a cross-correlation analysis, which showed that the maximum correlation between EC and Q is relatively constant presenting a time lag between 1 and 3 hours during the melting season, while much larger oscillations occur outside this period.

Furthermore, the analysis of EC and Q diurnal cycles highlighted interesting features: (i) the shifting in the timing of occurrence of maximum Q provides qualitative information about the snow dynamics, which is different every year, and also on the dynamics of catchment's travel time that changes with the progress of the season; (ii) the amplitude of EC and Q diurnal cycles can be used for estimating the daily contribution from snow-melting to streamflow on each year, yet the better results are obtained with the signal of Q.

Overall, the results of this work show that an individual analysis of electrical conductivity and streamflow signals gives limited information with respect to the combined analysis, which instead evidences a transient dynamics in the correlation between both signals, hence providing valuable insights into the catchment's hydrological characteristics. Therefore this study represents an important contribution in the context of Alpine catchments, which may lead to a more rigorous application of the EC-Q correlation for hydrological and geochemical purposes (for e.g., streamflow estimation, geochemical cycles and hydrograph separation) and can further support future studies on the different transfer functions that characterize water and solute transport in snow and glacier-melting dominated catchments.

*Chapter* 4

# Temporal variability of long-term hydrological time series

## 4.1 Introduction

Streamflow variability is the result of many intertwined hydrological and climate processes occurring at the catchment scale (Ceola et al., 2010). The variations on climate affect the temporal occurrence of hydrological patterns, more specifically, catchments with strong seasonal precipitation cycles have considerable regularity of high and low flow periods with respect to catchments with a more uniform precipitation (Carey et al., 2013).

Traditional hydrological long-term time series (i.e., precipitation, temperature and streamflow) can provide significant contributions into the study of streamflow variability. Recent studies have focused their attention on the relationship between precipitation (P) and streamflow (Q) and the link between storage and discharge, with the final aim of defining a joint concept for catchment response (Kirchner, 2009; Ali et al., 2011; Peters and Aulenbach, 2011; Shook and Pomeroy, 2011). However, the main mechanisms controlling streamflow generation in Alpine catchments, i.e., melting and snow accumulation, are driven by the sensitivity of these systems to temperature (T) changes (see e.g., Kuhn and Batlogg, 1998; Barnett et al., 2005; Stewart, 2009; DeBeer et al., 2010; Tobin et al., 2013; Penna et al., 2014; Engel et al., 2015). Therefore these regions are expected to be significantly affected by the rise of temperature due to climate change (Barnett et al., 2005). The previous highlights the importance to explore likewise the nature of variability between temperature and streamflow fluctuations.

Moreover, given the complexity characterizing Alpine environments, the need to understand how short and long-term climate variations may influence streamflow variability calls for the use of alternative techniques for the analysis of hydrological time series. By comparing streamflow variability between catchments and exploring the relationship between atmospheric forcing and streamflow, the identification of similarities and differences in the observed patterns can contribute to a better understanding of these systems, allowing us to improve existing concep-

tual models or to define more suitable frameworks for future model applications. Only few studies focused on studying the relationship P-Q have included specific analyses of snow-dominated catchments (Carey et al., 2013). Therefore, the combined analysis of the relationships P-Q and T-Q may provide further insights into the hydrological response or the sensitivity of Alpine systems to climate changes.

On this chapter, we investigate two nearby Alpine catchments located in North-Eastern Italy, both with similar features: Vermigliana ($78.9km^2$) and Sarca di Genova ($77.52km^2$), characterized by the presence of glaciers in their upper part. Daily records of observed precipitation, temperature and streamflow from the period 1996-2014 are available for both study cases. We use Hovmöller diagrams (Hovmöller, 1949) and the continuous wavelet transform (Torrence and Compo, 1998) to investigate daily and seasonal climate influences on streamflow variability. Furthermore, we use wavelet coherence (Grinsted et al., 2004) to explore the correlation (periods on which two time series experience oscillations at a similar frequency) between P-Q and T-Q at different temporal scales.

The main objectives of this chapter are: (i) to explore patterns and scales of variability of the hydrological time series of two case studies within the Alpine region using two different tools (i.e., Hovmöller diagrams and continuous wavelet transform); (ii) to further investigate the link between the variability of P-Q and T-Q using the wavelet coherence.

## 4.2 Study cases and available data

### 4.2.1 Vermigliana and Sarca di Genova catchments

Two nearby catchments were considered for this study: the Vermigliana (see description in Chapter 2) and Sarca di Genova, both located in North-East Italy with elevations that range from 1165 m.a.s.l. to 3548 m.a.s.l. in the case of Vermigliana and from 1119 m.a.s.l. to 3422 m.a.sl. for the Sarca di Genova. Figure 4.1 shows the boundaries of the study area and the location of the meteorological and hydrometric monitoring sites used in the analysis.

Sarca di Genova river drains a catchment area of $77.52km^2$ at the gauging station of Ponte Santa Maria (1119 m.a.s.l.). Like Vermigliana, this catchment can be considered in pristine conditions and is characterized by two important glaciers: Mandrone and Passo della Lobbia, that combined, cover about 25% of the total catchment area (see more details in Ranzi et al. (2010)). Main features of both catchments are reported on Table 4.1.

Both catchments present similar characteristics and the main difference can be found in the glacier coverage, which is three times larger in Sarca di Genova with respect to Vermigliana. Likewise, the runoff coefficient $C_{flux}$, is two times larger on Sarca di Genova, indicating a higher contribution from glacier melting in this catchment. The previous suggests a significant retreat of the glaciers within the catchment. Notice that Ice mass losses take place with fragmentations processes that generate a larger number of glaciers of smaller size and therefore less resistant to climate changes. Glaciers in the European Alps lost almost 50% in area from 1850 to 2000 (Zemp et al., 2006). In particular, during a recent campaign (2010-

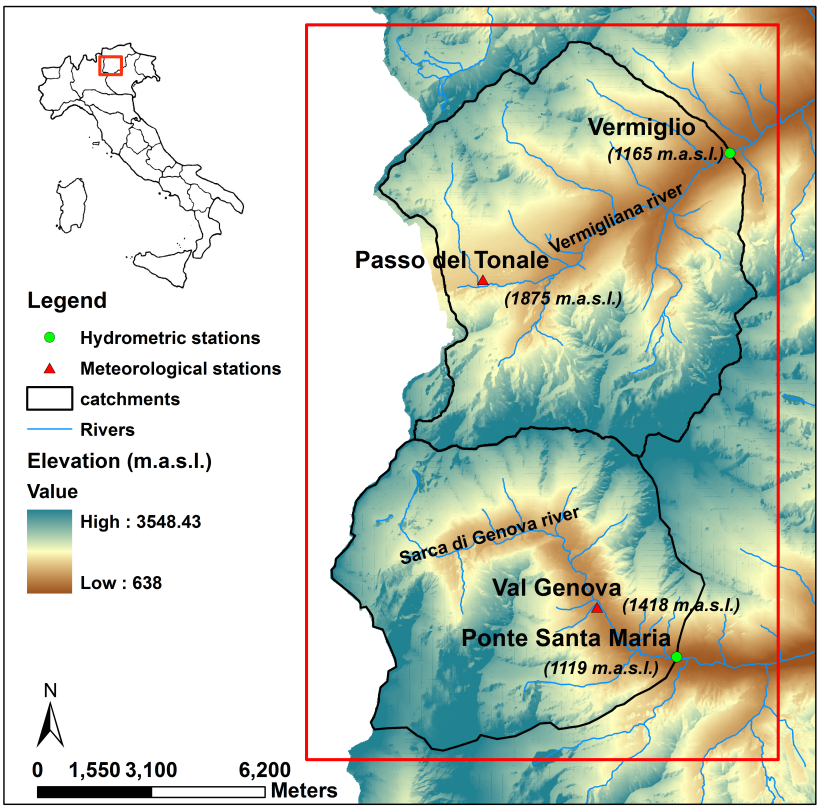


Figure 4.1: Location map of the catchments under study and monitoring stations. The map is coloured by elevation which ranges from 638 to 3548 m.a.s.l. Red triangles indicate meteorological stations: Passo del Tonale (PT) and Val Genova (VG) while green dots indicate the location of the hydrometric stations for the continuous monitoring of streamflow: Vermiglio and Ponte Santa Maria. The upper left inset shows the location of the catchments within the Italian territory.

2011) performed in the ablation area of the Mandrone glacier, in the proximities of left and right margins, intense melting phenomena was observed at the base of the glacier, which could have produced fragmentations on the glacier surface (Provincia Autonoma di Trento, Meteotrentino, 2012).

### 4.2.2 Observed time series

Precipitation and air temperature at daily time scale were provided by MeteoTrentino (http://www.meteotrentino.it) and streamflow records at hourly resolution by the Ufficio Dighe of the Province of Trento (http://www.floods.it). Streamflow data were after averaged into mean daily values. Figures 4.2 and 4.3 show the available data for Vermigliana and Sarca di Genova catchments respec-

Table 4.1: Vermigliana and Sarca di Genova main features.

| **Main characteristics** | **Vermigliana** | **Sarca di Genova** |
|---|---|---|
| Observation period | 1996-2014 | 1996-2014 |
| Catchment area $[km^2]$ | 78.9 | 77.52 |
| Mean elevation $(m.a.s.l.)$ | 2357 | 2392 |
| Meteorological station $(m.a.s.l.)$ | 1875 | 1418 |
| Hydrometric station $(m.a.s.l.)$ | 1165 | 1119 |
| Glacier coverage [%] | 8.55 | 25 |
| Mean annual precipitation[a] [mm] | 1351 | 1203 |
| $C_{flux}$[b] [-] | 0.82 | 1.63 |

[a]calculated from observation period

[b]$C_{flux}$=Runoff volume per year/Precipitation volume per year, calculated from observation period

tively.

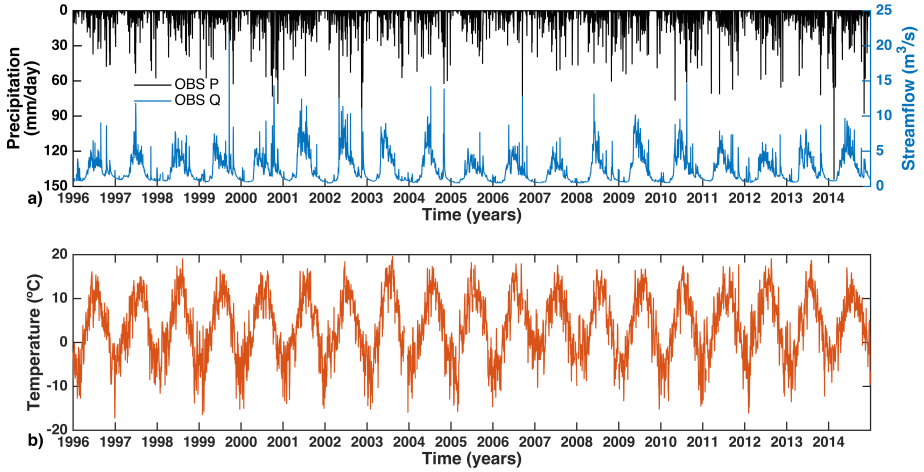


Figure 4.2: Vermigliana observed daily time scale data from the period 1996-2014: a)streamflow (blue line) and precipitation (black bars), b) temperature data.

Observed precipitation in the Vermigliana catchment (Figure 4.2a) presents slightly higher intensities with respect to Sarca di Genova (Figure 4.3a) and analogously, daily observed temperature is relatively higher in Sarca di Genova (Figure 4.3b) with respect to the Vermigliana (Figure 4.2b). These differences can be attributed to the location of the metereological stations: Passo del Tonale station is located at a higher altitude with respect to Val Genova station (see Figure 4.1).

In general, both catchments present high peaks on streamflow from May to August, with higher values observed on Sarca di Genova catchment (figure 4.3a), up to $68m^3/s$, while the maximum daily value registered on the Vermigliana is $22m^3/s$ (figure 4.2a). During the rest of the year (September to April) Vermigliana

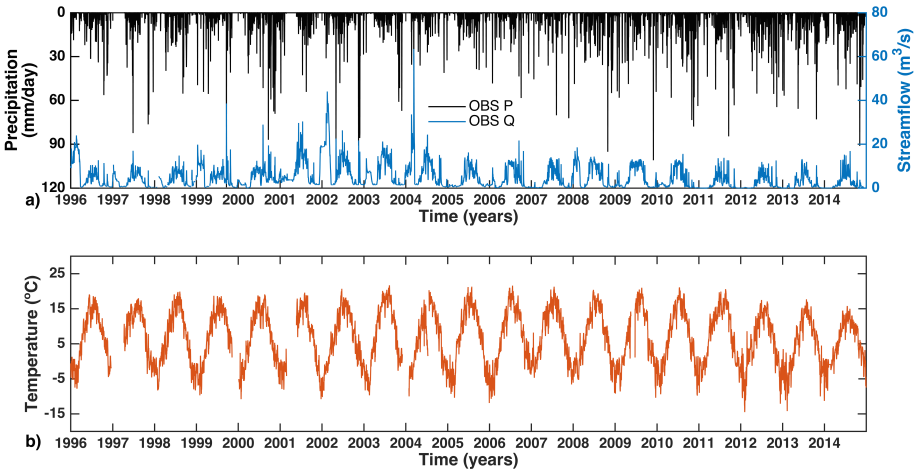


Figure 4.3: Sarca di Genova observed daily time scale data from the period 1996-2014: a) streamflow (blue line) and precipitation (black bars), b) temperature data.

shows a constant low-flow regime with few peaks around October-November due to very intense precipitation events. Sarca di Genova instead presents unusual high peaks around December-February during the period 1996-2005, which in most of the cases coincide with intense rainfall events. However, from 2006 a regular low-flow regime is observed from September to April with some high-peaks during October-November. Temperature time series (figures 4.2b and 4.3b) show a very clear and persistent annual cycle.

On the following section, the observed time series (i.e., precipitation, temperature and streamflow) of Vermigliana and Sarca di Genova catchments are analysed and compared using two different tools: Hovmöller diagrams and wavelet analysis.

## 4.3 Methods

We provide a detailed description of the methods applied for the identification of patterns and scales of variability of the observed time series (i.e., Hovmöller diagrams and continuous wavelet transform) and to explore the link between atmospheric forcing and streamflow (i.e., wavelet coherence).

### 4.3.1 Hovmöller diagrams

Hovmöller diagrams (see Hovmöller, 1949) are commonly used for plotting meteorological data in order to highlight the role of waves. On these diagrams, axes are typically represented by longitude or latitude (abscissa) and time (ordinate), with the value of some field represented through colour or shading. However,

Hovmöller diagrams have also been used to plot the time evolution of vertical profiles of scalar quantities (e.g., temperature, density, depth, pressure) (see e.g., Marengo et al., 2011).

Hovmöller plots were built by displaying, as an image, monthly averaged values from the observed time series using a range of colours, thus each element specifies the colour for one pixel of the image. The resulting time-time plot is an m-by-n grid of pixels where each column "m" indicates the year and each row "n" indicates the month.

### 4.3.2 Wavelet analysis

Wavelet analysis can be an useful tool to disentangle the periods of variations of hydrological signals and identify their change of strength in time. For details on the theoretical background of the continuous wavelet transform and wavelet coherence analysis, the reader may refer to Section 3.2.2. in Chapter 3.

In addition, in this chapter we applied the averaging in time and scale of the wavelet spectrum, thus we estimate the global wavelet power spectrum (i.e., averaging in time) and the scale-averaged wavelet power over a specific band (i.e., averaging in scale).

#### Global wavelet power spectrum

The time-averaged wavelet spectrum over a certain period is given by the following expression (Torrence and Compo, 1998):

$$\overline{W_n}^2(s) = \frac{1}{n_a} \sum_{k=n_1}^{n_2} |W_n(s)|^2 \tag{4.1}$$

where the index $k$ is arbitrarily assigned to the midpoint of $n_1$ and $n_2$, and $n_a = n_2 - n_1 + 1$ is the number of points averaged over. By applying equation (4.1) at all available discrete time steps a smoothed wavelet plot is obtained. However, if equation (4.1) is averaged over all the local wavelet spectra, we obtain the global wavelet spectrum, which provides an unbiased and consistent estimation of the true power spectrum of a time series (Torrence and Compo, 1998):

$$\overline{W}^2(s) = \frac{1}{N} \sum_{n=0}^{N-1} |W_n(s)|^2 \tag{4.2}$$

where $N$ is the number of points in the time series.

#### Scale-averaged wavelet power

In order to investigate the fluctuations in wavelet power over a range of scales, Torrence and Compo (1998) have defined the scale-averaged wavelet power as a time series of the average variance in a certain band, calculated as the weighted sum of the wavelet power spectrum over scales $s_1$ to $s_2$:

$$\overline{W_n}^2 = \frac{\delta_j \delta_t}{C_\delta} \sum_{j=j_1}^{j_2} \frac{|W_n(s_j)|^2}{s_j} \tag{4.3}$$

## 4.4 Results and discussions

### 4.4.1 Catchment intercomparison with Hovmöller plots

The inter-comparison between both case studies allowed us to improve our understanding on the nature of variability in Alpine catchments. Following the method described on Section 4.3.1, Hovmöller plots were built from the observed time series of Vermigliana and Sarca di Genova catchments (see figures 4.4, 4.5 and 4.6). Each cell of the map corresponds to a monthly averaged value from the observed time series (i.e., precipitation, temperature and streamflow), thus each cell or pixel is coloured with the colour corresponding to the colour bar shown at the right side of each graph and white cells evidence missing data. The sum of

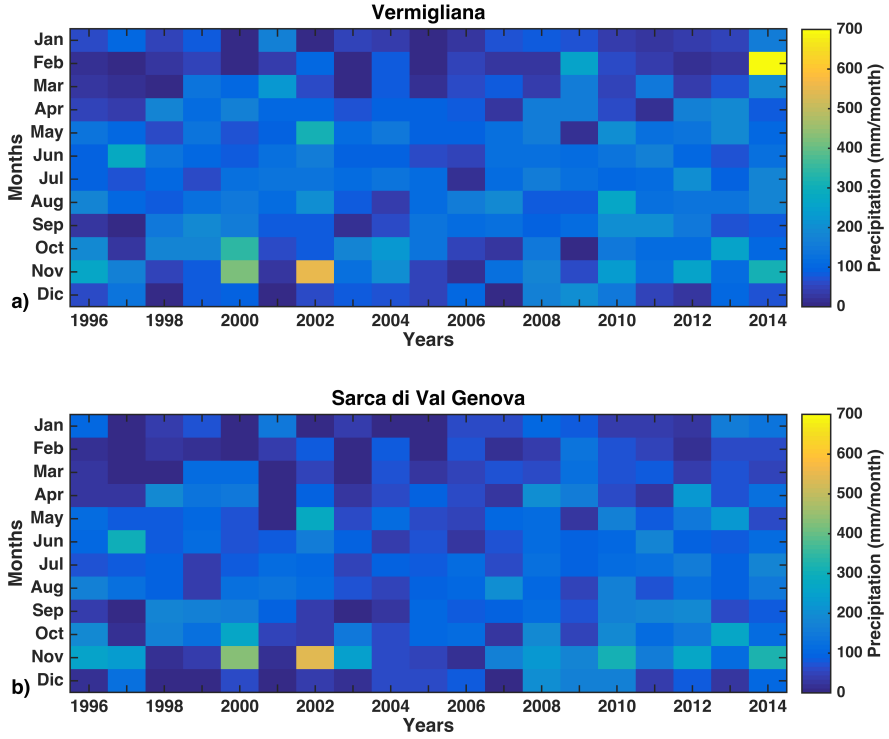


Figure 4.4: Hovmöller plots built from the observed precipitation time series: a)Vermigliana and b)Sarca di Genova. The colour bar at the right side of each graph indicates precipitation intensity (mm/month) and goes from dark blue to yellow. White cells indicate missing data

the total amount of rainfall on each month may be more useful with respect to an averaged monthly value when the objective of the analysis is to identify the existence of temporal patterns. Therefore, for the case of precipitation time series, we

used the accumulated precipitation at monthly scale instead of monthly averaged values. Figure 4.4 depicts Hovmöller plots built with precipitation data for Vermigliana (a) and Sarca di Genova (b) catchments. No particular patterns could be identified from this plots, although it is possible to make a division between the lowest observed monthly values (i.e., between 0 and $100mm$), which occur from December to February, from the rest of the year, on which monthly precipitation ranges between $100mm$ and $300mm$. High values are observed in November of the years 2000 (green) and 2002 (orange) on both catchments, corresponding to values of around $450mm$ and $600mm$ respectively. The highest value is observed on February 2014 in the Vermigliana catchment (figure 4.4a).

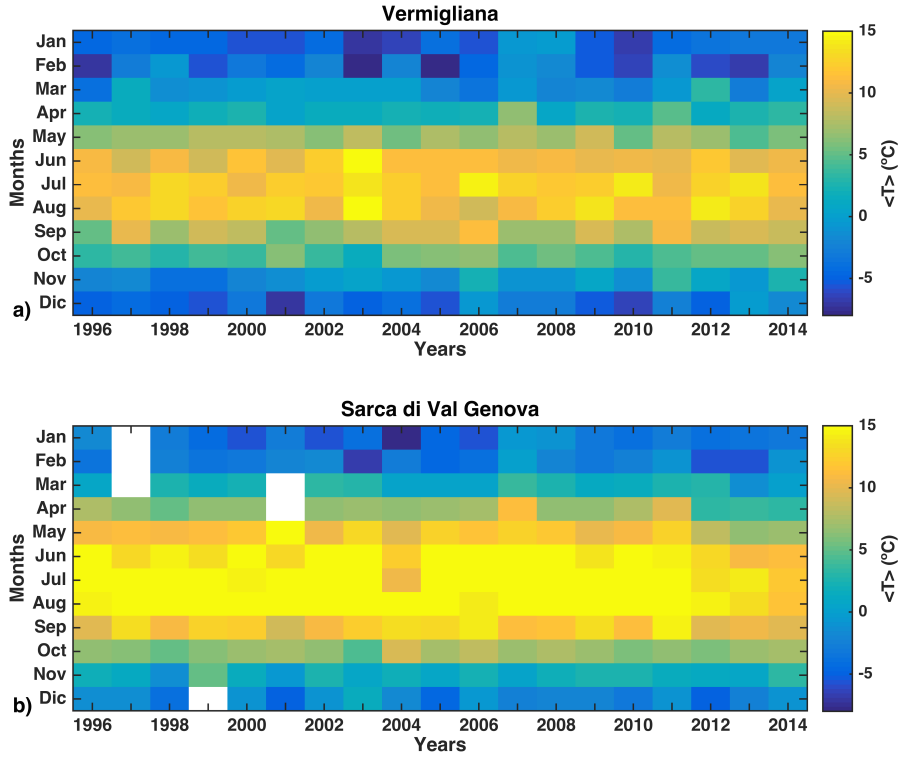


Figure 4.5: Hovmöller plots built from the observed temperature time series: a)Vermigliana and b)Sarca di Genova. The colour bar at the right side of each graph indicates monthly averaged values of air temperature ($C°$) and goes from dark blue ($-5°C$) to yellow ($15°C$). White cells indicate missing data

Hovmöller plots built from averaged monthly values obtained from temperature time series are shown in figure 4.5. As expected the graphics show a strong seasonality: the lowest temperature (i.e., below $0°C$) is observed mainly from December to February, followed by a transition period from March to May on which temperature gradually increases ranging from 0 to $10°C$. The highest tem-

peratures (i.e., higher than $10°C$) are observed from June to August, while from September to November a second transition period is observed, on which average temperature instead decreases, ranging from 10 to $0°C$. Overall, the meteorological station from Sarca di Genova catchment presents higher temperature values with respect to the Vermigliana. The seasonal pattern on streamflow time series

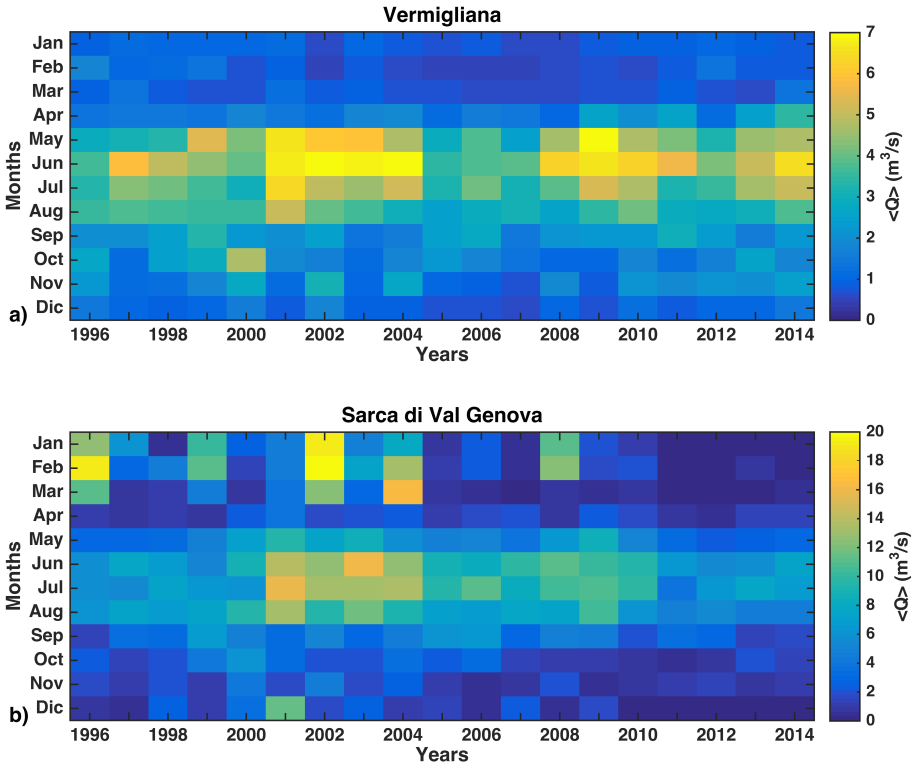


Figure 4.6: Hovmöller plots built from the observed streamflow time series: a)Vermigliana and b)Sarca di Genova. The colour bar at the right side of each graph indicates the range observed within the image and goes from minimum (dark blue) to maximum (yellow) values. White cells indicate missing data.

is likewise very clear in the Vermigliana catchment (figure 4.6a), which is characterized by high-flows observed mainly from May to August which range from 4 to 8 $m^3/s$, while the rest of the year (i.e., from September to April) is characterized by relatively constant low-flow regime that goes from 0.2 to values below $4m^3/s$. In addition, a second pattern can be identified: the highest streamflow values are observed along the band located between May and August of the periods 2001-2004 and 2008-2011. Sarca di Genova catchment (Figure 4.6b) shows a similar separation between high and low-flow seasons, with the first taking place from May to August and the second from September to April. The overall monthly values are nearly three times higher than in the Vermigliana catchment and the

second pattern, which includes the highest values along the entire observation period (from May to August), was found to occur in the same years and with the same frequency. On the other hand, in this catchment, high-flow values are also observed from January to March on the following years: 1996, 1999, 2002, 2004 and 2008.

As seen from figures 4.4, 4.5, and 4.6, Hovmöller plots constitute a simple approach useful to assess the temporal variability of hydrological time series. The time-time diagrams presented above disclosed interesting features that allowed us to make an initial catchment intercomparison. Precipitation time series does not show any particular patterns, yet in general both catchments present similar range of monthly values. Temperature however, evidences a very marked seasonality at the annual scale, which controls the main hydrological processes occurring on both catchments: snow accumulation during winter (December to February) due to low mean temperatures, while snow or ice-melting from May to August due to the significant increase of mean temperatures. The effect of temperature fluctuations on streamflow can also be observed on the Hovmöller plots (figure 4.6). High flow are observed from May to August with the main contribution coming from melting due to the rise of temperature above the freezing point also at high elevation, while a relatively constant low-flow regime during the rest of the year since at high elevations precipitation falls mostly as snow from December to February, this snow is accumulated and stored as snowpack due to the low temperatures. On the other hand, high-flows were also observed during winter in some years in Sarca di Genova catchment (figure 4.6b), which in most of the cases correspond to large precipitation events, as seen on figure 4.3a, and more important, do not affect significantly the annual pattern observed in the Hovmöller plot showing monthly data. Furthermore, an interesting second pattern during the melting period was observed in both catchments, with a duration of four consecutive years completing two cycles with a separation of three years between cycles. This last pattern is further analysed on the following section.

### 4.4.2 Catchment intercomparison with wavelet analysis

The Hovmöller plots presented in the previous section provide a preliminary identification of patterns between the observed time series of P, T and Q. To further explore the scales of variability of these patterns, we applied the continuous wavelet transform to the daily observed time series of both catchments. The results are presented in this section as figures composed by three panels, where the top left panel depicts the continuous wavelet power spectra (for further detailes on this method please refer to Section 3.2.2 in Chapter 3), on top right the global wavelet spectra calculated with equation 4.2 and, on the bottom panel, the scale-averaged wavelet power (equation 4.3) over the 0.5-2 year band. The wavelet power spectra ranges from blue, indicating low energy (i.e., small amplitude of the fluctuation at an specific period) to yellow, indicating instead high energy regions. Thick black contours denote the 5% significance level against red noise and the unreliable portion of the spectrum because of the edge effects is shown as a lighter shade.

Figures 4.7 and 4.8 depict the results of the wavelet analysis of precipitation

time series for Vermigliana and Sarca di Genova catchments, respectively. The wavelet power spectra (figures 4.7a and 4.8a) shows discontinuous small high energy regions distributed over the 2-30 days band. Large periodicities (i.e. periods larger than 128 days) evidence high energy regions persistent in time which appear to be particularly strong during the years 2000 to 2003 and 2009 to 2013. The global power spectrum of the Vermigliana (figure 4.7b) presents three important peaks, in correspondence to seasonal (i.e., 6 month), annual and bi-annual periodicities, while Sarca di Genova presents only two peaks (figure 4.8b), evidencing only seasonal and bi-annual periodicities. We then calculated the scale-averaged wavelet power over the 0.5-2 year band (figures 4.7c and 4.8c) and verify that these periodicities are of high energy in the periods 2000-2003 and 2010-2013.

The wavelet power spectra of the temperature time series (figures 4.9a and 4.10a) show small discontinuous high energy regions over the 2-15 days band, followed by clear and persistent in time high energy region at the annual scale. Consequently, the global wavelet spectra (figures 4.9b and 4.10b) shows only one peak, verifying a strong periodicity at the annual scale. The scale-averaged wavelet power at the 0.5-2 year band (figures 4.9c and 4.10c), shows several oscillations along the entire observation period. On the Vermigliana, we observed high energy content in 2003 (figure 4.9c), while on Sarca di Genova, energy increases gradually from 2001 to 2006 (figure 4.10c). In addition, both catchments show a sudden drop of energy at the year 2007.

Similarly, the wavelet power spectra of streamflow time series (figures 4.11a and 4.12a) exhibits discontinuous high energy regions extended over the 2-15 days band, although persistent in time high energy regions appear at seasonal and annual scales. The global power spectra (figures 4.11b and 4.12b) show peaks at the seasonal and annual scales. A third but smaller peak near the 1.5 year band appears on Sarca di Genova catchment. The scale-averaged wavelet power on the 0.5-2 year band (figures 4.11c and 4.12c) shows a periodic behaviour with energy that almost doubles in the highly energetic periods. The first large oscillations are observed from 2001 and 2004 while the second, from 2008 to 2011. A later increase in the oscillations is observed on 2014 only in the Vermgliana catchment.

The annual periodicity on temperature series as well as the oscillations on streamflow periodicities were also observed on the Hovmöller plots presented on the previous section (see figures 4.5 and 4.6), however no patterns were found on precipitation series. The more in-depth analysis of the variability across temporal scales of the hydrological time series with the continuous wavelet transform instead provides more detailed information. For instance, precipitation presents periodicities at seasonal, annual an bi-annual scales, as seen on the global wavelet spectra (see figures 4.7b and 4.8b), which may be enhanced in some specific years, probably due to the increase on precipitation intensity (see figures 4.7c and 4.8c), hence the resulting oscillations produce a periodic behaviour which probably mimics the climate pattern at the regional scale. On the contrary, temperature shows an unique and persistent in time high energy region, associated to the annual periodicity of the series (see figures 4.9b and 4.10b) with relatively constant oscillations along the entire observational period (figures 4.9c and 4.10c). Moreover, streamflow time series presents both seasonal and annual periodicities (figures

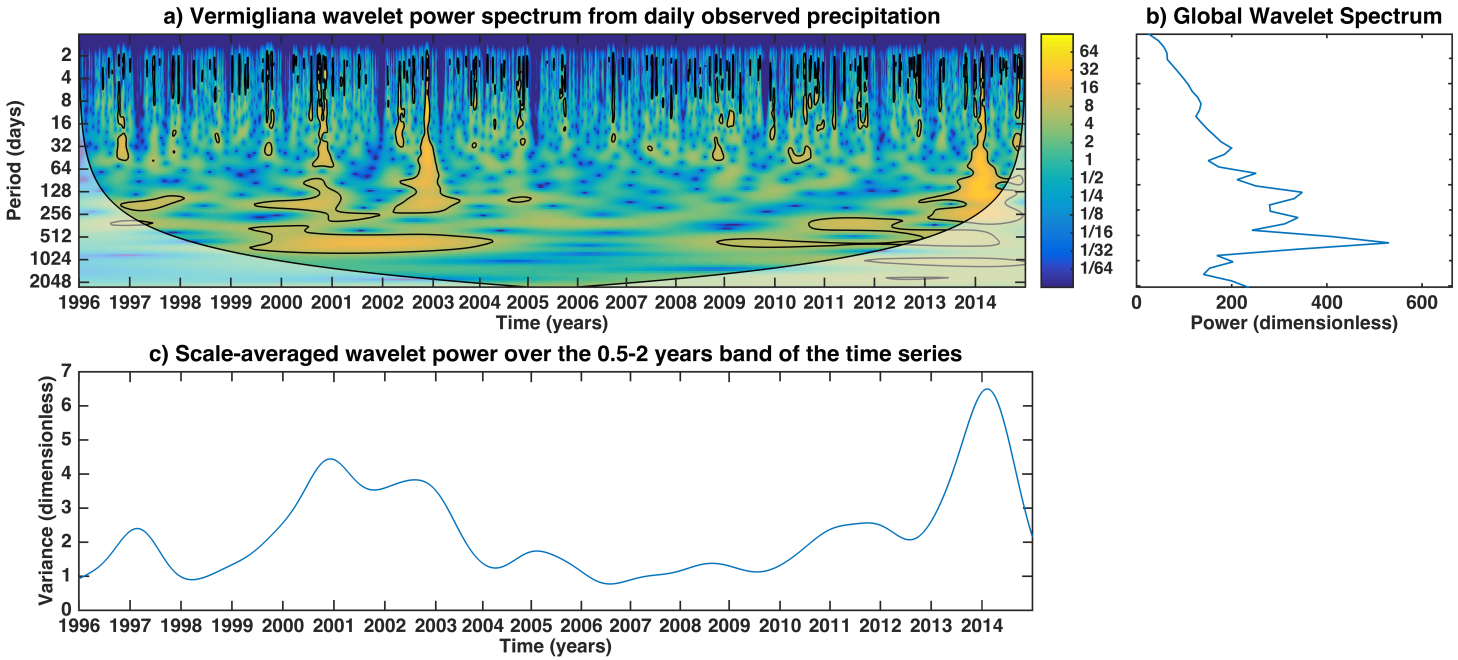


Figure 4.7: Application of the continuous wavelet transform to the daily precipitation time series of the Vermigliana catchment: a) wavelet power spectrum, b) global wavelet spectrum and, c) scale-averaged wavelet power over the 0.5-2 year band of the time series.

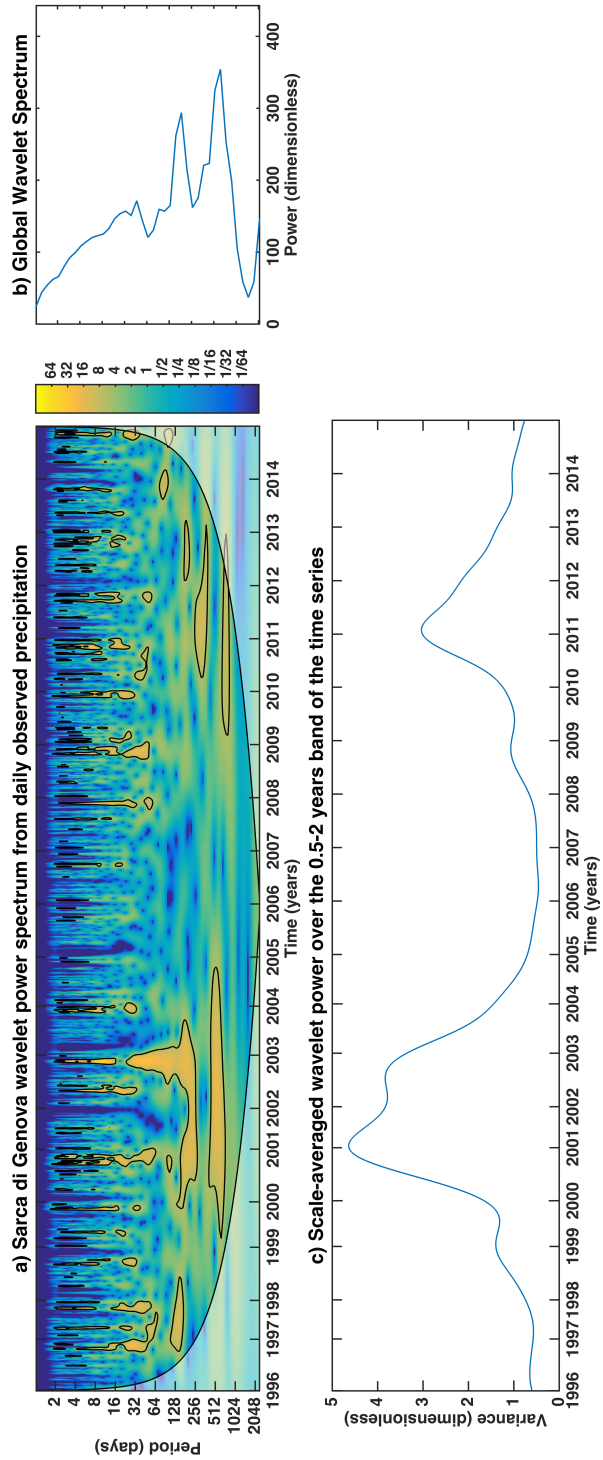


Figure 4.8: Application of the continuous wavelet transform to the daily precipitation time series of Sarca di Genova catchment: a) wavelet power spectrum, b) global wavelet spectrum and, c) scale-averaged wavelet power over the 0.5-2 year band of the time series.

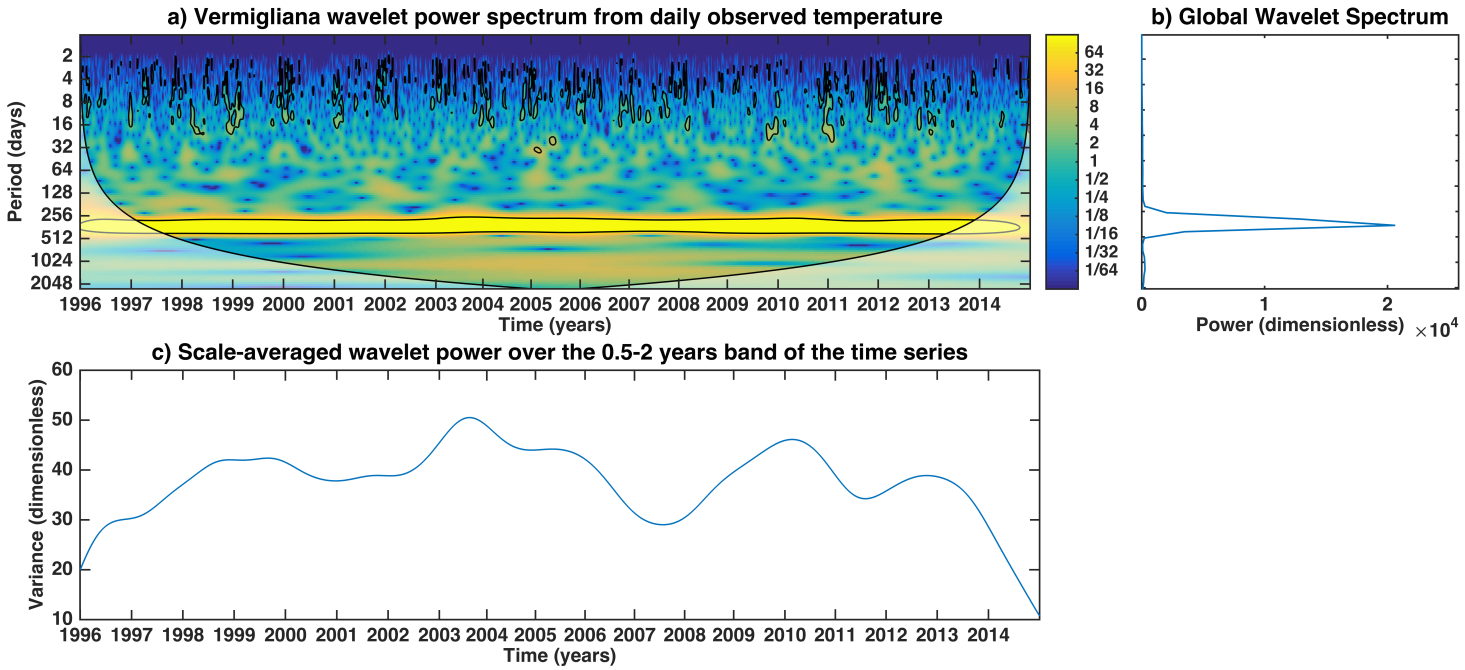


Figure 4.9: Application of the continuous wavelet transform to the daily temperature time series of the Vermigliana catchment: a) wavelet power spectrum, b) global wavelet spectrum and, c) scale-averaged wavelet power over the 0.5-2 year band of the time series.

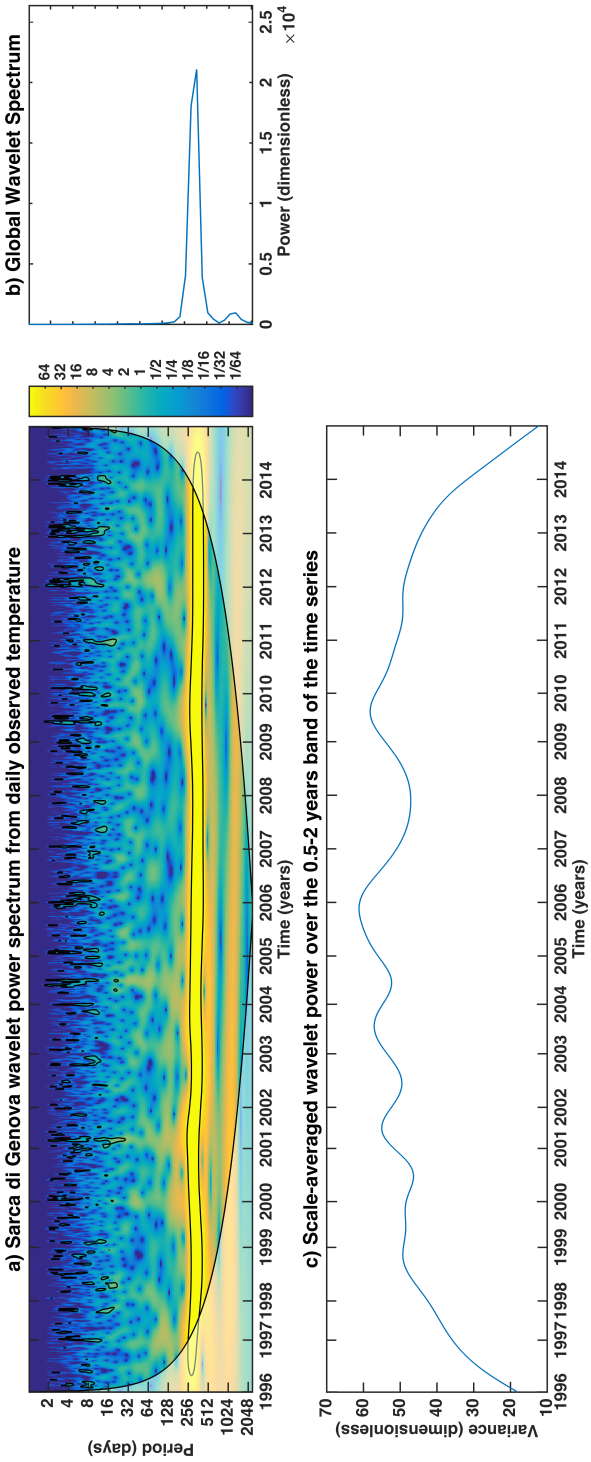


Figure 4.10: Application of the continuous wavelet transform to the daily temperature time series of Sarca di Genova catchment: a) wavelet power spectrum, b) global wavelet spectrum and, c) scale-averaged wavelet power over the 0.5-2 year band of the time series.

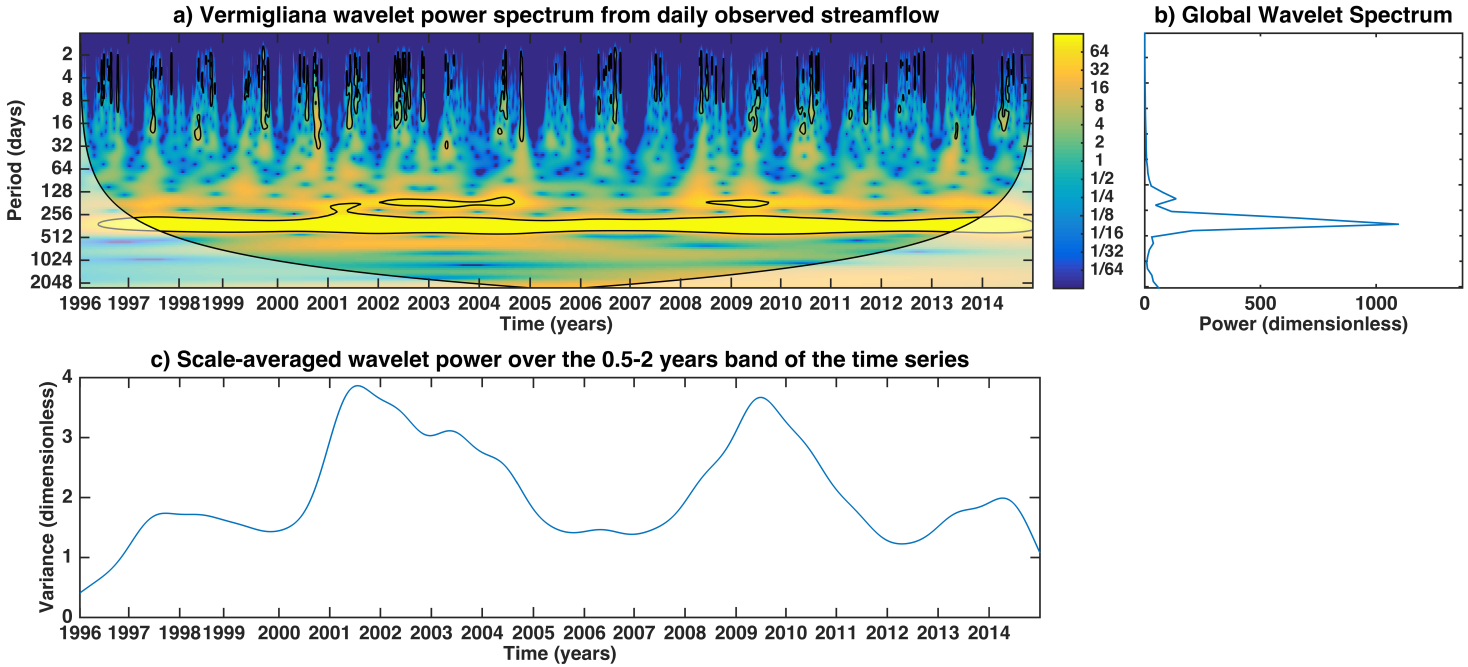


Figure 4.11: Application of the continuous wavelet transform to the daily streamflow time series of the Vermigliana catchment: a) wavelet power spectrum, b) global wavelet spectrum and, c) scale-averaged wavelet power over the 0.5-2 year band of the time series.

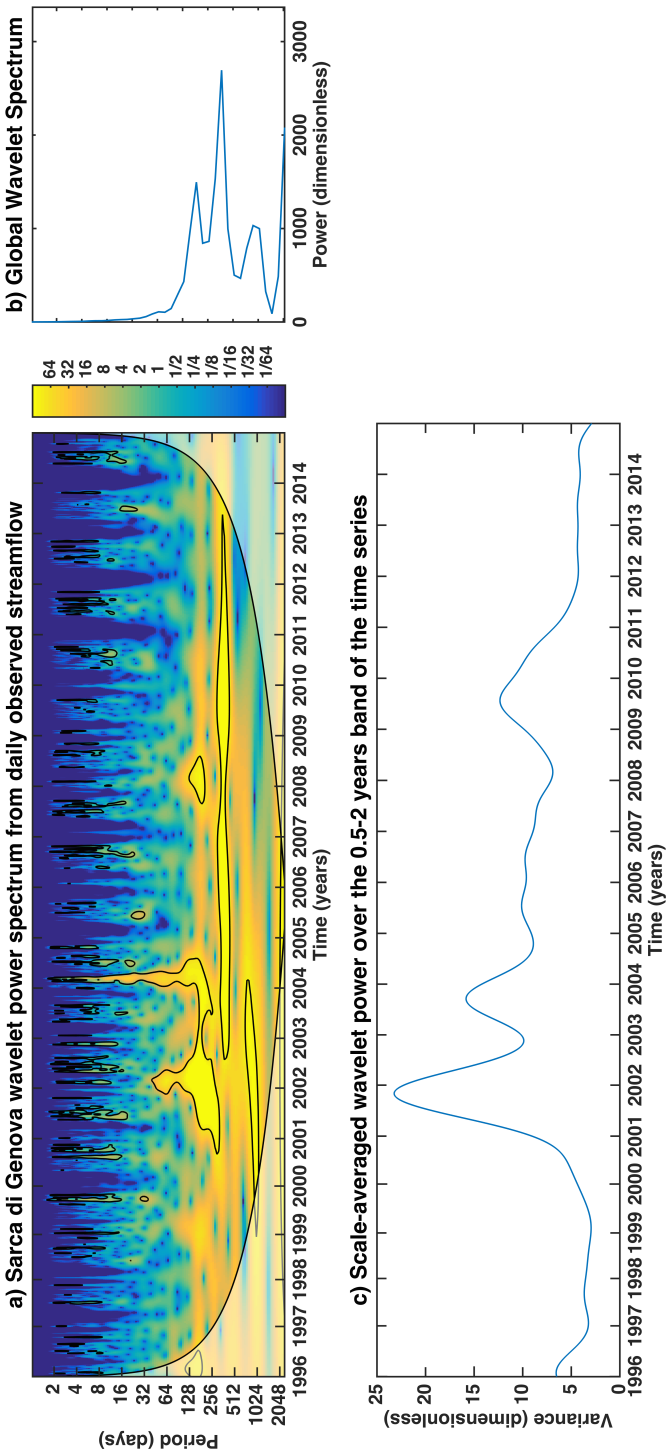


Figure 4.12: Application of the continuous wavelet transform to the daily streamflow time series of Sarca di Genova catchment: a) wavelet power spectrum, b) global wavelet spectrum and, c) scale-averaged wavelet power over the 0.5-2 year band of the time series.

4.11b and 4.12b), with the latter persistent in time during the entire observation period in the Vermigliana catchment (figure 4.11a), while on Sarca di Genova, the annual periodicity begins from the year 2003 (figure 4.12a). The scale-averaged power (figures 4.11c and 4.12c) illustrates a cyclical pattern similar to that observed on precipitation time series. Hence, streamflow is controlled by the atmospheric forcing (i.e., precipitation and temperature) with the most persistent periodicity at the annual scale.

The correlation between streamflow and atmospheric forcing has been explored by using wavelet coherence analysis (Grinsted et al., 2004). By correlation we mean that both signals present similar oscillations occurring in certain specific periods. Figures 4.13 and 4.14 show the results of the wavelet coherence analysis between precipitation and streamflow time series and, likewise, figures 4.15 and 4.16 the wavelet coherence between temperature and streamflow time series of Vermigliana and Sarca di Genova catchments, respectively. The colour bar at the right hand side of each figure indicates the level of correlation between two series and goes from 0 (uncorrelated) to 1 (fully correlated). Arrows indicate the phase relationship between the two time series: with the arrow pointing to the right indicating signals in phase, pointing to the left signal out of phase and arrow pointing upward indicating that the second series lags behind the first by 90◦. The thick black contours indicate the 5% significance level against red noise and the light shading shows the region influenced by edge effects excluded from the analysis.

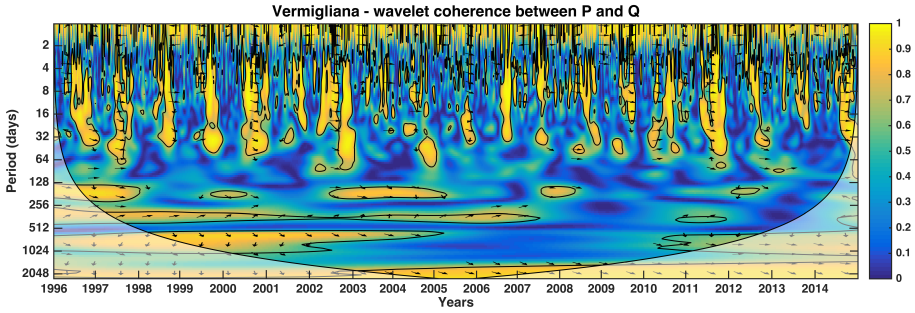


Figure 4.13: Wavelet coherence between precipitation (P) and streamflow (Q) time series of Vermigliana catchment.

Figures 4.13 and 4.14 show the results of the wavelet coherence analysis between precipitation and streamflow time series of Vermigliana and Sarca di Genova catchments. A variable correlation is observed over the 2-30 days band with an in-phase relationship along the entire observation period. This variable correlation disappears mainly during the snow accumulation period (December to February) and reappears when precipitation is liquid again. However, at larger scales, i.e., 256-1024 days, constant in time correlation can be found in the Vermigliana catchment from the years 1996 to 2006, while in Sarca di Genova, from 1999 to 2001 and from 2009 to 2013 but over the 128-256 days band.

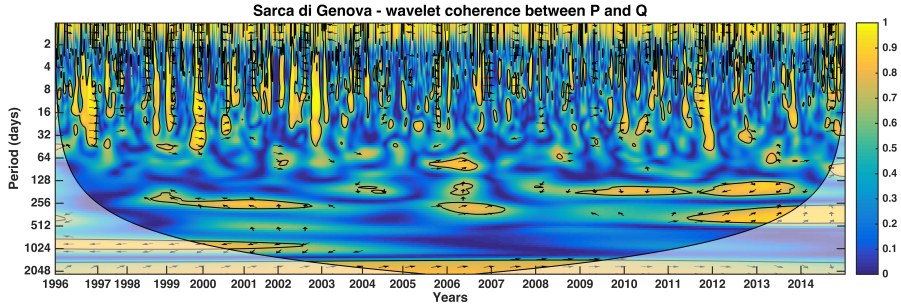


Figure 4.14: Wavelet coherence between precipitation (P) and streamflow (Q) time series of Sarca di Genova catchment.

Likewise, the correlation between temperature and streamflow time series (see figures 4.15 and 4.16) shows variability extended over the 2-30 days band, however the region with highest correlation appears between the 256-512-days band (i.e., annual scale) and presents a completely in-phase relationship, this means that when T increases also Q increases and vice-versa, when T decreases also Q decreases. The persistence on the annual correlation characterizes the entire observation period of Vermigliana, while in the Sarca di Genova, it is observed only from the year 2003, before that, there is no correlation between T and Q.

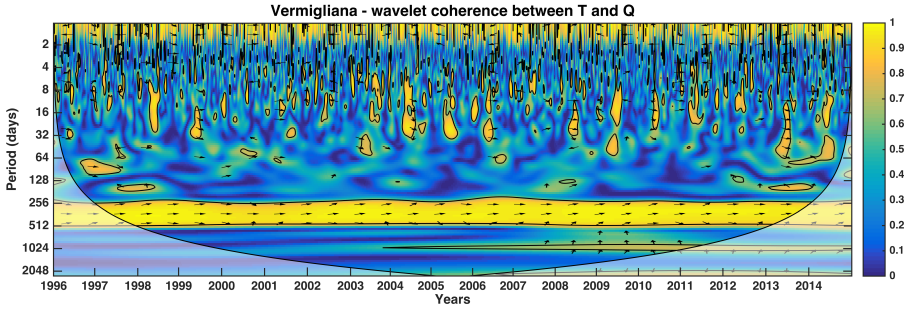


Figure 4.15: Wavelet coherence between temperature (T) and streamflow (Q) time series of Vermigliana catchment.

There is a need to explore alternative methods of data analysis and visualization to improve our understanding on catchment functioning (Carey et al., 2013), particularly in complex environments like Alpine regions. Investigating the nature of variability on hydrological time series and its consequent association to climate patterns provides further insights into the hydrological response and sensitivity of these systems to climate changes. Wavelet coherence can thus be useful to evidence the specific periods on which two signals are correlated and may also reveal significant information about the nature of their relationship. The results of

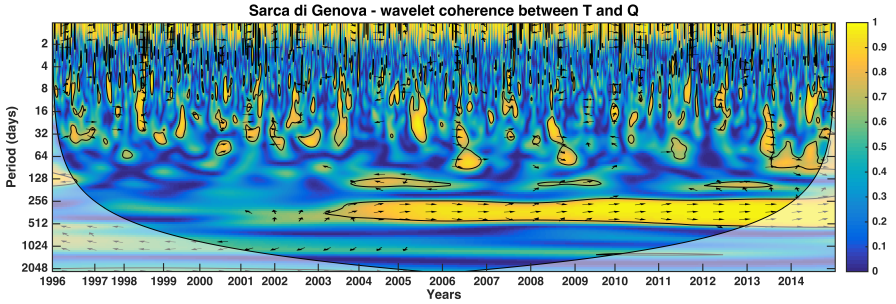


Figure 4.16: Wavelet coherence between temperature (T) and streamflow (Q) time series of Sarca di Genova catchment.

our analysis show how annual fluctuations on streamflow in these two catchments are mainly controlled by the fluctuations on air temperature, as seen from the wavelet coherence between T and Q (figures 4.15 and 4.16). Yet, in some cases these fluctuations may be increased by particularly intense precipitation periods, on which P and Q have also shown to be correlated (figures 4.13 and 4.14).

## 4.5 Conclusions

We explored the variability of the hydrological time series (i.e., precipitation, temperature and streamflow) of two Alpine catchments located in North-Eastern Italy, both characterized by the presence of glaciers, analysing nineteen years of data (1996-2014) using Hovmöller plots with averaged monthly values and applying the continuous wavelet transform to the daily time series.

Results showed that Hovmöller plots may be an useful tool to assess temporal variability of hydrological time series in a simplified way, evidencing significant patterns at different temporal scales. Results show a strong seasonality linking streamflow to temperature time series on the catchments under study, which is to be expected. An interesting pattern was instead observed to occur as a four year cycle on streamflow time series, which cannot be further explored with this method. In addition to the fact that no specific patterns could be identified on precipitation time series, the previous indicates very clearly the limitations on the use of these diagrams.

On the other hand, the continuous wavelet transform, a more complex technique, allowed us to perform an in-depth analysis of the variability across temporal scales of the hydrological time series, evidencing the occurrence of relatively constant periodicities. More specifically, the global wavelet spectra (i.e., the averaging in time of the wavelet spectra) evidenced the specific periods on which these periodicities occur: seasonal, annual and even bi-annual periodicities on the precipitation time series of Vermigliana, while seasonal and bi-annual periodicities in Sarca di Genova catchment. Temperature time series instead showed a constant annual periodicity on both cases, whereas streamflow showed annual

and bi-annual periodicities. The scale-averaged power of the wavelet spectra over the 0.5-2 years band, indicated the specific years in which oscillations of wavelet spectra were enhanced due to changes of precipitation time series. The continuous wavelet transform allowed us to explore the magnitude and persistence of variability in flows at different temporal scales: seasonal, annual. Moreover, besides snow and ice-melt, streamflow variability on both catchments is also dominated by 4 year cycles observed in precipitation time series, hence resulting on very strong fluctuations of flow and variability controlled by these climate patterns.

Furthermore, wavelet coherence analysis allowed us to identify the specific periods and temporal scales on which P-Q and T-Q presented similar oscillations (i.e., were correlated). Results showed similar coherence patterns on both catchments, as expected considering the common drivers for the hydrological processes. T and Q showed a constant correlation at the annual scale, while P and Q showed an variable correlation over the 2-30 days band, which disappears during the snow accumulation period (December to February) and reappears when precipitation is liquid again.

Studying the nature of variability of hydrological time series and its association to climate patterns provide further insights into the hydrological response and sensitivity of the systems under study to climate changes, which can lead to the further development of important applications in hydrology such as climate assessment tools. Moreover, the better comprehension of the variability in the relationship between atmospheric forcing and streamflow can lead to the improvement of current conceptual models or to define a suitable framework for future modelling studies in these complex contexts.

*Chapter* 5

# Stochastic streamflow pdf

## 5.1 Introduction

Alpine rivers host unique and fragile ecosystems (Bizzotto et al., 2009) and, from a functioning point of view, can storage large volumes of water as snow and ice, which induces both dial variations of streamflow during the melting season, as well as significant seasonal variations with glaciers playing a relevant role in regulating inter-annual variability (Kuhn and Batlogg, 1998; Stewart, 2009). Hence, characterization, as well as prediction of streamflow variability in Alpine catchments, can provide significant information for water resources management.

Fluctuations on streamflow can be described by the probability distribution function (pdf) of daily water discharge or the related flow duration curve (see e.g., Searcy, 1959; Moore, 1985; Sharma et al., 1997; Doyle et al., 2005; Castellarin et al., 2007; Botter et al., 2007b,c, 2008). Stochastic characterization and prediction of streamflow variability hence represents one of the major topics addressed in former and current hydrology.

In this context, Botter et al. (2009) have recently proposed a stochastic analytical framework which incorporates the effect of non-linear recessions on streamflow regimes in order to derive the statistical distribution and the duration curve of streamflow. This approach proved able to reproduce the main features of observed streamflow statistics (Ceola et al., 2010) and can provide tools of wide applicability through which interactions among hydrologic, climatic and geomorphic properties can be explicitly analysed (see e.g., Doulatyari et al., 2014, 2015). However, as we have seen in the previous chapter, streamflow dynamics in Alpine catchments can be strongly dominated by processes like snow-melting in summer and snow accumulation in winter. The effect of these processes may represent a temporal disconnection of one part of the catchment from the active streamflow network (DeBeer et al., 2010; Tobin et al., 2013), introducing a delay on the release at the outlet of the catchment. Schaefli et al. (2013) thus suggested an extension to the analytical approach proposed by Botter et al. (2009) in order to describe the pdf of winter streamflows affected by snow dynamics.

We applied an existing stochastic analytical modelling framework (Botter

et al., 2009) to the two case studies presented in Chapter 4: Vermigliana ($78.9km^2$) and Sarca di Genova ($77.52km^2$) catchments, both characterized by the presence of glaciers, covering $8.5\% and 25.0\%$ of the total catchment surface, respectively. The specific goals of this chapter area: (i) to test the model's ability to predict streamflow distribution on glacierized catchments on a season based approach and; (ii) to apply the model extension proposed by Schaefli et al. (2013) in order to predict winter streamflow pdf and further investigate the size of the non contributing part of the catchment during winter.

## 5.2 Methods

We provide a detailed description of the theoretical background for the stochastic analytical models applied in this chapter.

### 5.2.1 Analytical streamflow pdf

Streamflow characterization and prediction constitutes an important topic in hydrology and water management. In order to obtain new insights on streamflow distributions in Alpine catchments, we applied an existing analytical framework for the stochastic modelling of streamflow pdf of both the Vermigliana and Sarca di Genova rivers at the control sections indicated in Section 4.2.1.

To start, we refer to the analytical characterization of the probability distribution function (pdf) of base flows in river basins proposed by Botter et al. (2007a,c,b, 2008), which considers streamflow dynamics as the result of the superposition of a sequence of water flow impulses triggered by the precipitation.

Then we assume that the sequence of rainfall events generating streamflow are only a subset of rainfall events, which comprises the events with enough water to fill the deficit caused by plant transpiration in the root zone and therefore lead the soil water content above its retention capacity. Consequently, the excess of water this zone generates the runoff of the catchment. The model considers then subsurface storage as a linear reservoir, on which each pulse determines a sudden increase of the streamflow followed by an exponential-like recession. Thus, the stochastic dynamical expression for streamflow (Q) at a daily time scale is defined as:

$$\frac{dQ(t)}{dt} = -kQ(t) + \xi_t \tag{5.1}$$

where the first term at the right-hand side represents the exponential decay of Q between events, $k[T^{-1}]$ is the recession rate, which is the inverse of the mean residence time within the linear bucket representing soil storage, and $(\epsilon_t[L^3/T^2])$ is a random noise representing precipitation intensity. Rainfall is modelled by a marked Poisson process with frequency $\lambda_P[T^{-1}]$ and exponentially distributed depths with average $\alpha[L]$ (Rodriguez-Iturbe et al., 1999; Botter et al., 2007c; Rodríguez-Iturbe and Porporato, 2005). Effective rainfall events have an instantaneous duration and can be also approximated by a Poisson process characterized by a frequency $\lambda[T^{-1}]$, smaller than that of the overall rainfall (i.e., $\lambda < \lambda_P$). The

interarrival times between the jumps are therefore exponentially distributed with mean $1/\lambda$.

Under the above assumptions, $Q$ is given by sudden jumps followed by an exponential decay between the events. Thus, the resulting streamflow pdf associated to the process defined by equation 5.1 is expressed as a Gamma function and reads as follows (Botter et al., 2007b):

$$p(Q, t \to \infty) = \frac{1}{\Gamma(\frac{\lambda}{k})} \frac{1}{Q} \left( \frac{Q}{\alpha k A} \right)^{\frac{\lambda}{k}} \exp\left( -\frac{Q}{\alpha k A} \right) \tag{5.2}$$

where $\Gamma$ is the complete gamma function, $A$ is the catchment area, $\alpha$ is estimated as the mean depth of precipitation during rainy days, $\lambda$ is based on the mean observed (i.e., $\lambda = \langle Q \rangle / \alpha$) and $k$ can be deducted from recession analysis.

However, observational evidences and theoretical argument suggest that in several cases the storage-discharge relation can be non-linear (e.g., Amorocho and Orlob, 1961; Brutsaert and Nieber, 1977; Kirchner, 2009). Thus, the previous model was extended by Botter et al. (2009) so as to incorporate the effects of non-linear recessions on streamflow regime, providing a more realistic description of the hydrological response of the catchment. Considering power law decays in between events, as unstated by a non-linear storage-discharge relationship (Brutsaert and Nieber, 1977; Kirchner, 2009), the temporal dynamics of Q between effective rainfall events is described by the following stochastic differential equation:

$$\frac{dQ(t)}{dt} = -kQ(t)^a + \xi_t \tag{5.3}$$

where $a$ is a coefficient associated to the power law relation describing the rate of decrease of $Q$ during the recession. Consequently, the steady-state pdf of streamflow is derived from the solution of the master equation associated to equation 5.3:

$$p(Q, t \to \infty) = C \left\{ \frac{1}{Q^a} \exp\left[ -\frac{Q^{2-a}}{\alpha k A (2-a)} + \frac{\lambda Q^{1-a}}{k(1-a)} \right] + \frac{k}{\lambda} \delta(Q) H[1-a] \right\} \tag{5.4}$$

where $C$ is the normalization constant and $H$ corresponds to the Heaviside unit step function. In this way, $p(Q)$ is calculated as the sum of a continuous part of the pdf of Q, common for all cases, and an atom of probability in $Q = 0$ associated to the Dirac delta function only when $\alpha < 1$ (see Botter et al., 2009; Ceola et al., 2010).

The flow duration curve is expressed by the cumulative distribution function (cdf) of $Q$, calculated by integrating equation (5.4):

$$D(Q) = \int_Q^{+\infty} p(x)\, \mathrm{d}x. \tag{5.5}$$

Moreover, the model is based on spatially averaged, catchment-scale properties, therefore neglects effects related to a detailed description of network morphology and spatial distribution of soil properties (Botter et al., 2007c). Effects of

snow accumulation during winter are not explicitly included in the formulation, however the possible presence of carry over flow across different seasons can be accounted adjusting the frequency of effective events (Doulatyari et al., 2015). Applications of this model can be found in Ceola et al. (2010), Botter et al. (2013)., Doulatyari et al. (2014), Doulatyari et al. (2015),

**Parameters estimation - analytical streamflow pdf**

The model requires the definition of three parameters which are estimated from observed time series of precipitation, temperature and streamflow. The mean rainfall depth ($\alpha$), calculated as the mean precipitation during days with rainfall depth above zero (i.e., wet days). The frequency of rainfall events ($\lambda_P$), calculated as the relative fraction of days with rainfall on each season and, the frequency of effective rainfall events ($\lambda$), a ratio estimated from the mean observed streamflow and precipitation (i.e., $\lambda = \langle Q \rangle / \alpha$). The recession rate $k$, defined as the mean residence time in the catchment and the coefficient $a$ are estimated with the classical Brutsaert-Nieber recession analysis (Brutsaert and Nieber, 1977). Recession events are identified by a threshold-based selection approach which ensures a simple automatic selection for all catchments.

### 5.2.2 Analytical winter streamflow pdf

Alpine catchments are complex environment dominated by two main processes which are driven by the annual fluctuations in temperature: melting (from snow and also ice within the presence of a glacier) in summer resulting in high streamflow peaks and, snow accumulation in winter, with precipitation that falls as snow and is stored within the catchment such that low flow conditions prevailing in this season.

(Schaefli et al., 2013) presented an extension of the model described on the previous section which includes the effects of snow dynamics on the flow regime. The novelty in this approach is the addition of a delay on winter streamflow generation due to the temporary accumulation of snow at lower elevations, based on the existence of a temporary disconnection of high-elevation areas that experience freezing conditions during the winter season.

The theory behind this model is that the catchment can be conceptually divided into three zones during winter: Zone I, with occasional snowfall but no significant snowpack generation and therefore unaffected by snow dynamics; Zone II with regular snowfall followed by sporadic periods with enhanced snow-melt, thus significant snowpacks are formed in this zone but are assumed to melt during the same season and; Zone III, with precipitation that falls as snow and snowpack generation that lasts the entire winter, not contributing to streamflow during winter.

Winter streamflow is generated by the incoming precipitation pulses through the temporary accumulation of snow in the part that remains responsive during this season (i.e., Zone II), which introduces a delay in the catchment mean response time $\tau_w$ during this season (Schaefli et al., 2013):

$$\tau_w = \tau_k + \tau_D \tag{5.6}$$

where $\tau_k = k^{-1}[T]$ is the mean catchment response time in absence of snow and $\tau_D[T]$ is the delay in the catchment residence time due to temporary snow accumulation and can be estimated as a function of the freezing regime (for further details see (Schaefli et al., 2013)).

In this extension of the model, some important assumptions are made: (i) during winter there is no soil moisture loss through transpiration; (ii) soil moisture remains permanently close to its retention threshold; (iii) all precipitation events generate runoff and can be described as a Poisson process, therefore $\lambda = \lambda_P$, and; (iv) only a part of the catchment is responsive during winter.

Considering $A^*$ as the non-responsive part of the catchment during the entire winter (i.e., Zone III), the catchment area in equation 5.2 is replaced by the responsive area, $A - A^*$. Therefore, for the linear reservoir case, winter streamflow pdf is expressed as (Schaefli et al., 2013):

$$p(Q, t \to \infty) = \frac{1}{\Gamma(\frac{\lambda_P}{k_w})} \frac{1}{Q} \left[ \frac{Q}{\alpha k_w (A - A^*)} \right]^{\frac{\lambda_P}{k_w}} \exp \left[ - \frac{Q}{\alpha k_w (A - A^*)} \right] \tag{5.7}$$

where $k_w = \tau_w^{-1}$ and $A^*$ may be defined by establishing a threshold altitude value. This assumption stands only for catchments presenting temperatures above $0°C$ during winter. Analogously, if we consider instead a non-linear reservoir, winter streamflow pdf is described by the following equation:

$$p(Q, t \to \infty) = C \left\{ \frac{1}{Q^a} \exp \left[ - \frac{Q^{2-a}}{\alpha k_w (A - A^*)(2 - a)} + \frac{\lambda Q^{1-a}}{k_w (1 - a)} \right] + \frac{k_w}{\lambda} \delta(Q) H[1 - a] \right\} \tag{5.8}$$

The flow duration curve is expressed by the cumulative distribution function (cdf) of $Q$, defined by equation (5.5).

### Parameters estimation - analytical winter streamflow pdf

Besides the parameters described on the original model (i.e., $\alpha$, $\lambda_P$, and $\lambda$), this extension introduces two other parameters: $k_w$ and $A^*$. In order to estimate $k_w$, equation (5.6) should be solved, where the first term can be obtained considering the following relation: $\tau_k = 1/k$. The second term, $\tau_D$, is estimated based on the length of the periods in freezing conditions when precipitation falls as snow, accumulates on the ground and no melting occurs. Since temperature can be a good proxy for catchments dominated by melting processes, $\tau_D$ is assumed as the mean duration of periods with temperature below $0C°$ (i.e., freezing conditions) and therefore can be calculated from the observed temperature time series.

The second added parameter,is as a calibration parameter. Thus, once all the other parameters are estimated from observed time series, $A^*$ can be adjusted with a systematic search such as to minimize the bias between simulated and observed streamflow pdf.

## 5.3 Results and discussions

### 5.3.1 Inter-annual variations of the parameters controlling streamflow pdf

The catchment inter-comparison with Hovmöller plots and wavelet coherence analysis in Chapter 4 showed that both of the catchments under study are very sensitive to temperature changes and also, evidenced a clear distinction between two different flow regimes observed at the annual scale: (i) high-flow regime, from May to August, on which the main contribution comes from snow and ice-melting due to high temperatures and a smaller part comes from precipitation; (ii) low-flow regime, relatively constant and observed during the rest of the year, on this period part of the precipitation falls as snow and is stored within the catchment. Notice that on this second period the months of April and September are transition periods on which there is also an important contribution from rainfall. Likewise, October-November may present high precipitation events that can be enhanced by snow-melting producing rain-on-snow events. Nevertheless, we have included these transition periods within the low-flow regime and applied the analytical model described on section 5.2.1 considering hence two seasons: low-flow season (September to April) and melting season (May to June).

As exposed on section 5.2.1, the model has three parameters which can be estimated from observed time series of precipitation, temperature and streamflow: the mean rainfall depth ($\alpha$), the frequency of rainfall events ($\lambda_P$) and the frequency of effective rainfall events ($\lambda$). These parameters may display significant changes due to climate and landscape modifications (Doulatyari et al., 2014), thus, we first investigate their inter-annual fluctuations. Figures 5.1, 5.2 and 5.3 depict the temporal variation of $\alpha$, $\lambda_P$ and $\lambda$ for each season, where Vermigliana catchment is represented by the solid line while Sarca di Genova by the dashed line.

Both catchments present similar fluctuations on rainfall depth (figure 5.1), showing slightly lower values during the melting season with respect to low-flow season. Overall, on both seasons, oscillations in $\alpha$ show a slight but evident periodicity of four to five years. The inter-annual variability of $\alpha$ determines the frequency of rainfall events, $\lambda_P$, shown on figure 5.2. These parameter shows similar fluctuations on both catchments, although with lower values during the low-flow season with respect to the melting period.

Moreover, the inter-annual fluctuations of $\lambda$ during low-flow season (figure 5.3a) seem relatively constant, with values that range from 0.12 to 0.27 $d^{-1}$, on the other hand, Sarca di Genova instead presents higher values, ranging from 0.08 up to 1.12. During the melting season (figure 5.3b), $\lambda$ varies from 0.41 to 1.07 in Vermigliana catchment and from 0.63 to 3.35 in Sarca di Genova.

All the parameters (see tables 5.1 and 5.2) were estimated according to the methods described on section 5.2.1 for each season of the two catchments under study.

Figures 5.1, 5.2 and 5.3 illustrate the inter-annual variability of the driving hydro-climatic parameters controlling the shape of streamflow pdf reproduced by the model. While $\alpha$ and $\lambda_P$ are mainly associated to climatic changes, the inter-

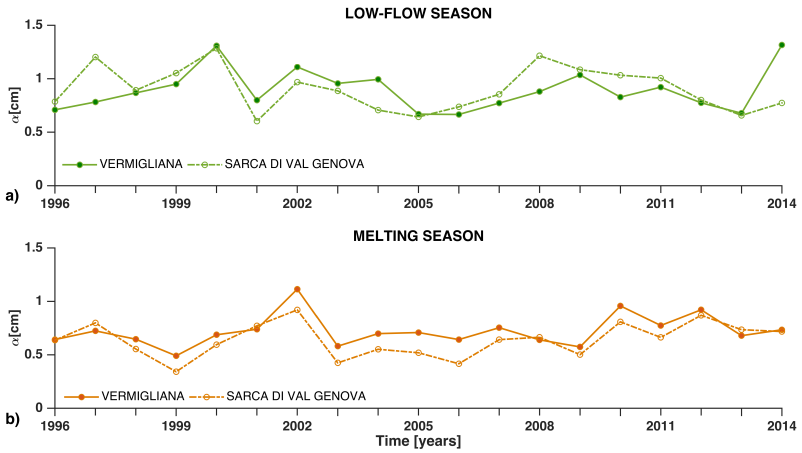


Figure 5.1: Inter-annual fluctuations of $\alpha$ on Vermigliana (solid line) and Sarca di Genova (dashed line) catchments: a)low-flow season and b)melting season

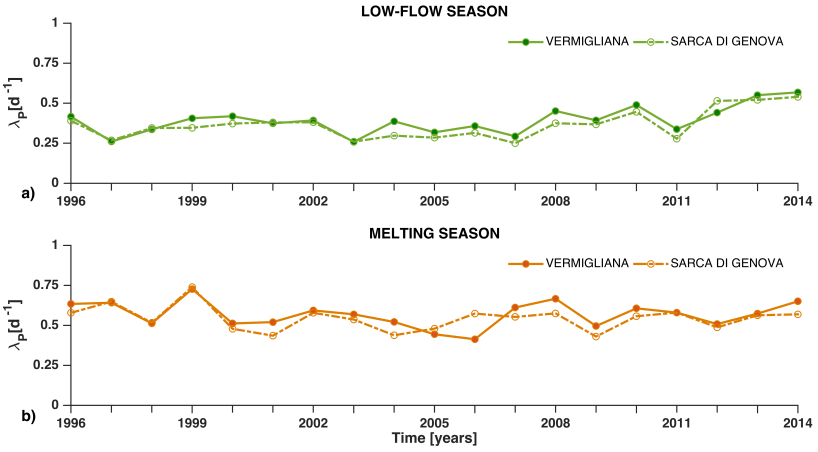


Figure 5.2: Inter-annual fluctuations of $\lambda_P$ on Vermigliana (solid line) and Sarca di Genova (dashed line) catchments: a)low-flow season and b)melting season

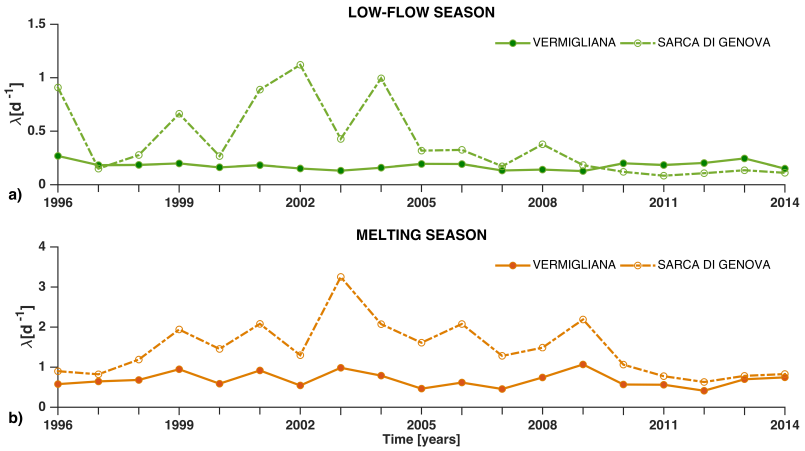


Figure 5.3: Inter-annual fluctuations of $\lambda$ on Vermigliana (solid line) and Sarca di Genova (dashed line) catchments: a)low-flow season and b)melting season

annual variations of $\lambda$ may capture not only the combined effect of changes in frequency and depth of precipitation, but in the case of the catchments under study, the significant variations observed during the melting season are also the result of processes like snow and ice-melting, which increase considerably the frequency of effective events, calculated from observed streamflow data. As for the low-flow season, we are not certain about the physical causes of the observed high winter flows. Besides the occurrence of particularly intense precipitation events in some of the cases, we find important to highlight that the data series is not validated, therefore data may be affected by not identifiable errors. This last hypothesis is supported by the fact that the wavelet coherence between observed temperature and streamflow time series (see figure 4.14 in Chapter 4), does not show correlation before 2004.

In addition, the values reported on tables 5.1 and 5.2, allowed us to further investigate the relationship between $\lambda_P$ and $\lambda$ on both catchments and hence, asses the model's applicability to our case studies. In the low-flow season, $\lambda < \lambda_P$ in the Vermigliana catchment while in Sarca di Genova this condition is true only on some specific years: 1997, 1998, 2000 and from 2006 until the end of the series. However, during the melting season, this relation varies in time in the Vermigliana catchment, i.e., $\lambda > \lambda_P$ on the following periods: 1998 to 2001, 2003 to 2006, 2008 to 2009, 2013 to 2014; the rest of the years $\lambda \leq \lambda_P$. In the melting season of Sarca di Genova, $\lambda > \lambda_P$ during the entire observation period.

The fact that $\lambda \geq \lambda_P$ in these two catchments, in particular during the melting season, is clearly an effect of snow and ice-melting processes and does not complain with one of the model main assumptions, i.e., $\lambda < \lambda_P$. Since the model does not take into account snow accumulation or melting, yet the parameter $\lambda$ may be used to account for the interference caused by these two processes (Doulatyari

Table 5.1: Inter-annual variations of the model parameters: Vermigliana catchment

| **Year** | **Low-flow** | | | | **Melting** | | | |
|---|---|---|---|---|---|---|---|---|
| | $\alpha[cm]$ | $\lambda_P[d^{-1}]$ | $\lambda[d^{-1}]$ | $k[d^{-1}]$ | $\alpha[cm]$ | $\lambda_P[d^{-1}]$ | $\lambda[d^{-1}]$ | $k[d^{-1}]$ |
| 1996 | 0.71 | 0.42 | 0.27 | 0.05 | 0.64 | 0.63 | 0.58 | 0.13 |
| 1997 | 0.78 | 0.26 | 0.18 | 0.04 | 0.72 | 0.64 | 0.64 | 0.12 |
| 1998 | 0.87 | 0.34 | 0.18 | 0.06 | 0.65 | 0.51 | 0.68 | 0.13 |
| 1999 | 0.95 | 0.41 | 0.20 | 0.04 | 0.49 | 0.73 | 0.95 | 0.13 |
| 2000 | 1.31 | 0.42 | 0.16 | 0.05 | 0.69 | 0.51 | 0.59 | 0.11 |
| 2001 | 0.80 | 0.37 | 0.18 | 0.06 | 0.74 | 0.52 | 0.92 | 0.15 |
| 2002 | 1.11 | 0.39 | 0.15 | 0.05 | 1.11 | 0.59 | 0.54 | 0.16 |
| 2003 | 0.96 | 0.26 | 0.13 | 0.05 | 0.58 | 0.57 | 0.98 | 0.09 |
| 2004 | 0.99 | 0.39 | 0.16 | 0.05 | 0.70 | 0.52 | 0.79 | 0.11 |
| 2005 | 0.67 | 0.32 | 0.19 | 0.06 | 0.71 | 0.44 | 0.46 | 0.09 |
| 2006 | 0.67 | 0.36 | 0.19 | 0.07 | 0.64 | 0.41 | 0.62 | 0.14 |
| 2007 | 0.77 | 0.29 | 0.13 | 0.06 | 0.75 | 0.61 | 0.45 | 0.12 |
| 2008 | 0.88 | 0.45 | 0.14 | 0.04 | 0.64 | 0.66 | 0.74 | 0.12 |
| 2009 | 1.04 | 0.39 | 0.13 | 0.05 | 0.57 | 0.50 | 1.07 | 0.11 |
| 2010 | 0.83 | 0.49 | 0.20 | 0.07 | 0.96 | 0.61 | 0.57 | 0.10 |
| 2011 | 0.92 | 0.34 | 0.18 | 0.07 | 0.77 | 0.58 | 0.56 | 0.15 |
| 2012 | 0.77 | 0.44 | 0.20 | 0.05 | 0.92 | 0.51 | 0.41 | 0.15 |
| 2013 | 0.67 | 0.55 | 0.25 | 0.08 | 0.68 | 0.57 | 0.70 | 0.13 |
| 2014 | 1.32 | 0.57 | 0.15 | 0.06 | 0.74 | 0.65 | 0.75 | 0.07 |

et al., 2015), we decided to test the model's ability to reproduce the observed streamflow pdf under these conditions. The results may provide further insights into catchment functioning of the study cases, thus improving our knowledge on the variability of streamflow pdf in Alpine environments.

Table 5.2: Inter-annual variations of the model parameters: Sarca di Genova catchment

| **Year** | **Low-flow** | | | | **Melting** | | | |
|---|---|---|---|---|---|---|---|---|
| | $\alpha[cm]$ | $\lambda_P[d^{-1}]$ | $\lambda[d^{-1}]$ | $k[d^{-1}]$ | $\alpha[cm]$ | $\lambda_P[d^{-1}]$ | $\lambda[d^{-1}]$ | $k[d^{-1}]$ |
| 1996 | 0.79 | 0.39 | 0.91 | 0.07 | 0.64 | 0.58 | 0.90 | 0.16 |
| 1997 | 1.21 | 0.27 | 0.15 | 0.06 | 0.80 | 0.65 | 0.82 | 0.21 |
| 1998 | 0.89 | 0.35 | 0.27 | 0.08 | 0.55 | 0.52 | 1.19 | 0.22 |
| 1999 | 1.05 | 0.35 | 0.66 | 0.08 | 0.34 | 0.74 | 1.94 | 0.25 |
| 2000 | 1.28 | 0.37 | 0.27 | 0.16 | 0.59 | 0.48 | 1.45 | 0.21 |
| 2001 | 0.60 | 0.38 | 0.88 | 0.09 | 0.77 | 0.44 | 2.08 | 0.25 |
| 2002 | 0.97 | 0.38 | 1.12 | 0.13 | 0.92 | 0.58 | 1.29 | 0.26 |
| 2003 | 0.89 | 0.26 | 0.43 | 0.09 | 0.42 | 0.54 | 3.25 | 0.10 |
| 2004 | 0.71 | 0.30 | 0.99 | 0.15 | 0.55 | 0.44 | 2.07 | 0.12 |
| 2005 | 0.64 | 0.28 | 0.32 | 0.09 | 0.52 | 0.48 | 1.61 | 0.16 |
| 2006 | 0.74 | 0.32 | 0.32 | 0.14 | 0.42 | 0.57 | 2.08 | 0.23 |
| 2007 | 0.85 | 0.25 | 0.17 | 0.11 | 0.64 | 0.55 | 1.28 | 0.19 |
| 2008 | 1.22 | 0.38 | 0.38 | 0.09 | 0.66 | 0.57 | 1.49 | 0.08 |
| 2009 | 1.08 | 0.37 | 0.18 | 0.14 | 0.50 | 0.43 | 2.19 | 0.10 |
| 2010 | 1.03 | 0.45 | 0.12 | 0.19 | 0.81 | 0.56 | 1.06 | 0.26 |
| 2011 | 1.00 | 0.28 | 0.08 | 0.27 | 0.66 | 0.58 | 0.77 | 0.38 |
| 2012 | 0.80 | 0.51 | 0.11 | 0.25 | 0.87 | 0.49 | 0.63 | 0.23 |
| 2013 | 0.66 | 0.52 | 0.13 | 0.17 | 0.74 | 0.56 | 0.78 | 0.17 |
| 2014 | 0.77 | 0.54 | 0.11 | 0.18 | 0.72 | 0.57 | 0.82 | 0.37 |

### 5.3.2 Analytical streamflow pdf

Streamflow distributions for each season were predicted for both catchments under study by applying the analytical approach described on section 5.2.1. Figure 5.4 shows the graphical comparison between analytical (solid line) and observed (bars) streamflow pdf during low-flow and melting seasons for Vermigliana and Sarca di Genova catchments. Results suggest that the model captures the shape of the observed streamflow pdf relatively well on both seasons in the Vermigliana (figures 5.4a and 5.4c), while in Sarca di Genova, the model fails to reproduce the shape of streamflow pdf on both seasons.

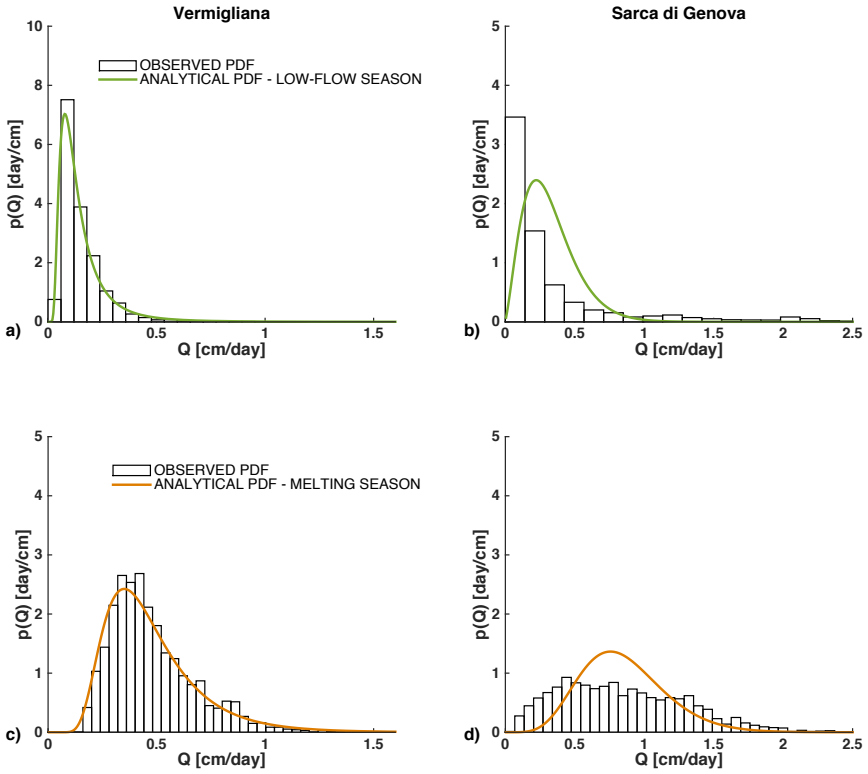


Figure 5.4: Comparison between the analytical streamflow pdf obtained with equation (5.4) for low-flow (green line) and melting seasons (orange line) estimated from observed data (bars): a-c) Vermigliana catchment, b-d) Sarca di Genova catchment.

In order to test the ability of the model to reproduce the observed streamflow pdf, we compared the cumulative distribution frequency (cdf), calculated by equation (5.5), with the one obtained from the observed data by using probability plots (Chambers, 1983). Thus, figure 5.5 compares the quantiles of modelled

versus observed cdfs, where top panels (a-b) correspond to low-flow and bottom (c-d) to melting season. To assess how well the model reproduce streamflow pdf, we plot a 45° reference line (dashed grey line), if the points fall along this line it means the model is able to reproduce the observed streamflow statistics.

In the Vermigliana catchment (figures 5.5a and 5.5c), the agreement between the model and the data is very good up to quantiles of 0.6 and 0.5 for low-flow and melting seasons respectively, while higher quantiles are underestimated by the model. In Sarca di Genova, the model is unable to capture the quantiles. In the low flow season (figure 5.5b) the model underestimates the small quantiles (up to 0.2) and overestimates quantile higher than this value. Model performance is in this case on satisfactory.

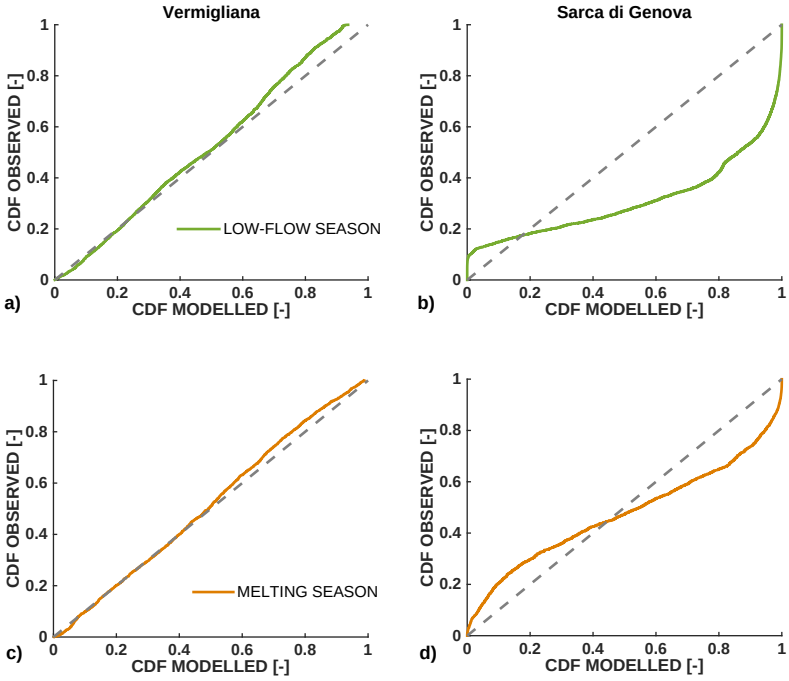


Figure 5.5: Probability plot between modelled and observed cdfs of low-flow and melting seasons: a-c) Vermigliana, b-d) Sarca di Genova catchment.

Graphically, the general agreement between modelled and observed daily streamflow pdfs is satisfactory in the case of Vermigliana for both seasons. However, on Sarca di Genova, the model fails to reproduce streamflow distribution during the low-flow season, while on the melting season, values are underestimated until the 0.5 quantile and overestimated above this threshold but to a lesser extent with respect to the previous case. Furthermore, the ability of the model to capture the observed streamflow pdf was also quantitatively assessed by computing the

Table 5.3: Qualitative and quantitative comparison of modelled and observed mean streamflow pdf

| Catchment | Season | Peak value | Mode location | K-S test |
|---|---|---|---|---|
| Vermigliana | low-flow | Ok | Ok | 0.07 |
| | melting | Ok | Ok | 0.06 |
| Sarca di Genova | low-flow | Too low | Slight right | 0.27 |
| | melting | Too high | Right | 0.21 |

Kolmogorov–Smirnov test and the results of the qualitative and quantitative assessments are reported on table 5.3.

Overall, the model is able to reproduce the streamflow statistics on the Vermigliana catchment, as seen by the low K-S values. On Sarca di Genova K-S values are instead significantly higher, while in addition the peak value and mode location differ from the observed data in both seasons. Moreover, The "s" like shape on the probability plot of the melting season on Sarca di Genova catchment (figure 5.5), is an effect of the bi-modal distribution observed on figure 5.4d, hence indicating the existence of two different dynamics controlling the shape of streamflow pdf: the first mode corresponds to snow-melting while the second is due to ice-melting, which obviously represents a significant contribution to streamflow on Sarca di Genova with respect to the Vermigliana, in particular considering the major difference on glacier size.

Therefore, the analytical model used in this chapter is able to reproduce relatively well streamflow statistics on both melting and low-flow seasons only in the case of glacierized catchments that have small glacier contribution. When glacier size and possibly, the consequent contribution to streamflow from this source significantly increases, the higher level of complexity on the system makes streamflow prediction a more difficult task.

### 5.3.3 Analytical winter streamflow pdf

Considering the results of the analytical approach used on the previous section, in particular for the low-flow season, we have also applied the extension of the model for winter streamflow described on section 5.2.2 to both case studies, hoping to improve the prediction of streamflow statistics on this season. This extended model has one calibration parameter A*, i.e., the non-responsive part of the catchment during winter. We investigate then the effect of increasing this parameter, while all the other parameters are kept constant, therefore testing the sensitivity of the model to variations on A*.

The other model parameters were estimated according to the methods described on section 5.2.2 for the two catchments under study and the mean values over the entire observational period are reported on table 5.4.

Table 5.4: Mean values of the analytical winter model parameters

| **Catchment** | $\alpha[cm]$ | $\lambda_P[d^{-1}]$ | $\tau_k[d]$ | $\tau_D[d]$ |
|---|---|---|---|---|
| Vermigliana | 0.9085 | 0.3881 | 18.55 | 9.27 |
| Sarca di Genova | 0.8948 | 0.3617 | 7.81 | 9.21 |

Figure 5.6 shows how the variations in A* produce a noticeable change on the shape of streamflow pdf: as A* increases, the peak on streamflow pdf also increases. In the Vermigliana (figure 5.6a) a relatively good fit seems to be obtained with A*=50%, while on Sarca di Genova the model is not able to capture the shape of observed streamflow pdf.

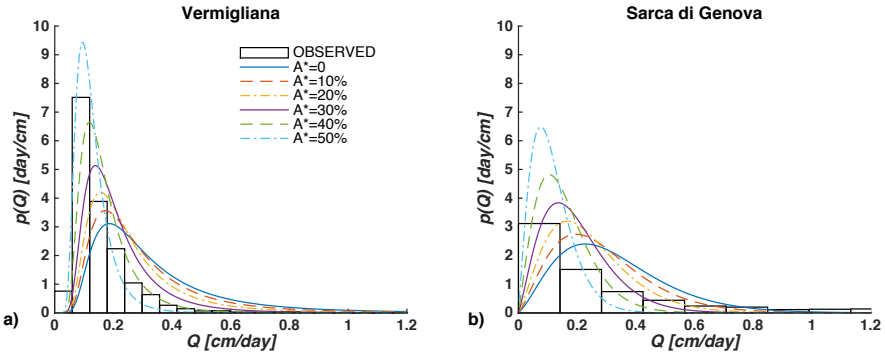


Figure 5.6: Comparison between analytical (obtained with equation (5.8) and observed (bars) streamflow pdfs during low-flow season. Effect of increasing the non-responsive part of the catchment, A*. A*(%)=[0,10,20,30,40,50]: a)Vermigliana cathment, b) Sarca di Genova.

Model performance is assessed qualitatively and quantitatively, the first analysing probability plots that compare the cumulative distribution function of analytical against observed streamflow pdf for both catchments (see figure 5.7) and the second by computing the Kolmogorov–Smirnov test (i.e., K-S test), with the results reported on table 5.5. From the probability plots, it can be easily noticed that the best fit for the Vermigliana is obtained with A*=50%: from quantiles up to 0.5 the model is underestimating while above this value the fit is relatively good. On Sarca di Genova, the model completely misses the shape of the observed streamflow pdf for all values of A*. Table 5.5 shows the details of both qualitative and quantitative evaluations of the model considering the effects of varying the parameter A*.

From figure 5.6 we have seen that an increase on A* results on the increase of the peak on modelled streamflow pdf and, according to table 5.5 also to a reduction of the mean. K-S test values decrease as A* increases and approximates to the value which gives the best fit. Moreover, the results of the K-S test for the low-flow season are higher than the ones obtained on the previous section with the original model (see table 5.3). Nevertheless, this extension of the model allowed us to identify the non-responsive part of the catchment during the low-flow season, which corresponds to 50% of the total area in the Vermigliana.

The analytical approach applied on this section describes the winter hydrological response of snow-dominated catchments and its applicability has been tested in undisturbed headwater catchments with no significant glaciers (Schaefli et al., 2013). On this study, we have considered two case studies located in the Italian

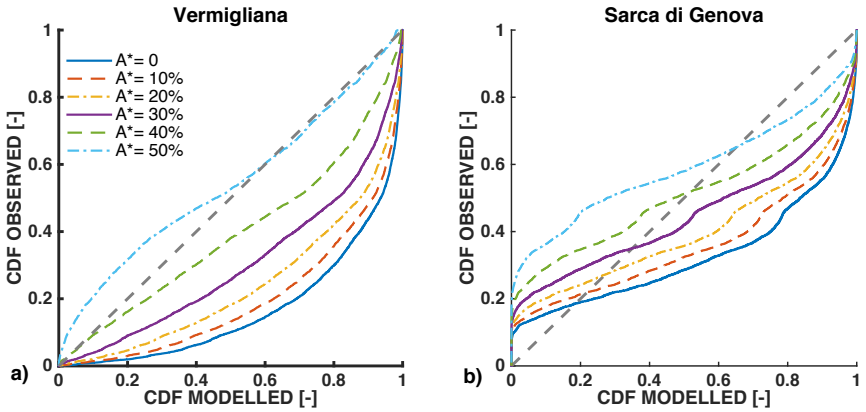


Figure 5.7: Probability plot with observed against analytical cumulative distribution functions for the low-flow season. Effect of increasing the non-responsive part of the catchment, with A*(%)=[0,10,20,30,40,50]: a)Vermigliana, b) Sarca di Genova.

Table 5.5: Effect of the increase of A* on analytical winter streamflow pdf.

| Catchment | A* | Peak value | Mode location | Mean | K-S test |
|---|---|---|---|---|---|
| Vermigliana | 0 | Too low | Right | 0.3476 | 0.5032 |
| | 10 | Too low | Right | 0.3060 | 0.4507 |
| | 20 | Too low | Right | 0.2627 | 0.3813 |
| | 30 | Too low | Slightly right | 0.2185 | 0.3133 |
| | 40 | Slightly low | Slightly right | 0.1739 | 0.2027 |
| | 50 | High | Ok | 0.1293 | 0.1182 |
| Sarca di Genova | 0 | Low | Right | 0.3236 | 0.3512 |
| | 10 | Low | Right | 0.2819 | 0.3136 |
| | 20 | Ok | Right | 0.2401 | 0.2703 |
| | 30 | Slightly high | Slightly right | 0.1984 | 0.2155 |
| | 40 | High | Slightly right | 0.1566 | 0.2066 |
| | 50 | Too high | Ok | 0.1149 | 0.2791 |

Alps, Vermigliana and Sarca di Genova, with glacier coverage of 8.55% and 25% respectively. The simulations highlighted the strong influence of the relative size of the non-responsive part of the catchment on shaping of streamflow pdf (figure 5.6).

Furthermore, the model provides a relatively good estimation of winter streamflow pdf for the Vermigliana catchment, inferring the average responsive part of the catchment during the low-flow season, which allowed us to obtain simplified but still, interesting information about the snow dynamics of this catchment (see table 5.5). On the other hand, there is an almost constant underestimation of the modelled streamflow pdf in the Sarca di Genova catchment (see figures 5.6b and 5.7b). This underestimation may be caused by the rough estimation of the delayed residence time $\tau_w$, calculated with equation (5.6). There are two important sources of uncertainty affecting $\tau_w$, first the melt of permanent snow and ice on

a catchment with a significant glacier coverage like Sarca di Genova may lead to estimates of $\tau_k$ that are not representative of the catchment average behaviour, as seen from table 5.4, the value for this parameter is very different on Sarca di Genova when compared to Vermigliana, while the rest of the parameters are instead very similar. Second, the location of the meteorological station (i.e., low altitude), may the responsible of an underestimation on the average temperature conditions in the responsive area, thus affecting the delay parameter $\tau_D$, which is very sensitive to the temperature dataset.

## 5.4 Conclusions

On this chapter, we applied an existing stochastic analytical modelling approach in order to predict streamflow distribution on two case studies within the Alpine region, Vermigliana and Sarca di Genova catchments, both with similar features but characterized by the presence of different glacier size, 8.5% and 25.0% of total catchment area respectively.

As seen in Chapter 4, both catchments present two seasons characterized by different flow regimes: a melting season, showing high flows (May to August) which main contribution comes from snow and ice-melting, followed by a low-flow season, during which the catchment experiences snow accumulation due to low temperatures (September to April). Thus, we applied an existent stochastic modelling framework (see Botter et al., 2007a,b,c, 2009), on a seasonal basis, with parameters estimated from the observed precipitation, temperature and streamflow time series presented in Chapter 4.

Glaciers can temporarily store water as snow and ice (Kuhn and Batlogg, 1998; Stewart, 2009). The subsequent release of this storage, is controlled by both climate and internal drainage mechanisms (Hock et al., 2005) and directly affect diurnal variations of streamflow during the melting season, as well as significant seasonal variations that regulate inter-annual variability. Therefore, glaciers are characteristic features of these complex environments that can have strong influence on catchment runoff quantity and distribution (Hock et al., 2005). The results of this chapter evidence that the size of glacier coverage on these type of catchments represents a very important feature of the system which cannot be neglected. The dynamics given by ice-melting and snow-melting theoretically can be implicitly taken into account by the model with the parameter representing the frequency of effective events. Yet, in Sarca di Genova, characterized by a considerably glacier coverage, these dymanics could not be captured, while instead in the Vermgiliana, which is mainly dominated by snow-melting and a smaller glacier size, the dynamics were captured relatively well.

Furthermore, we investigated the relative size of the non-responsive area during winter by applying an extension of the previous model (see Schaefli et al., 2013) to the low-flow season data in both catchments. Results show that the size of the non-responsive area during winter has a strong influence on the shape of streamflow pdf, providing a relatively good estimation on the Vermigliana catchment with a non-responsive area equal to 50% of the total surface, hence providing simplified, yet new information on catchment functioning. However, on Sarca di

Genova, the model showed a constant underestimation of streamflow pdf caused by the rough estimation of the delayed residence time due to snow accumulation during winter.

In conclusion, glaciers in the European Alps have lost almost 50% of their surface from 1850 to 2000 (Zemp et al., 2006). In particular, the Mandrone (Sarca di Genova catchment), has experienced intense melting phenomena at the base of the glacier in the past years (Provincia Autonoma di Trento, Meteotrentino, 2012). Taking into account that these catchments are expected to be significantly affected by the rise of temperature due to climate change (Barnett et al., 2005) and considering the importance of preserving these sources of freshwater, an adequate characterization and prediction of streamflow distribution becomes essential. Thus, we suggest that future research should be focused on improving the mathematical formulation of these models in order to include an explicit representation of snow and ice-melting dynamics.

*Chapter* 6

# Conclusions

Alpine headwaters present large streamflow variability over many temporal scales, which can be influenced by different features, such as climate patterns, temperature changes, diurnal variations on streamflow, snow dynamics and catchment's storage capacity. Streamflow generation is controlled by a multiplicity of sources, such as rain, snow-melt, glacier-melt and groundwater, therefore understanding streamflow variability and quantifying its sources becomes essential to characterize catchment's hydrological functioning in these complex environments. Likewise, a better understanding of the nature and variability of the relationship between atmospheric forcing and streamflow can give valuable information about the sensitivity of Alpine systems to climate changes, useful to assess the applicability of hydrological models to this context and to improve existing analytical frameworks or contribute to the development of new modelling structures.

Moreover, the use of alternative information sources, such as geochemical data, to supplement traditional hydrological observations, provides new insights that lead to a better comprehension of the hydrological response of Alpine systems. Our knowledge about the complex hydrological dynamics occurring in these catchments can still be enriched throughout studies based on the combined use of hydrological and geochemical information obtained from field experiments, and finally be used as support to water resources management of such important environments.

The aim of this doctoral thesis was to provide new insights that broaden our knowledge on the multi-faceted aspects of streamflow generation in Alpine region catchments, exploring the different roles played by hydrological and geochemical information to investigate the mechanisms controlling streamflow generation on real case studies, applying different techniques and considering a variability of temporal scales.

For this purpose, the work has been structured into four research elements. On the first, information on streamflow source components during significant hydrological events has been obtained by applying a two-component mixing analysis based mainly on the use of environmental tracers (Chapter 2). The outcomes of this analysis lead us to a more detailed study on the nature and variability of the relationship between electrical conductivity and streamflow (Chapter 3) in

order to understand the limits on the use of EC for different purposes (e.g., using EC as a proxy for water discharge or to estimate estimating daily contribution from snow-melting). Furthermore, the nature and variability of the relationship between streamflow and atmospheric forcing was also investigated (Chapter 4), trough the application of alternative methods for data analysis and visualization in order to obtain new insights into catchment functioning, allowing us to improve the conceptual model, followed by the application of an existing stochastic framework for characterization and prediction of streamflow distribution (Chapter 5). The main contributions of each element have been summarized as follows:

**Streamflow variability during single events:** The maximum contribution of event water estimated with the two-component mixing analysis applied to four significant hydrological events ranged from 45% to 71%, with a significant difference in the rate of increase of the rising part of the hydrograph. Moreover, the study of dynamics of new water contribution during these events provided new insights into catchment functioning, suggesting that the relative contribution of event water with respect to pre-event water does not change only according to the magnitude of the precipitation event or to temperature changes, but it also depends on the amount of snow accumulated prior to the event. Likewise, the occurrence as well as the size of the hysteresis loops found between streamflow and tracer concentration (clockwise direction when using EC while counter-clockwise direction with stable isotopes), are also related to the presence and thickness of the snowpack: small hysteresis loops can be observed in total absence of snow cover or in presence of very thin snowpack, while very wide hysteresis loops appear in the presence of thick snowpacks. More importantly, it was found that this hysteresis can be suppressed by considering a delay time between EC and Q signals, which varies according to the thickness of the snowpack present during each event, suggesting that the thicker the snowpack the longer the delay time. Overall, hydrological data complemented with other sources of information, such as geochemical data, provide important additional insights on system functioning (Pellerin et al., 2008; Laudon and Slaymaker, 1997; Finger et al., 2015).

**Nature and variability of the relationship between streamflow and electrical conductivity:** The relationship between electrical conductivity and water discharge is characterized by a wide hysteresis cycle at the seasonal scale, influenced by the amount of snow fallen in the previous winter season and by the snow cover duration within the catchment. Rain-on-snow events however, significantly depart from the annual cycle complicating the use of a single EC-Q relationship for the prediction of water discharge based on EC measurements. Moreover, the continuous wavelet transform of the signals analysed separately evidenced features like diurnal periodicities and the occurrence of high flow events. Yet, the most interesting information was obtained only when evidencing the modes of variation (periods) on which the two signals were correlated, thus wavelet coherence evidenced that EC and Q are out of phase and identified the periods on which snow and glacier-melting are triggered along the season. Also, a significant change can be observed in the temporal scales of variability and correlation between EC

and Q when the catchment shifts from a snow and glacier-melting regime to a rainfall controlled regime. A cross-correlation analysis of the two signals allowed us to verify the existence of a relatively constant time lag between 1 and 3 hours during the melting period. In addition, we showed how the analysis of EC and Q diurnal cycles can provide qualitative information about the snow dynamics of the snowpack on each year, while the amplitude of these cycles, can be used for estimating the daily contribution from snow-melting to streamflow, however the best results are still obtained with the signal of Q. Overall, the combined analysis of hydrological and geochemical information provided valuable insights into the catchment's hydrological characteristics.

**Temporal variability of the relationship between streamflow and atmospheric forcing:** Catchment inter-comparison trough the application of alternative methods of data analysis and visualization, such as Hovmöller diagrams and wavelet analysis, to identify specific patterns associated to the relationship between atmospheric forcing and streamflow, can provide further insights into the hydrological response of Alpine catchments. Hovmöller diagrams proved to be a simplified way to evidence the existence of patterns at different temporal scales. On the other hand, the continuous wavelet transform allowed us to perform a more in-depth analysis of the variability across temporal scales of hydrological time series, revealing seasonal, annual and even bi-annual periodicities depending on the case, while the global wavelet spectra evidenced the specific periods on which these periodicities occurred. The scale-averaged power of the wavelet spectra over specific bands instead indicated the years in which oscillations of wavelet spectra were enhanced due to changes on precipitation time series. Furthermore, wavelet coherence demonstrated the strong seasonality linking streamflow to temperature time series in the catchments under study. Yet, in some cases the fluctuations on streamflow were increased by particularly intense precipitation periods, these two signals were also highly correlated.

**Characterization and prediction of streamflow variability:** Assessing the applicability of streamflow probability distribution models to real case studies leads to a comprehensive knowledge on streamflow variability in Alpine rivers, which improves conceptual and analytical frameworks, that serve as support to water resources management on these environments. An existent stochastic modelling framework was applied (see Botter et al., 2007a,b,c, 2009), in order to predict streamflow distribution of two Alpine catchments characterized by the presence of glaciers of different size (8% and 25% of total catchment area). The model was able to reproduce the observed distribution of streamflow reasonably well on the catchment with the smaller glacier, however in the case with considerably larger glacier size, the model provide a poor representation of streamflow variability. Furthermore, an extension of the model (see Schaefli et al., 2013) allowed us to investigate the influence of the relative size of the non-responsive area during winter on the shape of streamflow pdf, hence providing simplified, yet new information on catchment functioning. Overall, results show that the size of glacier coverage on these type of catchments represents a very important feature

of the system and can have strong influence on catchment runoff quantity and distribution.

The analyses conducted in this thesis highlight the potential of geochemical data as an addition to hydrological information, in particular electrical conductivity continuous measurements. More specifically, the outcomes of Chapter 2 and 3 represent an important step towards future research on streamflow source components in Alpine rivers based on the combined use of hydrological and geochemical information at different temporal scales (event, seasonal and annual). In particular, future research should focus on the development of new methodologies to: (i) quantitatively correlate the time lag found between streamflow and precipitation peaks with respect to maximum event water contribution, to the thickness of the snowpack and; (ii) quantitatively relate the width of streamflow-tracer concentration hysteresis loops to the thickness of the snowpack during single events.

Additional insights on the nature and variability between electrical conductivity and streamflow can be obtained by including simplified quantitative approaches or analytical models that test the applicability of different relationships between EC and Q considering the limitations found in this thesis, hence leading to a more rigorous application of the EC-Q relationship for different hydrological and geochemical purposes. Moreover, the contributions from Chapter 3 can further serve as support for future research work on the different transfer functions that characterize water and solute transport in snow and glacier-melting dominated catchments.

Furthermore, the identification of particular patterns among catchments (Chapter 4) can be very useful to improve our understanding on the variability of long-term hydrological time series and to better comprehend the dominant mechanisms controlling streamflow generation in Alpine streams at large temporal scales (decades). Studies of this nature may be extended to develop methodologies that improve existing conceptual models and to built more adequate frameworks for different model applications in Alpine regions. On the other hand, the results from the stochastic analytical approach applied in Chapter 5, suggest that future studies should concentrate on improving the mathematical formulation of these type of models by including an explicit representation of snow and ice-melting dynamics or to consider these effects for instance, through the coupling with degree-day models.

# Bibliography


Ali, G. A., L'Heureux, C., Roy, A. G., Turmel, M.-C., and Courchesne, F. (2011). Linking spatial patterns of perched groundwater storage and stormflow generation processes in a headwater forested catchment. *Hydrological Processes*, 25(25):3843–3857.

Allamano, P., Claps, P., and Laio, F. (2009). Global warming increases flood risk in mountainous areas. *Geophysical Research Letters*, 36(24).

Amorocho, J. and Orlob, G. (1961). *Nonlinear analysis of hydrologic systems.* PhD thesis, University of California, Berkeley.

Barnett, T. P., Adam, J. C., and Lettenmaier, D. P. (2005). Potential impacts of a warming climate on water availability in snow-dominated regions. *Nature*, 438(7066):303–309.

Behrens, H., Bergmann, H., Moser, H., Rauert, W., Stichler, W., Ambach, W., Eisner, H., and Pessl, K. (1971). Study of the discharge of alpine glaciers by means of environmental isotopes and dye tracers. *Zeitscherkd Glazialgeo*, 7:79–102.

Birkel, C., Soulsby, C., Tetzlaff, D., Dunn, S., and Spezia, L. (2012). High-frequency storm event isotope sampling reveals time-variant transit time distributions and influence of diurnal cycles. *Hydrological Processes*, 26(2):308–316.

Bizzotto, E., Villa, S., and Vighi, M. (2009). Pop bioaccumulation in macroinvertebrates of alpine freshwater systems. *Environmental pollution*, 157(12):3192–3198.

Bolto, B., Hoang, M., and Xie, Z. (2012). A review of water recovery by vapour permeation through membranes. *Water research*, 46(2):259–266.

Botter, G., Basso, S., Rodriguez-Iturbe, I., and Rinaldo, A. (2013). Resilience of river flow regimes. *Proceedings of the National Academy of Sciences*, 110(32):12925–12930.

Botter, G., Bertuzzo, E., and Rinaldo, A. (2011). Catchment residence and travel time distributions: The master equation. *Geophysical Research Letters*, 38(11).

Botter, G., Peratoner, F., Porporato, A., Rodriguez-Iturbe, I., and Rinaldo, A. (2007a). Signatures of large-scale soil moisture dynamics on streamflow statistics across us climate regimes. *Water resources research*, 43(11).

Botter, G., Porporato, A., Daly, E., Rodriguez-Iturbe, I., and Rinaldo, A. (2007b). Probabilistic characterization of base flows in river basins: Roles of soil, vegetation, and geomorphology. *Water resources research*, 43(6).

Botter, G., Porporato, A., Rodriguez-Iturbe, I., and Rinaldo, A. (2007c). Basin-scale soil moisture dynamics and the probabilistic characterization of carrier hydrologic flows: Slow, leaching-prone components of the hydrologic response. *Water resources research*, 43(2).

Botter, G., Porporato, A., Rodriguez-Iturbe, I., and Rinaldo, A. (2009). Nonlinear storage-discharge relations and catchment streamflow regimes. *Water resources research*, 45(10).

Botter, G., Zanardo, S., Porporato, A., Rodriguez-Iturbe, I., and Rinaldo, A. (2008). Ecohydrological model of flow duration curves and annual minima. *Water resources research*, 44(8).

Box, G. E., Jenkins, G. M., and Reinsel, G. C. (2011). *Time series analysis: forecasting and control*, volume 734. John Wiley & Sons.

Brown, L. E., D M, H., A M, M., C, S., A J, H., and M J, B. (2006). Water source dynamics in a glacierized alpine river basin (Taillon-Gabiétous, French pyrénées). *Water Resources Research*, 42(8):W08404.

Brutsaert, W. (2005). *Hydrology: an introduction*. Cambridge University Press.

Brutsaert, W. and Nieber, J. L. (1977). Regionalized drought flow hydrographs from a mature glaciated plateau. *Water Resources Research*, 13(3):637–643.

Burns, D. A., McDonnell, J. J., Hooper, R. P., Peters, N. E., Freer, J. E., Kendall, C., and Beven, K. (2001). Quantifying contributions to storm runoff through end-member mixing analysis and hydrologic measurements at the panola mountain research watershed(georgia, usa). *Hydrological Processes*, 15(10):1903–1924.

Burt, T. and McDonnell, J. (2015). Whither field hydrology? the need for discovery science and outrageous hydrological hypotheses. *Water Resources Research*, 51(8):5919–5928.

Buttle, J. (1994). Isotope hydrograph separations and rapid delivery of pre-event water from drainage basins. *Progress in Physical Geography*, 18(1):16–41.

Cable, J., Ogle, K., and Williams, D. (2011). Contribution of glacier meltwater to streamflow in the wind river range, wyoming, inferred via a bayesian mixing model applied to isotopic measurements. *Hydrological Processes*, 25(14):2228–2236.

Caine, N. (1992). Modulation of the diurnal streamflow response by the seasonal snowcover of an alpine basin. *Journal of Hydrology*, 137(1):245–260.

Carey, S. and Quinton, W. (2005). Evaluating runoff generation during summer using hydrometric, stable isotope and hydrochemical methods in a discontinuous permafrost alpine catchment. *Hydrological Processes*, 19(1):95–114.

Carey, S. K., Tetzlaff, D., Buttle, J., Laudon, H., McDonnell, J., McGuire, K., Seibert, J., Soulsby, C., and Shanley, J. (2013). Use of color maps and wavelet coherence to discern seasonal and interannual climate influences on streamflow variability in northern catchments. *Water Resources Research*, 49(10):6194–6207.

Castellarin, A., Camorani, G., and Brath, A. (2007). Predicting annual and long-term flow-duration curves in ungauged basins. *Advances in Water Resources*, 30(4):937–953.

Ceola, S., Botter, G., Bertuzzo, E., Porporato, A., Rodriguez-Iturbe, I., and Rinaldo, A. (2010). Comparative study of ecohydrological streamflow probability distributions. *Water Resources Research*, 46(9).

Chambers, J. M. (1983). *Graphical methods for data analysis*.

Chiogna, G., Majone, B., Paoli, K. C., Diamantini, E., Stella, E., Mallucci, S., Lencioni, V., Zandonai, F., and Bellin, A. (2015). A review of hydrological and chemical stressors in the adige catchment and its ecological status. *Science of The Total Environment*.

Chiogna, G., Santoni, E., Camin, F., Tonon, A., Majone, B., Trenti, A., and Bellin, A. (2014). Stable isotope characterization of the vermigliana catchment. *Journal of Hydrology*, 509:295–305.

Chow, V. T. et al. (1964). Handbook of applied hydrology; a compendium of water-resources technology. Technical report.

Christophersen, N. and Hooper, R. P. (1992). Multivariate analysis of stream water chemical data: The use of principal components analysis for the end-member mixing problem. *Water Resources Research*, 28(1):99–107.

Christophersen, N., Neal, C., Hooper, R. P., Vogt, R. D., and Andersen, S. (1990). Modelling streamwater chemistry as a mixture of soilwater end-members—a step towards second-generation acidification models. *Journal of Hydrology*, 116(1):307–320.

Collins, D. N. (1979). Hydrochemistry of meltwaters draining from an alpine glacier. *Arctic and Alpine Research*, pages 307–324.

Coulibaly, P. and Burn, D. H. (2004). Wavelet analysis of variability in annual Canadian streamflows. *Water Resour. Res.*, 40(3).

Crouzet, E., Hubert, P., Olive, P., Siwertz, E., and Marce, A. (1970). Le tritium dans les mesures d'hydrologie de surface. determination experimentale du coefficient de ruissellement. *Journal of Hydrology*, 11(3):217–229.

DeBeer, C., Pomeroy, J., et al. (2010). Simulation of the snowmelt runoff contributing area in a small alpine basin. *Hydrology and Earth System Sciences*, 14(7):1205–1219.

Dincer, T., Payne, B., Florkowski, T., Martinec, J., and Tongiorgi, E. (1970). Snowmelt runoff from measurements of tritium and oxygen-18. *Water Resources Research*, 6(1):110–124.

Doulatyari, B., Basso, S., Schirmer, M., and Botter, G. (2014). River flow regimes and vegetation dynamics along a river transect. *Advances in Water Resources*, 73:30–43.

Doulatyari, B., Betterle, A., Basso, S., Biswal, B., Schirmer, M., and Botter, G. (2015). Predicting streamflow distributions and flow duration curves from landscape and climate. *Advances in Water Resources*, 83:285–298.

Doyle, M. W., Stanley, E. H., Strayer, D. L., Jacobson, R. B., and Schmidt, J. C. (2005). Effective discharge analysis of ecological processes in streams. *Water Resources Research*, 41(11).

Dzikowski, M. and Jobard, S. (2012). Mixing law versus discharge and electrical conductivity relationships: application to an alpine proglacial stream. *Hydrological Processes*, 26(18):2724–2732.

Elmore, A. J. and Kaushal, S. S. (2008). Disappearing headwaters: patterns of stream burial due to urbanization. *Frontiers in Ecology and the Environment*, 6(6):308–312.

Engel, M., Penna, D., Bertoldi, G., Dell'Agnese, A., Soulsby, C., and Comiti, F. (2015). Identifying runoff contributions during melt-induced runoff events in a glacierized alpine catchment. *Hydrological Processes*, pages n/a–n/a.

Evans, C. and Davies, T. D. (1998). Causes of concentration/discharge hysteresis and its potential as a tool for analysis of episode hydrochemistry. *Water Resources Research*, 34(1):129–137.

Finger, D., Vis, M., Huss, M., and Seibert, J. (2015). The value of multiple data set calibration versus model complexity for improving the performance of hydrological models in mountain catchments. *Water Resources Research*, 51(4):1939–1958.

Foufoula-Georgiou, E. and Kumar, P. (1994). *Wavelets in geophysics*, volume 4. Academic Press.

Garvelmann, J., Pohl, S., and Weiler, M. (2015). Spatio-temporal controls of snowmelt and runoff generation during rain-on-snow events in a mid-latitude mountain catchment. *Hydrological Processes*.

Gaucherel, C. (2002). Use of wavelet transform for temporal characterisation of remote watersheds. *Journal of hydrology*, 269(3):101–121.

Genereux, D. (1998). Quantifying uncertainty in tracer-based hydrograph separations. *Water Resources Research*, 34(4):915–919.

Grinsted, A., Moore, J. C., and Jevrejeva, S. (2004). Application of the cross wavelet transform and wavelet coherence to geophysical time series. *Nonlinear processes in geophysics*, 11(5/6):561–566.

Guan, K., Thompson, S. E., Harman, C. J., Basu, N. B., Rao, P. S. C., Sivapalan, M., Packman, A. I., and Kalita, P. K. (2011). Spatiotemporal scaling of hydrological and agrochemical export dynamics in a tile-drained midwestern watershed. *Water Resources Research*, 47(10):n/a–n/a.

Gurnell, A. and Fenn, C. (1984). Flow separation, sediment source areas and suspended sediment transport in a pro-glacial stream. *Catena, Suppl*, 5:109–119.

Gurnell, A. and Fenn, C. (1985). Spatial and temporal variations in electrical conductivity in a pro-glacial stream system. *Journal of Glaciology*, 31(108):108–114.

Hayashi, M., Vogt, T., Mächler, L., and Schirmer, M. (2012). Diurnal fluctuations of electrical conductivity in a pre-alpine river: Effects of photosynthesis and groundwater exchange. *Journal of Hydrology*, 450:93–104.

Hock, R., Jansson, P., and Braun, L. N. (2005). Modelling the response of mountain glacier discharge to climate warming. In *Global Change and Mountain Regions*, pages 243–252. Springer.

Hooper, R. P. (2001). Applying the scientific method to small catchment studies: a review of the panola mountain experience. *Hydrological Processes*, 15(10):2039–2050.

Hooper, R. P. (2003). Diagnostic tools for mixing models of stream water chemistry. *Water Resources Research*, 39(3).

Hooper, R. P., Christophersen, N., and Peters, N. E. (1990). Modelling streamwater chemistry as a mixture of soilwater end-members?an application to the panola mountain catchment, georgia, usa. *Journal of Hydrology*, 116(1):321–343.

Hovmöller, E. (1949). The trough-and-ridge diagram. *Tellus*, 1(2):62–66.

Huth, A., Leydecker, A., Sickman, J., and Bales, R. (2004). A two-component hydrograph separation for three high-elevation catchments in the sierra nevada, california. *Hydrological processes*, 18(9):1721–1733.

Kirchner, J. W. (2003). A double paradox in catchment hydrology and geochemistry. *Hydrological Processes*, 17(4):871–874.

Kirchner, J. W. (2009). Catchments as simple dynamical systems: Catchment characterization, rainfall-runoff modeling, and doing hydrology backward. *Water Resources Research*, 45(2).

Klaus, J. and McDonnell, J. (2013). Hydrograph separation using stable isotopes: Review and evaluation. *Journal of Hydrology*, 505:47–64.

Kuhn, M. and Batlogg, N. (1998). Glacier runoff in alpine headwaters in a changing climate. *International Association of Hydrological Sciences, Publication*, (248):79–88.

Kumar, P. and Foufoula-Georgiou, E. (1993). A multicomponent decomposition of spatial rainfall fields: 1. segregation of large-and small-scale features using wavelet transforms. *Water Resources Research*, 29(8):2515–2532.

Ladouche, B., Probst, A., Viville, D., Idir, S., Baqué, D., Loubet, M., Probst, J.-L., and Bariac, T. (2001). Hydrograph separation using isotopic, chemical and hydrological approaches (strengbach catchment, france). *Journal of hydrology*, 242(3):255–274.

Lau, K. and Weng, H. (1995). Climate signal detection using wavelet transform: How to make a time series sing. *Bulletin of the American Meteorological Society*, 76(12):2391–2402.

Laudon, H., Hemond, H. F., Krouse, R., and Bishop, K. H. (2002). Oxygen 18 fractionation during snowmelt: Implications for spring flood hydrograph separation. *Water Resources Research*, 38(11):40–1.

Laudon, H. and Slaymaker, O. (1997). Hydrograph separation using stable isotopes, silica and electrical conductivity: an alpine example. *Journal of Hydrology*, 201(1):82–101.

Lee, J., Feng, X., Faiia, A., Posmentier, E., Osterhuber, R., and Kirchner, J. (2010). Isotopic evolution of snowmelt: A new model incorporating mobile and immobile water. *Water Resources Research*, 46(11).

Leibundgut, C., Maloszewski, P., and Külls, C. (2011). *Tracers in hydrology*. John Wiley & Sons.

Lischeid, G. (2008). Combining hydrometric and hydrochemical data sets for investigating runoff generation processes: tautologies, inconsistencies and possible explanations. *Geography Compass*, 2(1):255–280.

Liu, F., Williams, M. W., and Caine, N. (2004). Source waters and flow paths in an alpine catchment, colorado front range, united states. *Water Resources Research*, 40(9).

Lundquist, J. D. and Cayan, D. R. (2002). Seasonal and spatial patterns in diurnal cycles in streamflow in the western united states. *Journal of Hydrometeorology*, 3(5):591–603.

Lundquist, J. D. and Dettinger, M. D. (2005). How snowpack heterogeneity affects diurnal streamflow timing. *Water resources research*, 41(5).

Lundquist, J. D., Dettinger, M. D., and Cayan, D. R. (2005). Snow-fed streamflow timing at different basin scales: Case study of the tuolumne river above hetch hetchy, yosemite, california. *Water resources research*, 41(7).

Marengo, J. A., Tomasella, J., Alves, L. M., Soares, W. R., and Rodriguez, D. A. (2011). The drought of 2010 in the context of historical droughts in the amazon region. *Geophysical Research Letters*, 38(12).

Martinec, J. (1975). Subsurface flow from snowmelt traced by tritium. *Water Resources Research*, 11(3):496–498.

Martinec, J., Siegenthaler, U., Oeschger, H., and Tongiorgi, E. (1974). New insights into the run-off mechanism by environmental isotopes. Technical report, Federal Inst. for Snow and Avalanche Research, Weissfluhjoch, Switzerland.

Maurya, A., Shah, M., Deshpande, R., Bhardwaj, R., Prasad, A., and Gupta, S. (2011). Hydrograph separation and precipitation source identification using stable water isotopes and conductivity: River ganga at himalayan foothills. *Hydrological Processes*, 25(10):1521–1530.

McCabe, G. J., Hay, L. E., and Clark, M. P. (2007). Rain-on-snow events in the western united states. *Bulletin of the American Meteorological Society*, 88(3):319–328.

McCuen, R. H. et al. (1982). *A guide to hydrologic analysis using SCS methods*. Prentice-Hall, Inc.

McGlynn, B. L. and McDonnell, J. J. (2003). Quantifying the relative contributions of riparian and hillslope zones to catchment runoff. *Water Resources Research*, 39(11).

Merz, R. and Blöschl, G. (2003). A process typology of regional floods. *Water Resources Research*, 39(12).

Meteotrentino (2011). Evoluzione e monitoraggi recenti dei ghiacchiai trentini. *Meteorological Office of the Trentino Province*.

Molini, A., Katul, G. G., and Porporato, A. (2011). Maximum discharge from snowmelt in a changing climate. *Geophysical Research Letters*, 38(5).

Moore, R. (1985). The probability-distributed principle and runoff production at point and basin scales. *Hydrological Sciences Journal*, 30(2):273–297.

Muir, D. L., Hayashi, M., and McClymont, A. F. (2011). Hydrological storage and transmission characteristics of an alpine talus. *Hydrological Processes*, 25(19):2954–2966.

Muñoz-Villers, L. E. and McDonnell, J. J. (2012). Runoff generation in a steep, tropical montane cloud forest catchment on permeable volcanic substrate. *Water Resources Research*, 48(9).

Mutzner, R., Weijs, S. V., Tarolli, P., Calaf, M., Oldroyd, H. J., and Parlange, M. B. (2015). Controls on the diurnal streamflow cycles in two subbasins of an alpine headwater catchment. *Water Resources Research*.

Ohlanders, N., Rodriguez, M., and McPhee, J. (2013). Stable water isotope variation in a central andean watershed dominated by glacier and snowmelt. *Hydrology and Earth System Sciences*, 17(3):1035–1050.

Pellerin, B. A., Wollheim, W. M., Feng, X., and Vörösmarty, C. J. (2008). The application of electrical conductivity as a tracer for hydrograph separation in urban catchments. *Hydrological processes*, 22(12):1810–1818.

Penna, D., Engel, M., Mao, L., Dell'Agnese, A., Bertoldi, G., and Comiti, F. (2014). Tracer-based analysis of spatial and temporal variation of water sources in a glacierized catchment. *Hydrology and Earth System Sciences Discussions*, 11(5):4879–4924.

Penna, D., Meerveld, H., Oliviero, O., Zuecco, G., Assendelft, R., Dalla Fontana, G., and Borga, M. (2015). Seasonal changes in runoff generation in a small forested mountain catchment. *Hydrological Processes*, 29(8):2027–2042.

Peters, N. E. and Aulenbach, B. T. (2011). Water storage at the panola mountain research watershed, georgia, usa. *Hydrological Processes*, 25(25):3878–3889.

Pinder, G. F. and Jones, J. F. (1969). Determination of the ground-water component of peak discharge from the chemistry of total runoff. *Water Resources Research*, 5(2):438–445.

Provincia Autonoma di Trento, Meteotrentino (2012). Annale Glaciologico Trentino 2010-2011.

Ranzi, R., Grossi, G., Gitti, A., and Taschner, S. (2010). Energy and mass balance of the mandrone glacier (adamello, central alps). *Geografia Fisica e Dinamica Quaternaria*, 33(1):45–60.

Richards, G. and Moore, R. (2003). Suspended sediment dynamics in a steep, glacier-fed mountain stream, place creek, canada. *Hydrological Processes*, 17(9):1733–1753.

Rinaldo, A., Benettin, P., Harman, C. J., Hrachowitz, M., McGuire, K. J., Van Der Velde, Y., Bertuzzo, E., and Botter, G. (2015). Storage selection functions: A coherent framework for quantifying how catchments store and release water and solutes. *Water Resources Research*, 51(6):4840–4847.

Rodríguez-Iturbe, I. and Porporato, A. (2005). *Ecohydrology of water-controlled ecosystems: soil moisture and plant dynamics*. Cambridge University Press.

Rodriguez-Iturbe, I., Porporato, A., Ridolfi, L., Isham, V., and Coxi, D. (1999). Probabilistic modelling of water balance at a point: the role of climate, soil and vegetation. In *Proceedings of the Royal Society of London A: Mathematical, Physical and Engineering Sciences*, volume 455, pages 3789–3805. The Royal Society.

Saco, P. and Kumar, P. (2000). Coherent modes in multiscale variability of streamflow over the united states. *Water Resources Research*, 36(4):1049–1067.

Schaefli, B., Rinaldo, A., and Botter, G. (2013). Analytic probability distributions for snow-dominated streamflow. *Water Resources Research*, 49(5):2701–2713.

Searcy, J. K. (1959). *Flow-duration curves*. US Government Printing Office.

Sharma, A., Tarboton, D. G., and Lall, U. (1997). Streamflow simulation: A nonparametric approach. *Water Resources Research*, 33(2):291–308.

Shook, K. R. and Pomeroy, J. W. (2011). Memory effects of depressional storage in northern prairie hydrology. *Hydrological Processes*, 25(25):3890–3898.

Simoni, S., Padoan, S., Nadeau, D., Diebold, M., Porporato, A., Barrenetxea, G., Ingelrest, F., Vetterli, M., and Parlange, M. (2011). Hydrologic response of an alpine watershed: Application of a meteorological wireless sensor network to understand streamflow generation. *Water Resources Research*, 47(10).

Singh, P., Spitzbart, G., Hübl, H., and Weinmeister, H. (1997). Hydrological response of snowpack under rain-on-snow events: a field study. *Journal of Hydrology*, 202(1):1–20.

Sklash, M. G. and Farvolden, R. N. (1979). The role of groundwater in storm runoff. *Developments in Water Science*, 12:45–65.

Soulsby, C., Rodgers, P., Smart, R., Dawson, J., and Dunn, S. (2003). A tracer-based assessment of hydrological pathways at different spatial scales in a mesoscale scottish catchment. *Hydrological Processes*, 17(4):759–777.

Speed, M., Tetzlaff, D., Hrachowitz, M., and Soulsby, C. (2011). Evolution of the spatial and temporal characteristics of the isotope hydrology of a montane river basin. *Hydrological Sciences Journal–Journal des Sciences Hydrologiques*, 56(3):426–442.

Stewart, I. T. (2009). Changes in snowpack and snowmelt runoff for key mountain regions. *Hydrological Processes*, 23(1):78–94.

Suecker, J. K., Ryan, J. N., Kendall, C., and Jarrett, R. D. (2000). Determination of hydrologic pathways during snowmelt for alpine/subalpine basins, rocky mountain national park, colorado. *Water Resources Research*, 36(1):63–75.

Surfleet, C. G. and Tullos, D. (2013). Variability in effect of climate change on rain-on-snow peak flow events in a temperate climate. *Journal of Hydrology*, 479:24–34.

Tetzlaff, D., Waldron, S., Brewer, M., and Soulsby, C. (2007). Assessing nested hydrological and hydrochemical behaviour of a mesoscale catchment using continuous tracer data. *Journal of Hydrology*, 336(3):430–443.

Theakstone, W. H. (1988). Temporal variations of isotopic composition of glacier-river water during summer: observations at austre okstindbreen, okstindan, norway. *Journal of Glaciology*, 34(118):309–317.

Tobin, C., Schaefli, B., Nicótina, L., Simoni, S., Barrenetxea, G., Smith, R., Parlange, M., and Rinaldo, A. (2013). Improving the degree-day method for sub-daily melt simulations with physically-based diurnal variations. *Advances in Water Resources*, 55:149–164.

Toffolon, M., Siviglia, A., and Zolezzi, G. (2010). Thermal wave dynamics in rivers affected by hydropeaking. *Water Resources Research*, 46(8).

Torrence, C. and Compo, G. P. (1998). A practical guide to wavelet analysis. *Bulletin of the American Meteorological society*, 79(1):61–78.

Torrence, C. and Webster, P. J. (1999). Interdecadal changes in the enso-monsoon system. *Journal of Climate*, 12(8):2679–2690.

Uhlenbrook, S. and Hoeg, S. (2003). Quantifying uncertainties in tracer-based hydrograph separations: a case study for two-, three-and five-component hydrograph separations in a mountainous catchment. *Hydrological Processes*, 17(2):431–453.

Unnikrishna, P. V., McDonnell, J. J., and Kendall, C. (2002). Isotope variations in a sierra nevada snowpack and their relation to meltwater. *Journal of Hydrology*, 260(1):38–57.

Venugopal, V. and Foufoula-Georgiou, E. (1996). Energy decomposition of rainfall in the time-frequency-scale domain using wavelet packets. *Journal of Hydrology*, 187(1):3–27.

Walling, D. and Webb, B. (1986). Solutes in river systems. *Solute processes*, pages 251–327.

Weekes, A. A., Torgersen, C. E., Montgomery, D. R., Woodward, A., and Bolton, S. M. (2014). Hydrologic response to valley-scale structure in alpine headwaters. *Hydrological Processes*.

Weijs, S. V., Mutzner, R., and Parlange, M. B. (2013). Could electrical conductivity replace water level in rating curves for alpine streams? *Water Resources Research*, 49(1):343–351.

Wenninger, J., Uhlenbrook, S., Tilch, N., and Leibundgut, C. (2004). Experimental evidence of fast groundwater responses in a hillslope/floodplain area in the black forest mountains, germany. *Hydrological Processes*, 18(17):3305–3322.

Williams, M. W., Seibold, C., and Chowanski, K. (2009). Storage and release of solutes from a subalpine seasonal snowpack: soil and stream water response, niwot ridge, colorado. *Biogeochemistry*, 95(1):77–94.

Yuan, F. and Miyamoto, S. (2008). Characteristics of oxygen-18 and deuterium composition in waters from the pecos river in american southwest. *Chemical Geology*, 255(1):220–230.

Zemp, M., Haeberli, W., Hoelzle, M., and Paul, F. (2006). Alpine glaciers to disappear within decades? *Geophysical Research Letters*, 33(13).

Zolezzi, G., Bellin, A., Bruno, M., Maiolini, B., and Siviglia, A. (2009). Assessing hydrological alterations at multiple temporal scales: Adige river, italy. *Water Resources Research*, 45(12).